INFORMATION TO USERS

This manuscript has been reproduced from the microfilm master. UMI films the text directly from the original or copy submitted. Thus, some thesis and dissertation copies are in typewriter face, while others may be from any type of computer printer.

The quality of this reproduction is dependent upon the quality of the copy submitted. Broken or indistinct print, colored or poor quality illustrations and photographs, print bleedthrough, substandard margins, and improper alignment can adversely affect reproduction.

In the unlikely event that the author did not send UMI a complete manuscript and there are missing pages, these will be noted. Also, if unauthorized copyright material had to be removed, a note will indicate the deletion.

Oversize materials (e.g., maps, drawings, charts) are reproduced by sectioning the original, beginning at the upper left-hand corner and continuing from left to right in equal sections with small overlaps.

Photographs included in the original manuscript have been reproduced xerographically in this copy. Higher quality 6" x 9" black and white photographic prints are available for any photographs or illustrations appearing in this copy for an additional charge. Contact UMI directly to order.

Bell & Howell Information and Learning
300 North Zeeb Road, Ann Arbor, MI 48106-1346 USA

UMI®
800-521-0600

Infrared Multiple-Photon Dissociation of Small Organic Sulfoxides

by

Marko Peter Banjavčić
B.Math., University of Waterloo, 1988
M.Sc., University of Waterloo, 1990

A Thesis Submitted in Partial Fulfillment of the
Requirements for the Degree of
DOCTOR OF PHILOSOPHY
in the
Department of Chemistry

We accept this thesis as conforming
to the required standard

Dr. T. E. Gough, Supervisor (Department of Chemistry)

Dr. W. J. Balfour, Departmental Member (Department of Chemistry)

Dr. C. Qian, Departmental Member (Department of Chemistry)

Dr. G.A. Beer, Outside Member (Department of Physics)

Dr. S.V. Filseth, External Examiner (Department of Chemistry, York University)

Supervisor: Dr. T.E. Gough

Abstract

The infrared multiple-photon dissociation of several small organic sulfoxides was studied in order to provide some insight in the dissociative product channels for this class of molecules. Vibrational excitation was achieved with a TEA CO_2 laser and photofragments were identified with a laser ionized time of flight mass spectrometer. A beam of 10.5 eV photons generated in a static xenon gas tripling cell from a tightly focused Nd:YAG third harmonic beam of light was used to ionize the molecules and fragment species.

The photoionization mass spectra were found to contain fewer fragmentation species than the corresponding electron impact ionization mass spectra. Numerous product species were observed from skeletal rearrangement reactions despite the lower level of energy excitation from the photoionization process.

The infrared photolysis wavelength dependence of dimethyl sulfoxide indicated that the maximum abundance for the major fragmentation species occurred at (or near) 1085.8 cm^{-1}. The major products at 1085.8 cm^{-1} were $[H_3CSO]^+$ and $[CH_3]^+$. Minor products were also observed at a higher output power threshold like the skeletal rearrangement species $[H_3CS]^+$ and $[OCH_3]^+$.

With the infrared photolysis wavelength dependence of methyl phenyl sulfoxide, the major product species ($[CH_3]^+$ and $[OSCH_3]^+$) had a maximum abundance near 1086.9 cm^{-1}. Small mass fragment species (like $[HCS]^+$, $[C_4H_5]^+$ and $[C_4H_3]^+$) had a

maximum abundance near 1080 cm^{-1} while large mass fragment species ($[C_6H_8S]^{+\bullet}$ and $[C_6H_5SO]^+$) had a maximum abundance that was further red-shifted (1058.9 and 1050.4 cm^{-1}, respectively). The photolysis at 1085.8 cm^{-1} generated the high mass fragment species ($[C_6H_5SO]^+$, $[C_6H_8S]^{+\bullet}$ and $[C_5H_5S]^+$) at all CO_2 laser output powers but a plateau in the abundance was observed at higher output powers. The smaller mass fragmentation species only appeared after a threshold power was surpassed.

The maximum abundance for the various fragmentation species of *sec*-butyl methyl sulfoxide occurred near 1072 cm^{-1}. The CO_2 laser output power dependence for the formation of the butane, butyl and butene ions indicated all three were generated at all output powers with an abundance plateau or decline occurring at higher output powers. Fragmentation species were observed from the butyl group primary products with the power threshold increasing for the sequentially smaller secondary species.

Examiners:

Dr. T. E. Gough, Supervisor (Department of Chemistry)

Dr. W. J. Balfour, Departmental Member (Department of Chemistry)

Dr. C. Qian, Departmental Member (Department of Chemistry)

Dr. G.A. Beer, Outside Member (Department of Physics)

Dr. S.V. Filseth, External Examiner (Department of Chemistry, York University)

Table of Contents

List of Tables

List of Figures

Acknowledgements

This project was like a journey that you walked a long distance to reach the final destination. Barriers were constantly encountered and decisions were made as to which direction to take to overcome the various problems. Then when the journey was finally over, you realized that you have ended up in Los Angeles when you really wanted to go to New York. When I first started this project, my goal was to use laser induced fluorescence to characterize the photofragment species but we never got around to this because of the numerous problems we encountered so the product fragments were characterized with a laser ionized time of flight mass spectrometer.

First of all, I would like to thank my supervisor, Professor Terry Gough for introducing me to the fascinating field of spectroscopy when I was an undergraduate student at the University of Waterloo. Over the past few years I have learnt a lot of information and, for that, I shall be forever grateful.

Next I would like to thank Dr. Jack Barnes and Dr. Wayne Ingham for their assistance with my project. Unfortunately, the majority of the synthesis work performed by Wayne was not used for this thesis. However, a valuable discussion with Wayne directed me towards investigating the skeletal rearrangement products after we had started the work with the sulfoxide molecules. Jack provided a lot of assistance with his skill and knowledge on designing and building electronic circuits, machining and glassware. Thanks to Jack, I did not have to go to the Machine Shop, the Glass Shop or the Electronics Shop very often. However, I still had to get some help from

Roy Bennett and Dick Robinson in the Machine Shop, Dave Searle and Sean Adams from the Glass Shop and Bob Dean and Terry Wiley in the Electronics Shop and so I would like to thank them as well. I would also like to thank Garth Irwin for the NMR spectra he recorded for me for dimethyl sulfoxide and methyl phenyl sulfoxide. The 70 eV electron impact mass spectra were recorded by Dave McGillivray.

I would also like to thank my fellow graduate students: Tangyu Wang, Terry Rowat, Roy Jensen and Marcell Stoer. Numerous discussions with Tangyu and Terry provided additional guidance during the early stages of my project. Roy was of some help to me when he was an undergraduate student but even more so over the past year since his return from his voluntary term of exile in Denver. My friendship with Marcell goes back to our undergraduate days at the University of Waterloo and we have been helping each other ever since. Felisa Stoer wrote the first version of the computer programme to collect data from the LeCroy 9450 digital oscilloscope which was subsequently modified by Marcell. The programme that I wrote to interface with the digital oscilloscope that replaced the analog switching box was too slow and so I decided to use the programme that they wrote and I would like to thank both of them. Also, the various discussions we have had over the years helped me tremendously so that I could re-focus my energy on my project.

Finally, I would like to thank my parents, my sister Carol and my brother Frank for their encouragement over the years. Without their support during the many rough times, I would not have been able to complete this degree.

To my parents.

Chapter 1

Introduction

Chemists have always been interested in observing, explaining and controlling chemical reactions. Observing a chemical reaction could be as simple as noting a colour change or detecting the distinct odour of a particular product. Unfortunately, qualitative observations are not as useful as quantitative results because more information can be obtained by investigating numerical trends in the data. For example, by studying the rate of formation of a particular product species, one could determine if the reaction proceeded in a linear relationship (usually referred to as first order) or a quadratic dependence (second order).

A greater understanding is obtained by being able to explain the outcome of a reaction. Just because a reaction is classified as being first order, it does not mean that everything is known about the reaction. A first order reaction in only one species which also has no dependence on any other species could be a unimolecular reaction.

Since a stable molecule will not spontaneously react to form products, this leads to the question, why did the molecule form the new product species? In order to explain the result of a reaction, scientists first propose a hypothesis to explain the reaction and if the observations agree with the predicted results, it becomes a theory describing the experimental process. Some of the theories that were used to explain unimolecular reactions will be considered later in this chapter.

The next logical step after being able to explain a reaction is controlling it so that a desired outcome is achieved. A part of a molecule which behaves as a separate unit and in a certain way is classified as a functional group. Sometimes chemists want a reaction to occur with one functional group but not with another one on the same molecule and so by preparing the molecule in an appropriate manner, a site-specific reaction could then occur.

One method of controlling a chemical reaction involves breaking a specific bond in a molecule. If a bond is considered to behave like a spring, one could (in principle at least) put enough energy into the vibrational mode associate with the bond so that it will rupture. Unfortunately, most of the vibrational modes are not associated with just one bond but describe a concerted motion of the molecule as a whole. In order to localize the vibration to a single bond, a linear combination of all of the modes needs to be considered such that motion of the other atoms not involved in the bond is cancelled out and the only one which changes in length is the desired bond.

The potential energy surface of a molecule is a useful way of representing the

interactions of the various atoms when the molecule moves according to the different vibrational modes. The potential energy surface can be visualized as being like a mountain range with peaks and valleys. Each valley represents a stable structure and the different valleys correspond to different isomers of the molecule. A plateau can be thought of as a dissociative product channel. A molecule in one stable structure undergoing a chemical reaction could then follow a variety of different product channels, some of which lead to different isomers while others lead to the dissociation of one or several bonds.

Although vibrationally exciting a molecule can result in the system entering a product channel which corresponds to cleavage of a single bond, various unexpected product channels can also become energetically accessible and can also be entered by the excited molecule. By studying the various species of the different product channels when some condition is changed (usually the amount of energy absorbed by the molecule), an understanding of the competing reactions and their respective reaction rates or likelihoods can be obtained.

From the title of this thesis, it should be clear that this work involved a study of some small (i.e. less than twenty-five atoms) organic sulfoxide molecules with an infrared laser and it is understood that some form of detection system was employed. The aim of this chapter is to provide background information on these three components of the experiment by first providing a general review of mass spectrometers, then about laser excitation and finally to discuss the previous mass spectrometry and

photolysis work performed on these small sulfoxide molecules. Chapter 2 outlines the experimental apparatus used in this work. The experimental results are presented in chapter 3. The last chapter provides some concluding remarks on this work and explains how it enhances the picture presented by the previous work.

1.1 Mass Spectrometers

Since the aim of this section is to provide a general review of mass spectrometers, an overview of two common instrumental techniques pertinent to this work will be presented. A more detailed description of these and other techniques is beyond the scope of this work but can be found in many other places (reference [1] to name just a single source). Because mass spectrometers detect fragmentation species in addition to (or sometimes instead of) the parent molecule, unimolecular reaction theories can assist in providing an understanding of the mechanisms involved in forming the various products. Consequently, this section will conclude with a discussion of this important topic.

1.1.1 Instrumentation

Mass spectrometers have three basic components: sample delivery system, mass separation unit and the detection system. The sample can be delivered into the mass spectrometer in several different ways. For a gaseous sample, an effusive source could

be used to leak the sample into the mass spectrometer at the desired location. A pulsed molecular beam with a carrier gas could be used to increase the molecular density in the mass spectrometer. Non-gaseous samples could be inserted into the mass spectrometer by placing the sample on a probe and then positioning the probe at the desired location inside the system.

Before covering the mass separation unit, some methods of detecting the sample will be covered. In some of the first mass spectrometers, the detection system was a photographic plate [2–4]. Although this did provide an indication of which masses were present over a wide range, it was very difficult to quantitatively determine how much of a certain species was observed. Replacement of the photographic plate with a position sensitive detector would provide a complete spectrum where the intensity for a certain mass could be recorded. A more common substitution is to use a single channel detector instead of the photographic plate and vary an instrumental parameter to generate the desired mass spectrum.

Mass separation of the sample represents the heart of a mass spectrometer. By ionizing the sample, separation can be achieved because of the unique mass-to-charge ratio for the ions of a certain mass. The ionization process most commonly occurs by colliding the neutrally charged molecule with a highly energetic electron (usually around 70 eV of kinetic energy). The neutral molecule absorbs some energy from the electron and emits an electron to become an ion. Colliding the neutral sample molecule with a positively charged ion is another way of producing a charged species

and this method is referred to as chemical ionization. Another common technique involves using a laser to photoionize the sample. In all of these cases, the ionization process occurs within an electric field so that once the sample has been ionized, the ions are accelerated towards the mass analyzer.

Magnetic Sector Deflection Analyzers

The most common method of separating the different masses uses a magnetic sector. The ion beam is aligned to travel through the magnetic sector such that the trajectories of the different masses are deflected by a different amount. Thus, for a sector with a specific radius of curvature and a certain magnetic field, only the ions with the appropriate kinetic energy will travel through and reach the detector. Varying any one of these three parameters (radius of curvature, magnetic field or kinetic energy) while fixing the other two will generate a mass spectrum.

One problem with using only a single analyzer is that the ions of a certain mass can have a small range of kinetic energies due to the spread in the initial kinetic energy of the neutrally charged sample. The spread in kinetic energies results in a range of apparent masses for the ions which leads to a lower mass resolution for the instrument. If the ion beam travels through an energy analyzer before the magnetic sector, the ion beam will be dispersed from the central trajectory. A slit placed between the energy analyzer and the magnetic sector would then narrow the range of kinetic energies of the ions entering the magnetic sector by only allowing a narrow range of trajectories

to pass from the energy analyzer and into the magnetic sector. This method improves the mass resolution but at the expense of decreasing the number of ions which reach the detector.

Stable ions will travel from the ionization region through the analyzers and on to the detector without fragmenting. However, some ions will dissociate within the analyzers. This results in a broad peak in the mass spectrum at a different mass. Even though these metastable ions complicate the mass spectrum, they do provide some valuable information. The ion will have an apparent mass of m^* given by [5]

$$m^* = \frac{(m_d)^2}{m_p} \tag{1.1}$$

where m_p represents the mass of the unstable parent ion formed in the ionization region and m_d is the mass of the daughter ion formed while the parent ion was within the analyzers. The kinetic energy of the ion is given by

$$eV = \frac{1}{2} m_p v^2 \tag{1.2}$$

while the magnetic deflection of the ion is for the daughter ion and is a balance between the centripetal force and the centrifugal force. The velocity for the ion is then

$$v = \frac{eHr}{m_d} \tag{1.3}$$

where e is the charge on the ion and H is the magnetic field strength. Substitution of this term for the velocity into the kinetic energy equation with some additional rearrangements results in

$$\frac{(m_d)^2}{m_p}\frac{1}{e} = \frac{H^2r^2}{2V} \tag{1.4}$$

or

$$\frac{m^*}{e} = \frac{H^2r^2}{2V}. \tag{1.5}$$

The presence of a metastable peak in the mass spectrum thus provides a mechanism describing the formation of the daughter ion from the parent molecular ion.

Time of Flight Analyzer

A time of flight analyzer involves accelerating the ions from the ionization region towards the detector and achieves mass separation because all of the ions will have the same kinetic energy so ions of dissimilar masses will have different velocities. Hence, the time for ions of dissimilar masses to travel through a drift region of a fixed length will be different. Wiley and McLaren improved the resolution over a single accelerating region time of flight mass spectrometer by adding a second accelerating region right after the ionization region [6]. The time of flight mass spectrometer used in this work was based on the two-stage ion acceleration apparatus built by Wiley

and McLaren and the specifics are covered in more detail in section 2.3 starting on page 53. One advantage with using a time of flight mass analyzer instrument is that a complete mass spectrum can be obtained in a few microseconds. This would be an advantage in a system where the sample molecular density changes unexpectedly. A major disadvantage with a time of flight mass spectrometer is the lower mass resolution than with a magnetic sector analyzer.

The spread in the initial kinetic energy of the neutrally charged sample molecules is also a problem with a time of flight mass analyzer. The extreme situation involves considering two ions with the same initial kinetic energy, one initially moving towards the detector and the other moving away from the detector. The ion moving away from the detector will be decelerated until it stops and then the ion will be accelerated towards the detector. When the ion returns to the original position, it has the same kinetic energy as it initially had but it is now travelling towards the detector. The time that it takes the ion to return to the original position is referred to as the turn-around time and the total flight time for the two ions will differ by this amount.

The problem of the turn-around time can be corrected in several different ways. One method of dealing with this problem involves increasing the strength of the field in the ionization region. The time spread is decreased because the stronger field causes the ion travelling away from the detector to rapidly turn around and be accelerated in the opposite direction. Another method involves lengthening the drift region. This increases the total flight time and so the relative amount of time for the ion to turn

around (compared to the total flight time) is decreased.

The mass resolution can also be improved by adding an element to deal with the spread in the initial kinetic energies and one common type of instrument which does this is referred to as a reflectron time of flight mass spectrometer [7]. An ion mirror uses an electric field to decelerate the ion and then accelerate it again, usually in a different direction. Ions with a slightly higher kinetic energy will travel further in the ion mirror before being deflected away from the mirror. This results in a compression of the time spread due to the range of initial kinetic energies for ions of the same mass because the faster ions (with the larger initial kinetic energy) travel a longer distance from the ionization region to the detector.

1.1.2 Unimolecular Reaction Theory

As previously mentioned, mass spectrometers require ionizing the sample but, unfortunately, the ionization process can result in a parent ion that is unstable which can then dissociate. This type of behaviour is designated as a unimolecular reaction because it involves a single molecule reacting to form products. The formation of the fragmentation species in a mass spectrum could then be treated as being governed by rate processes of unimolecular reactions. Although this type of calculation was not performed for the work presented in this thesis, a historical overview of unimolecular reaction theories is provided because of the importance of this topic to the field of mass spectrometry.

The Radiation Hypothesis

The first somewhat successful attempt at explaining the mechanism behind unimolecular reactions was the radiation hypothesis developed primarily by Perrin in 1913 and further refined after World War I [8]. It stated that the energy necessary for the molecule to undergo either a rearrangement (i.e. isomerization) or a decomposition reaction was provided by the environment that the molecule was located in and the energy was in the form of a single photon of radiation. Some people have interpreted this to mean that the radiation must come from the walls of the container. The justification for this hypothesis was that unimolecular reactions followed a linear dependence on the pressure of the system, not quadratic as would be expected for bimolecular reactions which involve collisions to energize the molecule.

Unfortunately, at the time that Perrin and other researchers were spending so much effort refining the radiation hypothesis to fit the available data, there was no known reaction that was truly unimolecular; the reactions that were believed to follow a unimolecular mechanism were later shown to be complex in nature. One such example was the decomposition of N_2O_5 according to the reaction

$$2N_2O_5 \rightarrow 4NO_2 + O_2 \tag{1.6}$$

investigated by Daniels and Johnston [9, 10]. The experimentally observed rate of N_2O_5 consumption was first order in N_2O_5 (and zero order in everything else) and

so the authors believed they had found a unimolecular reaction. Subsequent work determined that the decomposition was explained by the following mechanism [11–14]

$$N_2O_5 \xrightarrow{k_1} NO_2 + NO_3 \tag{1.7}$$

$$NO_2 + NO_3 \xrightarrow{k_{-1}} N_2O_5 \tag{1.8}$$

$$NO_2 + NO_3 \xrightarrow{k_2} NO_2 + O_2 + NO \tag{1.9}$$

$$NO + N_2O_5 \xrightarrow{k_3} 3NO_2 \tag{1.10}$$

with the rate of N_2O_5 consumption given by [15]

$$-\frac{d[N_2O_5]}{dt} = \frac{2k_1k_2}{k_{-1}+k_2}[N_2O_5]. \tag{1.11}$$

The rate of N_2O_5 consumption denoted by equation 1.11 is first order but the decomposition of N_2O_5 does not occur by an elementary unimolecular reaction.

One of the opponents of the radiation hypothesis was Langmuir who pointed out that there was no direct evidence supporting this theory [16]. He believed that unimolecular reactions had to be explained in terms of quantum mechanics. Langmuir stated that every chemical reaction was a discontinuous process, going from reactants to products. His main objection to the radiation hypothesis was that the refinements that were necessary in order to explain the experimental evidence complicated the simple picture of unimolecular reactions to the point of making this theory rather absurd.

The chief detractor of the radiation hypothesis was Lindemann who pointed out that for the inversion of sucrose, the radiation hypothesis did not predict the correct relative rate of reaction in sunlight compared with in darkness [17]. The intensity of 1.05 μm light is 5×10^{13} times greater in sunlight than in the dark and so should correspond with a much higher rate in sunlight while the experimental evidence suggested that the reaction proceeded at about the same rate with or without sunlight. Lindemann later pointed out an inconsistency between the supporters of the radiation hypothesis [18] when Perrin suggested that the rate of inversion of sucrose was dependent upon the absorption of sunlight in several bands, not just at 1.05 μm [19] while Lewis had found a single band which supported the position of the radiation hypothesis in this reaction [20].

The Lindemann Mechanism

Instead of just arguing against the radiation hypothesis, Lindemann also proposed that the molecule was energized by a collision with another molecule before a unimolecular reaction occurred [17]. This could be accounted for with the following mechanism

$$A + A \xrightarrow{k_1} A^* + A \tag{1.12}$$

$$A^* + A \xrightarrow{k_{-1}} A + A \tag{1.13}$$

$$A^* \xrightarrow{k_2} (Products) \tag{1.14}$$

where A^* represents a molecule with sufficient energy to surpass the barrier to reaction. The rate of producing the energized species is $k_1[A]^2$ while the rate of consuming the energized species is the sum of $k_{-1}[A^*][A]$ and $k_2[A^*]$.

For high pressures, the rate of de-energizing A^* ($k_{-1}[A^*][A]$) will be much greater than the rate of product formation ($k_2[A^*]$). In this situation, the rate of forming the energized species is equal to the rate of de-energizing A^*. Thus,

$$k_1[A]^2 = k_{-1}[A^*][A] \tag{1.15}$$

or, in terms of solving for $[A^*]$,

$$[A^*] = \frac{k_1}{k_{-1}}[A]. \tag{1.16}$$

The rate of product formation is then equal to $(k_1k_2/k_{-1})[A]$ and is first order in $[A]$. Thus, a collisional energization mechanism could account for the observed first order behaviour of unimolecular reactions.

For low pressures, the rate of de-energizing A^* is much smaller than the rate of product formation. The rate of product formation is then equal to the rate of forming the energized species and is second order ($k_1[A]^2$). This result was a significant change from the radiation hypothesis which stated that unimolecular reactions were first order at all pressures. The second order dependence at low pressures was experimentally verified in 1927 by Ramsperger [21] and effectively closed the door on the

radiation hypothesis.

An alternate derivation of the unimolecular reaction rate involves using the steady-state approximation, which states that the change in the concentration of intermediate species over time is equal to zero (i.e. the concentration, whatever it might be, does not change significantly). This approach yields

$$[A^*] = \frac{k_1[A]^2}{k_{-1}[A] + k_2} \tag{1.17}$$

and the rate of product formation is

$$k_2[A^*] = \frac{k_1 k_2[A]^2}{k_{-1}[A] + k_2}. \tag{1.18}$$

At high pressures, $k_{-1}[A]$ is much larger than k_2 and the reaction rate becomes

$$\frac{k_1 k_2}{k_{-1}}[A] \tag{1.19}$$

just as before. At low pressures, k_2 is much larger than $k_{-1}[A]$ and the reaction rate simplifies to

$$k_1[A]^2 \tag{1.20}$$

which, again, is the same result as was previously obtained.

Since the rate of a unimolecular reaction is also given in terms of the apparent first

order rate coefficient (k) by $k[A]$, the following expression is obtained by equating the apparent rate of the reaction to the rate of product formation

$$k = \frac{k_1 k_2 [A]}{k_{-1}[A] + k_2} \tag{1.21}$$

or

$$k = \frac{k_1 k_2 / k_{-1}}{1 + k_2/(k_{-1}[A])}. \tag{1.22}$$

An alternative representation, which is more useful, is to consider the reciprocal of k

$$\frac{1}{k} = \frac{k_{-1}}{k_1 k_2} + \frac{1}{k_1 [A]}. \tag{1.23}$$

A plot of $1/[A]$ against $1/k$ should yield a straight line with slope $1/k_1$ and intercept $k_{-1}/(k_1 k_2)$. Unfortunately, experimental results show a significant deviation from this expected linearity and this problem must be addressed by a successful theory.

Approach Made By Hinshelwood

In 1927, Hinshelwood refined Lindemann's mechanism by allowing the energy available to the molecule to be distributed among the s vibrational modes of the molecule [22]. Since each vibrational mode involves two quadratic energy terms, the following expression for the fraction of molecules above the threshold energy E_0 is

obtained

$$f = \frac{1}{(s-1)!}\left(\frac{E_0}{k_B T}\right)^{s-1} \exp(-E_0/k_B T) \tag{1.24}$$

where k_B is the Boltzmann constant and T is the temperature in kelvin. The rate coefficient for a reaction is taken to be proportional to the fraction of molecules above the threshold energy so k_1/k_{-1} is given by

$$\begin{aligned} \frac{k_1}{k_{-1}} &= \frac{f}{1} \\ \frac{k_1}{k_{-1}} &= \frac{1}{(s-1)!}\left(\frac{E_0}{k_B T}\right)^{s-1} \exp(-E_0/k_B T) \end{aligned} \tag{1.25}$$

where it is assumed that there is no energy barrier for the de-energizing reaction and so the fraction of molecules above the threshold energy is unity.

Although this expression provides much higher rates for the activation reaction and better agreement with experimental results, Hinshelwood's approach still has some problems. The most significant problem was that only about half of the number of vibrational modes needed to be considered to provide agreement with experimental data. Another problem was that f, the fraction of molecules above the threshold energy, introduced a term with a strong temperature dependence but there is no experimental evidence to support this claim. Also, just as with Lindemann's treatment, a plot of $1/[A]$ against $1/k$ should still be linear.

Rice-Ramsperger-Kassel Treatment

A problem with the treatment made by Lindemann and Hinshelwood is that the apparent first order rate coefficient given by

$$k = \frac{k_2 k_1 / k_{-1}}{1 + k_2/(k_{-1}[A])} \tag{1.26}$$

involves rate coefficients which are independent of the amount of energy in the excited molecule. The energizing reaction rate coefficient (k_1) should increase as the energy content is increased because the more energy a molecule has, the greater the probability that a collision will produce an energized molecule. Thus, k_1/k_{-1} should be dependent upon the energy content of the molecules.

The rate coefficient for the product forming reaction (k_2) should also be dependent upon the energy content. The probability that some internal mode will contain enough energy to surpass the reaction barrier will increase as the energy content of the molecule is increased. An improvement to Lindemann and Hinshelwood's theories would, therefore, treat k_1/k_{-1} and k_2 as being dependent on the energy.

In 1927, Rice and Ramsperger published a paper which allowed the energy to be distributed among the various individual energy terms of the molecule [23, 24]. A reaction would occur when the critical term surpassed some threshold energy. Shortly thereafter, Kassel published a similar treatment but he allowed the energy to be distributed among the various vibrational modes of the molecule [25]. This classical me-

chanics treatment of the energy distribution was followed up with a similar quantum mechanical treatment [26]. Because the treatment made by Rice and Ramsperger was so similar to that made by Kassel, people refer to this as the RRK theory of unimolecular reactions.

The expression for k_1/k_{-1} is obtained by starting with equation 1.25 and allowing the energy in the critical mode to vary above the threshold value. This yields

$$\frac{dk_1}{k_{-1}} = \frac{1}{(s-1)!}\left(\frac{E^*}{k_BT}\right)^{s-1} \exp(-E^*/k_BT)\frac{dE^*}{k_BT} \tag{1.27}$$

where E^* refers to an amount of energy above the minimum value. The energy-dependent product formation rate coefficient is taken as being proportional to the probability of the reaction occurring. This is the ratio of the number of ways of distributing the energy above the threshold value in all of the oscillators to the number of ways of distributing all of the energy in all of the oscillators. Using this approach for both the classical and quantum mechanics treatments results in a reaction probability given by [25, 26]

$$P = \left(\frac{E - E_0}{E}\right)^{s-1}. \tag{1.28}$$

Rice-Ramsperger-Kassel-Marcus (RRKM)

The Rice-Ramsperger-Kassel treatment was extended by Marcus and Rice in 1950 [27, 28] by including transition-state theory and once again in the early 1960s by Wieder and Marcus [29] where a quantum mechanical approach was incorporated. The reaction scheme is given by

$$A + M \xrightarrow{k_1} A^* + M \tag{1.29}$$

$$A^* + M \xrightarrow{k_{-1}} A + M \tag{1.30}$$

$$A^* \xrightarrow{k_a(E^*)} A^\ddagger \tag{1.31}$$

$$A^\ddagger \xrightarrow{k_3} (Products) \tag{1.32}$$

where the rate coefficients for the energization step (k_1) and the activation step ($k_a(E^*)$ given by reaction 1.31) are both taken as being energy-dependent. It can be shown that [30–32]

$$k_a(E^*) = \frac{1}{hN^*(E^*)} \sum_{E^\ddagger_{vr}=0}^{E^\ddagger} P(E^\ddagger_{vr}) \tag{1.33}$$

where h is Planck's constant, $N^*(E^*)$ is the density of states at energy E^*, $E^\ddagger_{vr}$ is the energy in the vibrational and rotational modes of $A^\ddagger$, $P(E^\ddagger_{vr})$ is the number of vibrational-rotational states of $A^\ddagger$ with energy exactly equal to $E^\ddagger_{vr}$ and the summation denotes all of the levels with energy less than or equal to $E^\ddagger_{vr}$. The unimolecular

rate coefficient can then be shown to be

$$k_{uni} = \frac{1}{hq_A} \int_{E_0}^{\infty} \frac{(\sum P(E_{vr}^{+})) \exp(-E^{+}/k_B T)\, dE^{+}}{1 + k_a(E^{*})/k_{-1}[M]}. \tag{1.34}$$

Since the extension of the Rice-Ramsperger-Kassel model made by Marcus is so dependent upon RRK theory, it is commonly referred to as RRKM theory to honour all four contributors. The success of RRKM theory in estimating unimolecular reaction rates over the past fifty years has led it to become the standard theory used to describe unimolecular reactions.

1.2 Laser Excitation

In the previous section, an overview of some of the theories describing unimolecular reactions was presented in order to provide an understanding of what happens when an energetically excited molecule fragments. The work presented in this thesis used a CO_2 laser to vibrationally excite a molecule still at the electronic ground state as opposed to most of the other photolysis work reviewed in the next section which utilized a vacuum ultraviolet laser to raise the molecule to an excited electronic state. Staying at the electronic ground state simplifies the analysis of unimolecular reactions because a change in the electronic level does not need to be considered. This section starts with a general discussion on how a multiple number of objects (atoms, molecules or photons) interact to form some other molecule (in the case of atoms and

molecules) or an excited species (when an atom or molecule absorbs several photons). This discussion is of some benefit when laser initiated unimolecular dissociation is considered. In addition, an overview of infrared multiple-photon dissociation is provided to connect the two other subsections together with the apparatus used for this work.

1.2.1 Interaction of Multiple Objects

This section deals with the interaction of multiple objects through some type of reaction. The objects could all be molecules (or molecules and atoms) in which case the interaction is a collision. The other possibility that will be considered is the case where one atom or molecule interacts with an electric field from a laser beam. In this case, the other objects are photons and the interaction is an absorption process. The subsequent paragraphs are left a bit general to deal with these two possibilities. The section will end with a treatment of the differences in the analysis due to the separate cases.

If one considers the interaction of one species, generically designated as A, with a multiple number of another species, B, the process where species A absorbs a multiple number of species B may be represented by

$$A + nB \rightarrow AB_n. \tag{1.35}$$

If this chemical equation represents an elementary process, the rate law for this reaction would be

$$v = k[A][B]^n \tag{1.36}$$

and the reaction would be of order n in species B and overall order $(n + 1)$.

The interaction represented by equation 1.35 involves $(n + 1)$ species but the likelihood of $(n + 1)$ species simultaneously interacting, under normal circumstances, decreases rapidly as n increases. A more likely scenario involves a sequential interaction as denoted by the following reaction scheme

$$A + B \xrightarrow{k_1} AB \tag{1.37}$$

$$AB + B \xrightarrow{k_2} AB_2 \tag{1.38}$$

$$\vdots$$

$$AB_{(j-1)} + B \xrightarrow{k_j} AB_j \tag{1.39}$$

$$\vdots$$

$$AB_{(n-1)} + B \xrightarrow{k_n} AB_n \tag{1.40}$$

and the rate law for the equation where j copies of B have been absorbed by the complex is

$$v = k_j[AB_{(j-1)}][B]. \tag{1.41}$$

Each of these chemical equations represents an elementary bimolecular process which is first order in species B and second order overall.

The rate law for equation 1.40 is

$$v = k_n[AB_{(n-1)}][B] \tag{1.42}$$

and it involves the intermediate species $AB_{(n-1)}$. If the steady-state approximation is used, then the rate of formation of this species equals the rate of depletion which is depicted mathematically as

$$\begin{aligned} \frac{d[AB_{(n-1)}]}{dt} &= k_{(n-1)}[AB_{(n-2)}][B] - k_n[AB_{(n-1)}][B] \\ &= 0 \end{aligned} \tag{1.43}$$

or

$$[AB_{(n-1)}] = \frac{k_{(n-1)}[AB_{(n-2)}][B]}{k_n[B]}. \tag{1.44}$$

Substituting this expression for $[AB_{(n-1)}]$ into equation 1.42 results in

$$\begin{aligned} v &= k_n \frac{k_{(n-1)}[AB_{(n-2)}]}{k_n}[B] \\ &= k_{(n-1)}[AB_{(n-2)}][B]. \end{aligned} \tag{1.45}$$

Continuing this process of dealing with the various $[AB_{(j-1)}]$ intermediate species yields

$$v = k_1[A][B] \tag{1.46}$$

which is first order in species B and second order overall. This result is vastly different from the case where the reaction was treated as a single elementary reaction which was of order n with respect to B and order $(n+1)$ overall.

The problem with using the steady-state approximation is that it is possible that not all of an intermediate is used to make the next product. In the case where more of an intermediate is produced than consumed by a subsequent reaction, the rate of formation would be

$$\frac{d[AB_{(n-1)}]}{dt} > 0 \tag{1.47}$$

which yields

$$k_{(n-1)}[AB_{(n-2)}][B] > k_n[AB_{(n-1)}][B]. \tag{1.48}$$

The inequality can be re-arranged to give

$$[AB_{(n-1)}] < \frac{k_{(n-1)}}{k_n}[AB_{(n-2)}] \tag{1.49}$$

and substitution into equation 1.42 results in

$$v = k_n[AB_{(n-1)}][B] < k_n \frac{k_{(n-1)}}{k_n}[AB_{(n-2)}][B]. \quad (1.50)$$

Repeating this substitution procedure for the other intermediates yields

$$v < k_1[A][B]. \quad (1.51)$$

The apparent rate constant must be less than k_1 and once again the order of the reaction is clearly not n with respect to species B.

When species B is either an atom or a molecule, it is very rare that two (or more) of them will collide simultaneously with species A because it is highly unlikely that three (or more) species travelling in random directions will occupy the same volume of space at the same time. In this case, the sequential addition process predominantly occurs. However, when species B is a photon, a strong electric field (as occurs within a tightly focused laser beam) makes it possible for numerous photons to interact with the absorbing species within the short period of time that the photons take to travel through the interaction volume. In this fashion, the net result is that it appears that a multiple number of photons have been absorbed by species A in a single step. This is referred to as a multiphoton absorption process. In addition to the multiphoton process, the sequential photon absorption process can occur when the intermediate is a stable excited species with a finite lifetime. To emphasize the difference in the

photon absorption mechanism, the second case is occasionally referred to as multiple-photon absorption.

1.2.2 Infrared Multiple-Photon Dissociation

The previous section dealt with a molecule absorbing a multiple number of photons. On its own, this process has a limited appeal but it is very helpful in preparing the system for a subsequent reaction. In this section, this process is extended to the case where enough photons have been absorbed so that the molecule dissociates. Because the work for this thesis used a CO_2 laser to excite a molecule above the dissociation threshold, a review of vibrational modes and infrared multiple-photon dissociation will be briefly discussed.

By making the approximation that a bond behaves like a spring, the vibrating molecule undergoes a restoring force which is proportional to its displacement. This vibration can then be described as a harmonic oscillator. As such, it will have equally spaced energy levels which are separated by $h\nu$ where h is Planck's constant and ν is the frequency of the vibration. A laser of the same frequency could then excite the molecule above the vibrational ground state. Vibrational frequencies are usually around 500 to 3000 cm^{-1} which is in the infrared region of the electromagnetic spectrum.

Unfortunately, the simple picture of treating the vibrational mode as a harmonic oscillator is not correct. For a typical vibrational mode, the restoring force gets

weaker as the displacement increases. This results in the energy levels at the larger displacements being closer together than with a harmonic oscillator. Consequently, a laser which can excite a molecule in the ground state by the absorption of a single photon may not be able to further excite the molecule.

One way in which further excitation can be accomplished is by the absorption of a multiple number of photons as mentioned in the previous section. Unfortunately, the probability of absorbing a multiple number of photons in a single step is proportional to the laser intensity raised to the power of the number of photons (i.e. absorbing three photons would be proportional to the cubed power of the laser intensity) [33]. Since the dissociation energy of a polyatomic molecule is typically equivalent to about 20-30 infrared photons [34], this would require a laser intensity on the order of a gigawatt per square centimetre [35].

Although this intensity is attainable, efficient dissociation is possible at much lower intensities (about 5 MW/cm^2 [36]) which suggests that a different mechanism must be responsible for the dissociation process. The anharmonicity resulting from the weakened restoring force at larger displacements may also remove the independence of the normal vibrational modes. This coupling of vibrational modes allows the molecule to redistribute the energy from one mode into some of the other modes. For example, consider the case of three vibrational modes which are coupled together and where the frequency of one mode is equal to the sum of two other modes (i.e. $\nu_1 = \nu_2 + \nu_3$). In this case, the molecule can readily redistribute one quantum of

energy from the first mode into one quantum in both of the other two modes.

It should be pointed out that the coupling of vibrational modes is not as simple as was described in the previous paragraph. At low levels of excitation, anharmonicity plays a minor role and so the energy content tends to remain localized in the excited vibrational mode. One common method by which molecules redistribute energy to different vibrational modes is by a collision with another molecule. At higher levels of excitation, anharmonicity terms become important and an isolated molecule can redistribute energy amongst the various vibrational modes without collisions [37]. This intramolecular vibrational energy redistribution is quite fast (1-10 ps [38]) and usually occurs before the molecule dissociates.

This now provides a picture of the current model for the multiple-photon absorption process. Initially the excitation occurs in a single vibrational mode, but due to the anharmonicity, the molecule can only be excited a few levels above the ground state. Because of the coupling of the vibrational modes, energy can be redistributed from the absorbing mode and transferred into other modes. This allows the absorbing mode to be excited once again and the absorption-redistribution cycle can be repeated many times while the molecule is still in the electric field of the laser beam.

As more vibrational energy is put into the molecule, the number of permutations in how the energy can be distributed into the various vibrational modes increases. Since each permutation corresponds to a particular state of the molecule, the density of states at a particular energy level increases as more vibrational energy is put

into the molecule. So far, only the case where the states are at exactly the same energy level has been considered. Because of the frequency mismatch of the different vibrational modes, there will be some states at a slightly different energy level. For low levels of vibrational excitation, this energy gap will be quite large but the energy gap will become narrower as the molecule absorbs more vibrational energy. This results in an almost continuum of energy levels for the molecule. Once the molecule has been excited into this quasi-continuum, it can easily be further excited up to the dissociation threshold by the absorption of several photons, a single photon at a time. Another way of looking at this is that an increasing density of states means that the probability of the current energy level in the quasi-continuum being separated from a higher level by $h\nu$ increases the further the molecule has been excited up into the quasi-continuum. This, in turn, means that the likelihood of a photon being absorbed by the molecule increases. Consequently, the molecule can easily be excited up to the dissociation threshold by the absorption of a few photons at a time once it is in the quasi-continuum of energy levels.

The molecule can still be excited above the dissociation threshold but now two competing processes have to be considered: the molecule being further excited above the lowest dissociation energy threshold and the molecule fragmenting. The dissociation process can be thought of as rupturing a single bond in the molecule. In order for the bond to break, the corresponding vibrational mode(s) must be excited above the dissociation threshold. But because the modes are coupled together, the total vibra-

tional energy of the molecule when it dissociates is usually larger than the amount needed to reach this threshold. In other words, usually other vibrational modes are also excited above their ground state when the dissociating mode has enough energy for the molecule to fall apart.

1.2.3 Laser Initiated Unimolecular Dissociation

As previously mentioned, one of the first theories to try and explain unimolecular reactions was the radiation hypothesis (see section 1.1.2 on page 11). It essentially stated that the molecules obtained enough energy to react by absorbing radiation from the surrounding environment. At the time, this was only possible by thermally exciting the molecules. Because the amount of thermal energy available was generally insufficient to cause a reaction, the radiation hypothesis was dismissed. Another competing theory was that the molecules obtained the required energy through collisions with other molecules. Strictly speaking, collisions involve at least two molecules and so, technically, are not unimolecular but bimolecular reactions. However, as was previously shown, at higher pressures these reactions involve only the excited molecule and exhibit a unimolecular behaviour. It is interesting to note that the important point of both the radiation hypothesis and the collisional explanation of unimolecular reactions is that they both require that the reacting molecules obtain enough energy to surpass an energy barrier. With the development of high power lasers, it is now possible to study true unimolecular reactions by exciting the molecules with radiation

from the laser.

Undergraduate Physical Chemistry textbooks state that the rate of a reaction involving the absorption of a photon is given by the number of quanta absorbed per unit time per unit volume (I_{abs}) [39, 40]. With this in mind, consider the following reaction scheme:

$$A + h\nu_a \xrightarrow{I_{abs}} A^* \tag{1.52}$$

$$A + M \xrightarrow{k_2} A^* + M \tag{1.53}$$

$$A^* + M \xrightarrow{k_3} A + M \tag{1.54}$$

$$A^* \xrightarrow{k_4} A + h\nu_e \tag{1.55}$$

$$A^* \xrightarrow{k_5} A^\ddagger \tag{1.56}$$

$$A^\ddagger \xrightarrow{k_6} B + C \tag{1.57}$$

where M is some arbitrary bath gas molecule and B and C are the fragmentation products.

The second and third reactions account for collisional activation and de-activation of A. The fourth reaction represents the excited A molecule emitting a photon to de-energize A^*. Ideally, these three reactions should be negligible but are included here for the sake of completeness.

The rate of change of $[A^*]$ is given by

$$\frac{d[A^*]}{dt} = I_{abs}[A] + k_2[A][M] - k_3[A^*][M] - k_4[A^*] - k_5[A^*] \tag{1.58}$$

but because $[A^*]$ is a reaction intermediate, it is used up as soon as it is formed and so by the steady-state approximation the rate of change of $[A^*]$ should equal zero. This results in

$$[A^*] = \frac{I_{abs}[A] + k_2[A][M]}{k_3[M] + k_4 + k_5}. \tag{1.59}$$

Similarly, $[A^\ddagger]$ is given by

$$[A^\ddagger] = \frac{k_5}{k_6}[A^*] \tag{1.60}$$

which yields

$$[A^\ddagger] = \frac{k_5}{k_6}\frac{I_{abs}[A] + k_2[A][M]}{k_3[M] + k_4 + k_5}. \tag{1.61}$$

The rate of change of product B is

$$\frac{d[B]}{dt} = k_6[A^\ddagger] \tag{1.62}$$

$$= \frac{k_5 I_{abs}[A] + k_2 k_5[A][M]}{k_3[M] + k_4 + k_5}. \tag{1.63}$$

At low pressures, $[M] \rightarrow 0$ and

$$\frac{d[B]}{dt} \approx \frac{k_5 I_{abs}[A]}{k_4 + k_5} \tag{1.64}$$

and is first order in $[A]$ as required.

Although the final result presented in the previous paragraph was dependent upon the absorption of a single photon (equation 1.52 on page 32), the same result is obtained if this equation is replaced by

$$A + n\,h\nu_a \rightarrow A^* \tag{1.65}$$

where the excitation is considered to occur by a multiple-photon absorption process. In section 1.2.1 (starting on page 22), it was shown that the rate law for the sequential absorption of n photons was

$$v = k_1[B][A] \tag{1.66}$$

which becomes

$$v = k_1 I_{abs}[A] \tag{1.67}$$

with the notation used in this section. Since this is the same expression as was used for the development of equation 1.63, it stands to reason that the same result was

obtained when either equation 1.52 or 1.65 was used in the laser initiated unimolecular dissociation reaction scheme.

1.3 Small Organic Sulfoxide Molecules

As mentioned in the previous section, this work utilized a CO_2 laser to vibrationally excite a molecule in its ground electronic state. The major laser lines are around 9.6 and 10.6 μm (1040 and 940 cm^{-1}) and so whichever molecules are selected, they must absorb near one of these two bands. The original objective of this project was to vibrationally excite transition metal carbonyls to study the fragmentation mechanisms as the CO groups were lost from the parent molecule. Although the single metal atom carbonyl molecules were readily made, the molecules with a greater number of metal atoms were much more difficult to synthesize. At about this time, the time dependent infrared laser photolysis study on a few small organic sulfoxide molecules performed by Gross *et al.* [41] was published and it was decided that a complementary investigation could be conducted by our group.

In the 1960s, Rayner *et al.* proposed that thermal racemization of a group of diaryl, alkyl aryl and dialkyl sulfoxides occurred by pyramidal inversion from a molecular vibration without breaking a carbon-sulfur bond [42, 43]. Vibrational excitation of this class of molecules should yield some interesting results due to the motion of the sidegroups relative to the sulfur and/or oxygen atoms, maybe even the migration of part of the molecule in some instances. Because the experimental work for this the-

sis involved photofragmentation and then species identification with a time of flight mass spectrometer, a review of the previous mass spectrometry work performed on these molecules followed by an overview of the photolysis work will be provided in this section.

1.3.1 Electron Impact Mass Spectrometry

The first electron impact mass spectrometry investigation of sulfoxide and sulfone molecules was reported in the mid 1960s and provided unexpected results even for the smallest molecule of the group, dimethyl sulfoxide [44, 45]. A minor peak of significant intensity corresponded to the loss of OH from the parent molecular ion and this fragment species was not expected to be formed from a single step elimination process. The presence of the appropriate metastable species, however, indicated that a hydrogen migration must have occurred prior to the OH elimination reaction and that this dissociation did occur in a single step.

The most abundant ion in the 70 eV electron impact mass spectrum of dimethyl sulfoxide recorded by Bowie *et al.* was found to have a mass of 63 amu which correlates to the loss of a methyl group from the parent molecular ion [45]. Although a metastable peak connects this peak with a precursor species of mass 78 amu, it is not known if the precursor was the same species which led to the elimination of OH or not. Another unexpected species had a mass of 45 amu and was connected to the peak at 63 amu by the appropriate metastable species which indicates that H_2O had

been eliminated from the 63 amu mass species in a single step.

Another molecule investigated by Bowie *et al.* which had some unexpected results was methyl phenyl sulfoxide [45]. Minor product species were found at 94 and 112 amu which occurred by a single step elimination of H_2CS and CO, respectively, from the parent molecular ion as indicated by the appropriate metastable species. A major peak was observed at 125 amu which corresponds to the elimination of a CH_3 group from the parent molecular ion. A metastable peak connecting this 125 amu species to one at 97 amu was also present. Since this also indicates a loss of CO from a precursor species, some excited species must have been formed where a carbon atom migrated to the oxygen atom. Bowie *et al.* proposed a mechanism where the phenyl group migrated to the oxygen atom [45]. Siegel determined that the carbon atom of the phenyl group bonded to the sulfur atom was the one that migrated to the oxygen atom by isotope labelling this particular carbon atom [46].

Although Bowie *et al.* did not observe a similar migration to the oxygen atom in dimethyl sulfoxide, Amos *et al.* did with their investigation of the appearance potentials for $[H_3CS]^+$ and $[OCH_3]^+$ [47]. Instead of using 70 eV electrons, Amos *et al.* varied the potential energy from 0 to 20 eV. Consequently, they were able to observe $[H_3CS]^+$ with a relative intensity of 9.3% at an electron energy of 11.4 eV and 7.3% for $[OCH_3]^+$ at 12.2 eV. Since OCH_3 does not appear in the parent molecule as a separate unit, the energetically excited parent molecular ion must have undergone a rearrangement where a methyl group migrated to the oxygen atom.

The unexpected results for methyl phenyl sulfoxide noted by Bowie *et al.* were also observed for other aromatic sulfoxides and sulfones [45]. In particular, migrating one group from the sulfur atom to the oxygen atom with a subsequent rupture of the sulfur-oxygen bond was observed for diphenyl sulfoxide and di-*p*-tolyl sulfoxide. This rather interesting result prompted Gillis *et al.* to investigate the rearrangement in the unsaturated molecule methyl vinyl sulfoxide [48]. They found evidence for the migration of either the methyl moiety or the vinyl group to the oxygen atom. Kinstle and Oliver studied the mass spectra of styryl sulfoxides and also observed the similar sulfoxide rearrangement [49]. The complexity of the fragmentation mechanism of these and other exotic sulfoxide molecules is beyond the scope of this thesis but can be found in the review articles by Khmel'nitskii and Efremov [50] and by Pihlaja [51].

The lack of subsequent interest in aliphatic sulfoxide molecules could be attributed to Bowie *et al.* because they stated that the electron impact mass spectra were "relatively simple" [45]. However, this result may have been due to their selection of molecules. By choosing dialkyl sulfoxide molecules, the authors were limited to a rather small subset of aliphatic sulfoxides. Selecting molecules with different alkyl groups would provide information on competing dissociative reactions because the alkyl moieties would involve different fragmentation channels.

Fortunately, Smakman and de Boer continued the investigation of small aliphatic sulfoxide molecules with their study on hydrogen migration and fragmentation patterns [52]. They found that there was a nonspecific hydrogen migration to the oxy-

gen atom when the results were compared with the site-specific analogous deuterated molecules. In addition, Smakman and de Boer stated that breaking a carbon-sulfur bond without migrating a hydrogen atom rarely occurred with aliphatic sulfoxide molecules.

Unlike Bowie *et al.* [45], Smakman and de Boer selected unsymmetrical alkyl groups and obtained some rather interesting results [52]. With unbranched alkyl groups, the larger moiety was preferentially (but not exclusively) lost. Isopropyl *n*-butyl sulfoxide has two methyl groups connected to the carbon atom bonded to the sulfur atom in the isopropyl moiety and hydrogen migration from the smaller isopropyl group with cleavage of the bond to the sulfur atom resulted in the loss of a propene group from the parent molecular ion. In this manner, isopropyl *n*-butyl sulfoxide could lose either the larger butyl group or the smaller propene group in almost equal abundance.

1.3.2 Sulfoxide Photolysis

A common goal of researchers investigating the photolysis of sulfoxide molecules is to compare their results with those obtained with ketones. This leads back to the pioneering work performed by Norrish and associates in the 1930s [53–57]. For this work, they utilized a mercury lamp which generated photons over a 3000 to 2200 Å range but usually 2537 Å was selected.

The results for the photolysis of a generic ketone can be summarized by the

following chemical equations

$$R'COR'' + h\nu \rightarrow [R']^{\bullet} + [R''CO]^{\bullet} \quad (1.68)$$

$$R'COR'' + h\nu \rightarrow [R'CO]^{\bullet} + [R'']^{\bullet} \quad (1.69)$$

$$R'COCH_2CH_2CH_2R'' + h\nu \rightarrow R'COCH_3 + H_2C{=}CHR''. \quad (1.70)$$

The mechanism for equations 1.68 and 1.69 is believed to be direct dissociation to form the pair of radical species. The mechanism for equation 1.70 is more complicated because a hydrogen migration from the third carbon atom from the carbonyl group (a γ-carbon) to the oxygen atom and cleavage of the bond between the α-carbon and the β-carbon occurs.

Although the bonding appears to be similar between a carbonyl molecule and a sulfoxide, the bond angles are different due to the different electronic configuration between carbon and sulfur. The bond angle between the carbonyl oxygen atom and an α-carbon is governed by the sp^2 hybridization of the carbonyl carbon. Whereas with the sulfur atom in the sulfoxide functional group, the six valence electrons combine with four electrons from the bonded atoms to form five orbitals, four bonded orbitals and one with a lone pair of electrons. This results in a tetrahedral arrangement around the sulfur atom for the lone pair and three bonding orbitals. The net result is that the migrating hydrogen can be one atom closer to the oxygen atom in a sulfoxide molecule than with a carbonyl (i.e. hydrogen migration from a β-carbon instead of a

γ-carbon).

The photolysis of dimethyl sulfoxide in solutions was first investigated by Gollnick and Stracke in the early 1970s [58–60]. The photolysis was performed at 2537 Å with a mercury lamp. In addition to the expected dissociation reaction forming the methyl radical, Gollnick and Stracke reported the formation of dimethyl sulfone and dimethyl sulfide. This could be accounted for by the following mechanism

$$H_3C-SO-CH_3 + h\nu \rightarrow [H_3C-SO-CH_3]^* \quad (1.71)$$

$$[H_3C-SO-CH_3]^* + H_3C-SO-CH_3 \rightarrow H_3C-SO_2-CH_3 + H_3C-S-CH_3 \quad (1.72)$$

where the increased dimethyl sulfoxide concentration in the solutions makes the collisional reaction more likely to occur than if the photolysis would have been performed in the gas phase.

In addition to the photolysis work on dimethyl sulfoxide, Gollnick and Stracke presented a vacuum ultraviolet absorption spectrum and performed some electron density calculations for the frontier orbitals [60]. The vacuum ultraviolet absorption spectrum covered the region from 140 to 240 nm and was recorded at the vapour pressure of dimethyl sulfoxide at 25° C (0.5 Torr [61]). The most intense peak in the absorption spectrum had a maximum at 188 nm and was attributed to a $\pi \rightarrow \pi^*$ transition of the sulfoxide group.

The strong peak at 188 nm in the vacuum ultraviolet absorption spectrum allowed several researchers to use an ArF excimer laser (193 nm) to study various aspects of the photodissociation of dimethyl sulfoxide [62–66]. Zhao *et al.* used photofragmentation time of flight mass spectrometry to study the various dissociation product species [64]. In particular, they found the major species were H_3CSO, CH_3 and SO. In addition, they found no evidence for the formation of oxygen atoms in the dissociation of dimethyl sulfoxide so the species with a mass of 62 amu was attributed to H_2CSO instead of H_3CSCH_3.

Another photofragment translational spectroscopy investigation on the dissociation of dimethyl sulfoxide at 193 nm worth mentioning was performed by Blank *et al.* [65]. An investigation of the time of flight for the H_3CSO fragment determined that two photofragment channels produced a species with a mass of 63 amu. The majority (83%) was attributed to a slow channel which subsequently further dissociated according to the following reactions

$$H_3CSO \rightarrow H + H_2CSO \tag{1.73}$$

$$H_3CSO \rightarrow H_3C + SO \tag{1.74}$$

where the first equation accounted for less than 5% of the H_3CSO and the second equation involved 64%. Another interesting result was obtained when the authors switched to the fully deuterated analogue of dimethyl sulfoxide and found that the slow primary photofragment channel accounted for only 73% of D_3CSO. The sec-

ondary dissociation to give D_3C and SO accounted for 56% of the 73% of D_3CSO for the slow channel. There was no evidence for the formation of D_2CSO.

Blank *et al.* only considered the direct cleavage reaction, they did not consider the skeletal rearrangement reaction as suggested by Smakman and de Boer [52]. The *ab initio* work performed by Gozzo and Eberlin concluded that the dissociation of ionized dimethyl sulfoxide should occur primarily by the simple cleavage reaction but decomposition through a metastable species would involve hydrogen migration [67].

Using the information from the work by Gozzo and Eberlin, the fast photofragment channel observed by Blank *et al.* [65] should correspond to

$$(H_3C)_2SO \rightarrow H_3C + H_3CSO \tag{1.75}$$

while the slow channel would be

$$(H_3C)_2SO \rightarrow (H_3C)(H_2C)SOH \tag{1.76}$$

$$(H_3C)(H_2C)SOH \rightarrow H_3C + H_2CSOH. \tag{1.77}$$

Further support for this explanation is given by the consideration of the relative yields for the fully deuterated molecule. The review article by Schwarz on the mechanisms for unimolecular fragmentation reactions states that hydrogen migration is more likely to occur than deuterium migration [68]. This would mean that $(H_3C)_2SO$ would be more likely to rearrange than $(D_3C)_2SO$ and so the slow photofragment channel would

have a lower branching ratio in the deuterated molecule. It is rather surprising that Blank *et al.* did not take this into account with their paper [65].

An infrared laser study of dimethyl sulfoxide was performed by Gross *et al.* [41] and provided a different outlook on the photolysis as compared to the ArF excimer laser work. The use of a CO_2 laser allowed the authors to change the excitation wavelength and they found that the maximum dissociation occurred at the wavelength which was the closest to the maximum in the infrared absorption spectrum (1085.8 cm^{-1}). Although the use of the CO_2 laser only vibrationally excited the parent molecule, the formation of SO suggests that the authors were able to excite dimethyl sulfoxide to such a large extent that not just a single methyl group was lost, but both carbon-sulfur bonds were broken. Because Gross *et al.* used a static gas cell at a pressure of 0.24 Torr, it raises some doubts about their proposed mechanism for the generation of the SO species. At this pressure, collisions cannot be ignored and this would also explain why Gross *et al.* were not able to observe the intermediate H_3CSO species like the ultraviolet photofragmentation work [64, 65].

Chapter 2

Experimental Apparatus

This chapter will describe the apparatus used in this work. Since a detailed explanation will be covered in the subsequent sections, only a general outline will be given here. A schematic diagram of the apparatus built by our group is given in figures 2.1 and 2.2. A CO_2 laser was used to vibrationally excite a molecule in its electronic ground state to an energy level above the threshold of dissociation. A Nd:YAG laser was then used to ionize the fragments between the acceleration grids which caused the species to be accelerated towards the detector. A digital oscilloscope received the detector signal and performed the averaging of the signal traces (i.e. averaging the mass spectra). The averaged signal trace could then be downloaded to a microcomputer for storage and subsequent processing.

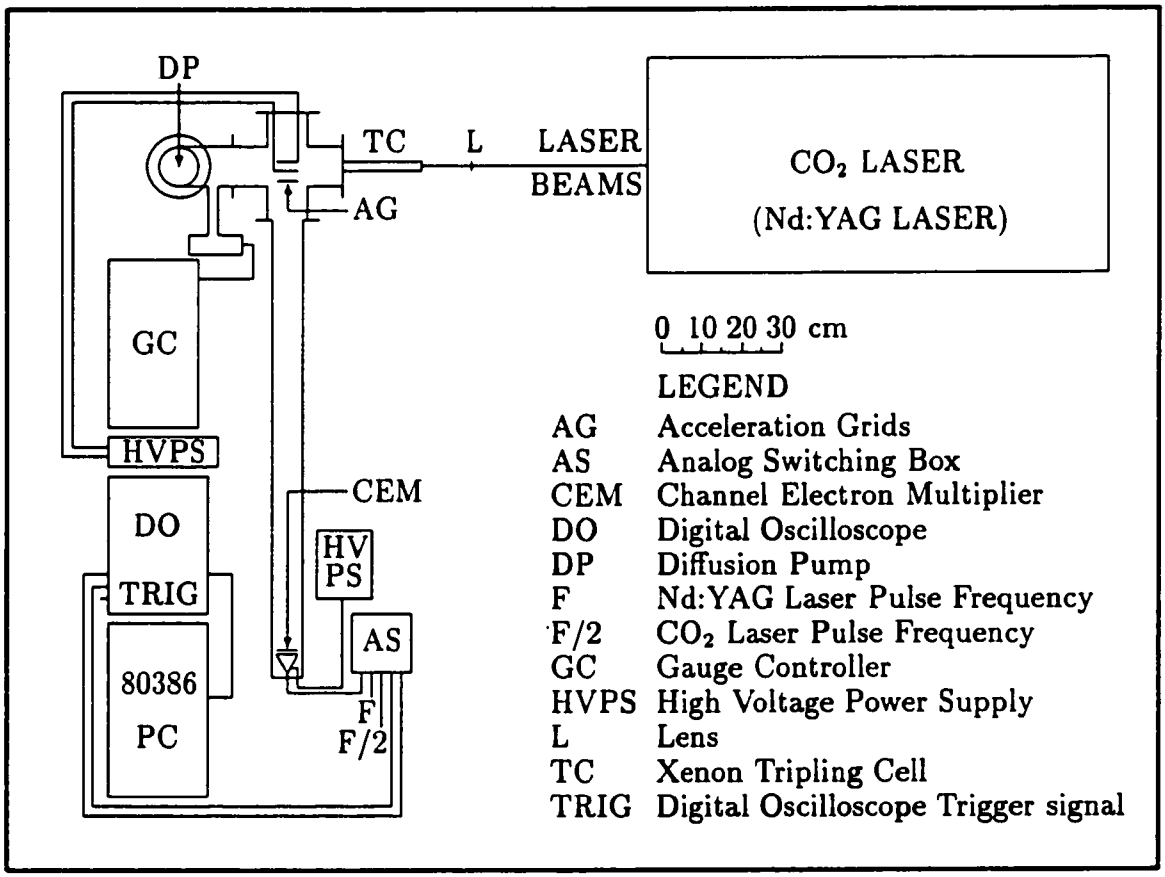

Figure 2.1: Schematic diagram representing the experimental apparatus as viewed from above. Note that the CO_2 laser is positioned on top of the Nd:YAG laser as illustrated in figure 2.2 on page 47.

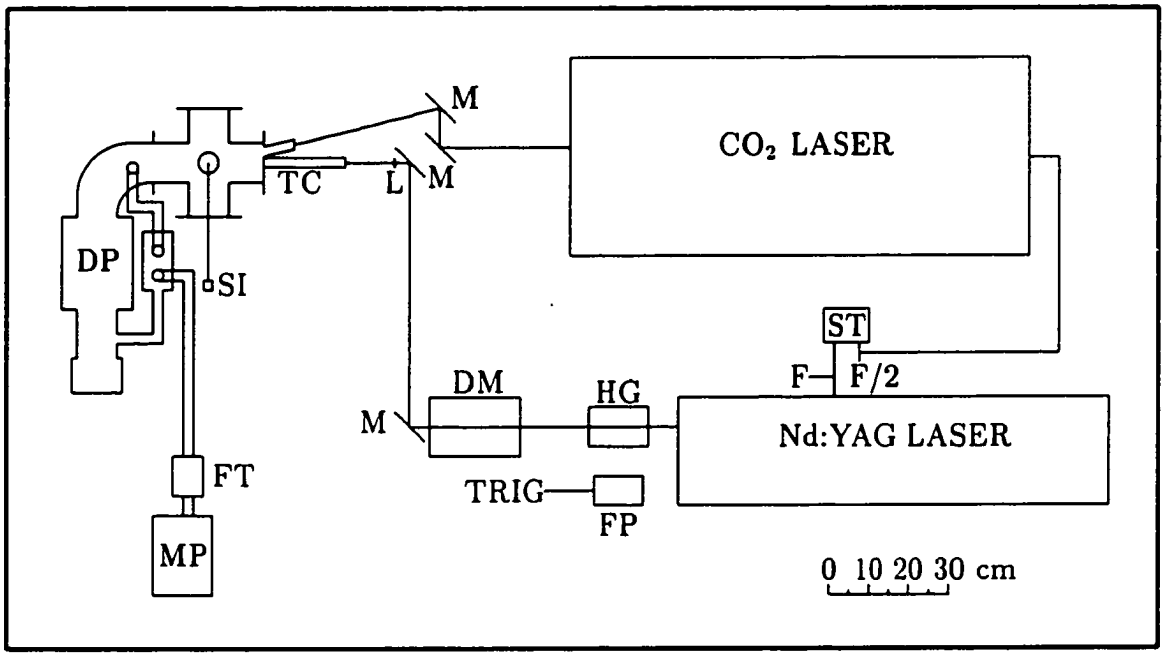

Figure 2.2: Schematic diagram representing the experimental apparatus as viewed from the side.

	LEGEND
DM	Dichroic Mirrors Box
DP	Diffusion Pump
F	Nd:YAG Laser Pulse Frequency
F/2	CO_2 Laser Pulse Frequency
FP	Fast Photodiode
FT	Foreline Trap
HG	Harmonic Generation Box
L	Lens
M	Mirror
MP	Mechanical Pump
SI	Sample Inlet
ST	Synchronization Trigger Box
TC	Xenon Tripling Cell
TRIG	Trigger for the Digital Oscilloscope

2.1 Time of Flight Vacuum Chamber

To study a unimolecular process, one needs to isolate a molecule from the rest of the system. An easy way of doing this is to work with the sample in the gas phase. One method utilizes a static cell which has a fixed number of sample molecules in a closed container. A disadvantage with using a static cell is that if highly reactive species are formed from a dissociation reaction, the products may recombine prior to being quantified.

Another method of working with gas phase molecules involves flowing the sample but this technique also has limitations and disadvantages. To have a flow of molecules it becomes necessary to pump out the system otherwise, once the system and the source are at the same pressure, a static arrangement develops. A simple method of flowing the sample involves an effusive source where the sample molecules effuse from an area of higher pressure (the source) to an area of lower pressure (the system).

The heart of the time of flight mass spectrometer chamber used in this work is a six-way cross tube with the ion acceleration grids in the centre. A 120 cm long ion flight tube is connected to one of the six arms. A Galileo model 4816 channeltron (also referred to as a channel electron multiplier or CEM) is located at the end of the ion flight tube usually at -2500 V from a Bertan model PMT-50A/N power supply connected to the front cone of the detector. A gain in the signal of greater than 10^7 was achieved for each initial ion and, typically, a single ion generated a 50 mV signal. The arm in the opposite direction of the six-way cross tube contains the electrical

feedthroughs and support rods for the ion acceleration grids. The acceleration is achieved by supplying a constant voltage to the back plate of the ionization region (2500 V) and a lower voltage to the first acceleration grid (2140 V) both from a Bertan model 365 high voltage power supply. The last acceleration grid was grounded so that the ions drift through the flight tube at the same velocity with which they left the second acceleration region.

Perpendicular to this axis for the flight tube and the acceleration grids are the two arms for the vacuum pumping system and the windows for the two laser beams. An Edwards mechanical pump (two stage model E2M5) with a maximum pumping speed of 113 litres per minute was used to lower the chamber pressure from atmosphere down to less than 0.05 Torr. Below this pressure pumping was then switched to an Edwards diffusion pump (model 100M) with a maximum pumping speed of 280 litres per second to lower the pressure down to approximately 9.0×10^{-7} Torr.

The CO_2 laser beam enters the chamber through a one inch diameter zinc selenide lens with a 20 cm focal length, located 20 cm from the centre of the six-way cross tube. The Nd:YAG laser beam enters the chamber from the xenon tripling cell and will be covered in the next section.

The sample molecules effuse into the system from a glass nozzle which is attached to the bottom arm of the six-way cross. The sample of methyl phenyl sulfoxide was purchased from the Aldrich Chemical Company while dimethyl sulfoxide, ethyl phenyl sulfoxide, *tert*-butyl methyl sulfoxide, *sec*-butyl methyl sulfoxide and *sec*-butyl

ethyl sulfoxide were obtained from Caledon Laboratories. All of the other molecules used for this work were prepared by Dr. W. Ingham. The individual samples were placed in a glass bulb located below the glass nozzle and were purified by repeated freeze-pump-thaw cycles to remove air and any other dissolved gases. A needlevalve provided control over the flow rate of the sample into the chamber. The needlevalve was opened to achieve a chamber pressure between 2 and 4×10^{-6} Torr as monitored with a Bayard-Alpert ionization gauge tube connected to a Granville-Phillips model 270 ionization gauge controller.

2.2 Photoionization of Molecules

For the sample to be accelerated toward the detector, the molecules must be ionized while they are between the back plate and the first acceleration grid. The 1064 nm Nd:YAG fundamental emits photons with an energy of 1.17 eV. Since this is well below the 10 eV required to ionize molecules, some method must be used to generate higher harmonics so that the molecules can be photoionized with a Nd:YAG laser. The Quanta-Ray GCR-3 Nd:YAG laser manufactured by Spectra-Physics was utilized in this work and this laser uses a potassium dideuterated phosphate (KD^*P) crystal to generate the second harmonic and then another KD^*P crystal to combine the fundamental and the second harmonic to generate the third harmonic.

The harmonic generation process described in the previous paragraph results in a beam which contains the 1064 nm fundamental, the 532 nm second harmonic and the

355 nm third harmonic and so some method of separating the wavelengths must be employed if only a single wavelength is desired. For this work, a pair of dichroic mirrors were used to separate the 355 nm third harmonic from the 1064 nm fundamental and 532 nm second harmonic. Another pair of dichroic mirrors (for the appropriate wavelength) can be used to separate the 532 nm second harmonic from the 1064 nm fundamental. In this manner, the three different wavelengths contained in the laser beam which leaves the harmonic generating box located at the front of the Nd:YAG laser can be separated and (effectively) isolated.

Although the 355 nm third harmonic corresponds to a 3.5 eV photon, this beam can only ionize molecules by either a multiphoton process or a multiple-photon absorption mechanism. A multiple-photon mechanism requires that the molecule can absorb a multiple number of single photons but this process cannot occur if the molecule does not absorb at 355 nm in the ultraviolet region of the electromagnetic spectrum. A multiphoton process does not have this problem but it does require a strong electric field which can be achieved by focusing a high powered laser beam.

Even though Nd:YAG lasers are becoming more common, the specifics for operation vary from one model to another so the performance of the Quanta-Ray GCR-3 Nd:YAG laser used for this work will be outlined in this paragraph. The Nd:YAG laser contains two Nd:YAG rods, one designated as the oscillator and the other as the amplifier. Each Nd:YAG rod can be separately excited with a pair of flash lamps located on either side of the Nd:YAG rod. A separate meter measures the amount

of energy discharged by the flash lamps on each laser pulse for both the oscillator and the amplifier. The Quanta-Ray GCR-3 Nd:YAG laser was operated at a 10 Hz repetition rate for all of the experiments presented in this work. The threshold for the laser to produce 1064 nm photons was a flash lamp setting of 28 J/pulse for the oscillator while the amplifier was off when the Nd:YAG laser was first installed. Since this threshold value is an indication of problems with the performance of the Nd:YAG laser, it was checked regularly and corrective actions were taken when the value increased above 30 J/pulse. The maximum energy produced by the oscillator for the 1064 nm fundamental was 371 mJ/pulse with the flash lamps set to 69 J/pulse. The maximum energy produced by the Nd:YAG laser increased to 925 mJ/pulse when the amplifier flash lamps were set to 65 J/pulse. The maximum energy for the 355 nm third harmonic was determined to be 319 mJ/pulse.

Although the Quanta-Ray GCR-3 Nd:YAG laser used for this work was powerful enough to multiphoton ionize the molecules with the third harmonic, a lower output energy could be used when the xenon gas cell was utilized to photoionize the sample. This had the added benefit of producing a mass spectrum with less noise than when the maximum energy was used. If the Nd:YAG laser output energy was decreased to the threshold level, the noise would decrease but, unfortunately, so would the ion signal. A flash lamp energy of 42 J/pulse for the oscillator while the amplifier was off, produced an output energy of approximately 10 mJ/pulse for the 355 nm third harmonic and generated photoionization mass spectra that had a strong ion signal

with few random ions that contribute to the background noise level.

In principle, the design of the xenon gas tripling cell should have been straight forward but because the cell was modified several times from the original design, a description of the final arrangement is in order. A mixture of argon and xenon (ratio of 430:1) in a static gas cell was determined to be quite effective at producing 118 nm (10.5 eV) photons from the 355 nm third harmonic [69]. Although using pure xenon is less efficient at generating the 10.5 eV photons, a gas cell with approximately 40 Torr of xenon was found to be adequate for this work and tremendously simplified the gas cell replenishing procedure. The 355 nm third harmonic was focused with a 15 cm focal length fused silica lens located 11 cm in front of the xenon gas cell. The xenon gas cell was made from a one inch diameter, 20 cm long glass tube. A one inch quartz window was epoxied (Master Bond EP21LV) to one end of the glass tube. The other end was sealed with an o-ring to a one inch diameter VUV magnesium fluoride plano-convex lens which, in turn, was sealed with an o-ring to the vacuum chamber at the flat surface of the lens. The diverging 118 nm beam passed through the 9.5 cm focal length MgF_2 lens and was focused towards the centre of the vacuum chamber.

2.3 Time of Flight Mass Spectrometer

The time of flight mass spectrometer used in this work, based on the two-stage system developed by W.C. Wiley and I.H. McLaren [6], will be outlined in this section. The ions are accelerated in two separate regions, the first region is the ionization region

and the second the acceleration region. The acceleration was achieved by supplying a positive voltage (2500 V) to the back plate of the ionization region and a smaller voltage (2140 V) to the grid between the ionization and acceleration regions. The voltage to the first acceleration grid was adjusted to minimize the time spread of ions due to the range of initial positions and velocities within the ionization region.

One difference between the apparatus described by Wiley and McLaren and the mass spectrometer used in this work is that the voltage to the back plate of the ionization region was not pulsed. Pulsing the voltage would ensure that all the ions start accelerating at the same time. However, the mass spectrometer used here ionized the sample with 118 nm photons generated in the xenon tripling cell and the narrow temporal profile of around 10 ns for the 118 nm beam of light resulted in a virtually simultaneous acceleration of the ions.

An advantage to using a time of flight mass spectrometer is that a complete mass spectrum was obtained in a few microseconds with each laser pulse. The apparatus used in this work recorded a mass spectrum up to 390 amu in 40 μs. The flight time of an ion travelling in the ionization region is given by

$$t_s = \sqrt{2m}\frac{s}{q(PV - GV)}\left(T_s^{1/2} \mp T_0^{1/2}\right) \tag{2.1}$$

where m is the mass of the ion, s is the length of the ionization region, PV is the voltage on the back plate of the ionization region, GV is the voltage on the grid between the ionization and acceleration regions, T_s is the kinetic energy of the ion

when it reaches the end of the ionization region and T_0 is the initial kinetic energy of the ion. The kinetic energy of the ion when it reaches the end of the ionization region is dependent upon the initial position of the ion in the region. The further the ion is from the end of the ionization region, the longer the time that the ion is accelerated. This results in ions starting further from the grid between the ionization and acceleration regions having a higher kinetic energy than ions starting closer to the grid. The plus and minus signs arise because the ions can either be accelerated in the same direction as the initial velocity or in the opposite direction. The minus sign refers to those ions initially moving towards the detector and the plus sign to the ions initially moving towards the back plate.

The time for the ion to travel through the acceleration region is

$$t_a = \sqrt{2m}\frac{a}{q(GV)}\left(T_a^{1/2} - T_s^{1/2}\right) \tag{2.2}$$

where a is the length of the acceleration region and T_a is the kinetic energy of the ion when it reaches the end of the acceleration region. Once the ions leave the acceleration region, they drift in a field free region so the voltage at the second grid must be the same as the voltage at the grid before the detector. For convenience, both grids are grounded (i.e. 0 V).

The time the ion takes to travel across the drift free region is just the length of

this region divided by the velocity of the ion. Thus,

$$t_d = d\sqrt{\frac{m}{2T_a}} \tag{2.3}$$

or

$$t_d = \sqrt{2m}\frac{d}{2T_a^{1/2}}. \tag{2.4}$$

The total flight time for the ion is the sum of the individual times through the three regions and so for an ion of mass m, this becomes

$$t_m = \sqrt{2m}\left[\frac{s}{q(PV-GV)}\left(T_s^{1/2} \mp T_0^{1/2}\right) + \frac{a}{q(GV)}\left(T_a^{1/2} - T_s^{1/2}\right) + \frac{d}{2T_a^{1/2}}\right]. \tag{2.5}$$

For distances measured in centimetres, kinetic energy in electron-volts and time in microseconds, a conversion factor of 1.018 is introduced to the expression for the flight time.

2.4 Vibrational Excitation of Molecules

Even though most of the material in this section can also be found elsewhere (references [70] and [71] to name just two), it is included here for completeness to explain the terminology used in dealing with the naming of the various CO_2 laser lines. The gaseous molecules studied in this work were vibrationally excited up to (and above)

the dissociation limit using a Lumonics series TEA-820 CO_2 laser. The gain medium is carbon dioxide gas mixed with nitrogen and helium. Excitation is achieved when a storage capacitor is discharged transversely across the gain medium. The discharged electron can collide with either a CO_2 or N_2 molecule as in the following chemical equations

$$e^- + CO_2(v_1=0, v_2=0, v_3=0) \rightarrow e^- + CO_2(0,0,n), \tag{2.6}$$

$$e^- + N_2(v=0) \rightarrow e^- + N_2(v=n) \tag{2.7}$$

where v_i refers to the number of quanta in the fundamental vibrational modes of CO_2 (illustrated in figure 2.3) and v is the number of quanta in the vibrational mode of N_2. For convenience, the v_i are omitted and the number of quanta in the vibrational modes are written down with the understanding that the numbers are listed in order.

Coincidentally, N_2 (v=n) and CO_2 (0,0,n) have almost the same amount of vibrational energy up to n=4 and a collision between a vibrationally excited N_2 molecule with an unexcited CO_2 molecule results in a transfer of vibrational energy as shown in the following reaction

$$N_2(v=n) + CO_2(0,0,0) \rightarrow N_2(v=0) + CO_2(0,0,n). \tag{2.8}$$

Because of this near degeneracy, regardless of which molecule (N_2 or CO_2) was vibrationally excited by the electron, the end result is CO_2 (0,0,n). A collision with a

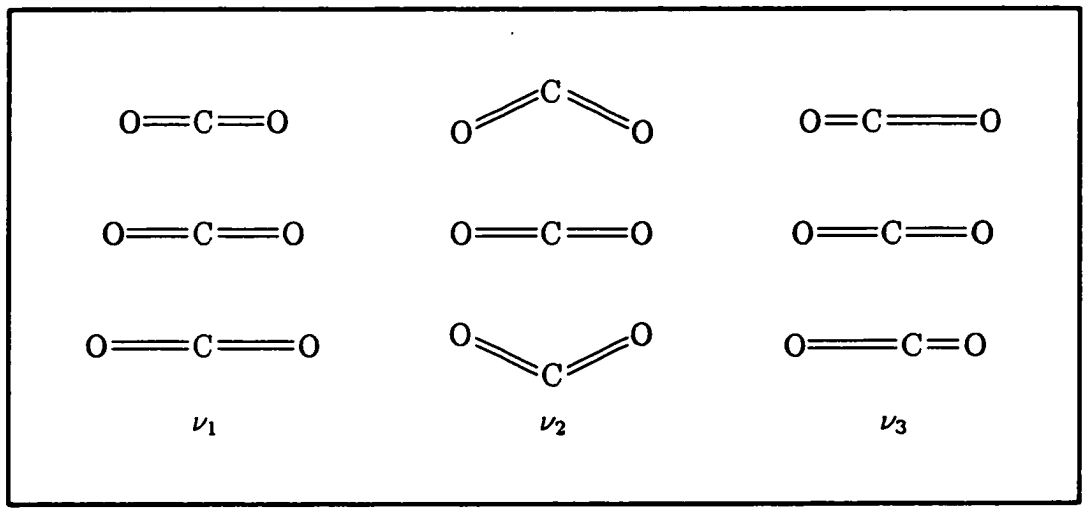

Figure 2.3: The vibrational modes of CO_2. The ν_1 mode is the symmetric stretch, ν_2 the bending mode and ν_3 is the asymmetric stretch. There is another bending mode orthogonal to the one shown which goes out of the plane of the page.

ground state CO_2 molecule as described by the following reaction

$$CO_2(0,0,n) + CO_2(0,0,0) \rightarrow CO_2(0,0,n-1) + CO_2(0,0,1) \qquad (2.9)$$

results in the rapid relaxation of the CO_2 molecules to CO_2 (001).

Figure 2.4 illustrates the relative energy levels of several vibrational states of CO_2. In this diagram, only the major laser transitions have been shown. A superscript has been introduced to describe the quantum state corresponding to the excitation of the ν_2 bending mode. Recall that the CO_2 molecule can bend in two orthogonal directions. Consequently, when quanta are added to the bending mode, the two orthogonal directions can combine to give an angular momentum term. This superscript to the

ν_2 quantum number describes the angular momentum of the two orthogonal bending modes.

The major laser transitions are given by the following equations

$$CO_2(00^01) \rightarrow CO_2(02^00) + h\nu_9 \tag{2.10}$$

for the 9 μm transition and

$$CO_2(00^01) \rightarrow CO_2(10^00) + h\nu_{10} \tag{2.11}$$

for the 10 μm transition. One relaxation pathway for CO_2 (10^00) is to CO_2 (02^00) which occurs since these two states are effectively coupled because the bending vibration induces a symmetric stretching in the molecule [71]. Another pathway for removing the ν_1 vibrational energy is

$$CO_2(10^00) + CO_2(00^00) \rightarrow CO_2(01^10) + CO_2(01^10) + \Delta E' \tag{2.12}$$

and collisions also convert CO_2 (02^00) by the following equation

$$CO_2(02^00) + CO_2(00^00) \rightarrow CO_2(01^10) + CO_2(01^10) + \Delta E''. \tag{2.13}$$

By introducing helium atoms, collisions with CO_2 (01^10) effectively transfer energy to the helium atoms and return the CO_2 molecule to the ground state.

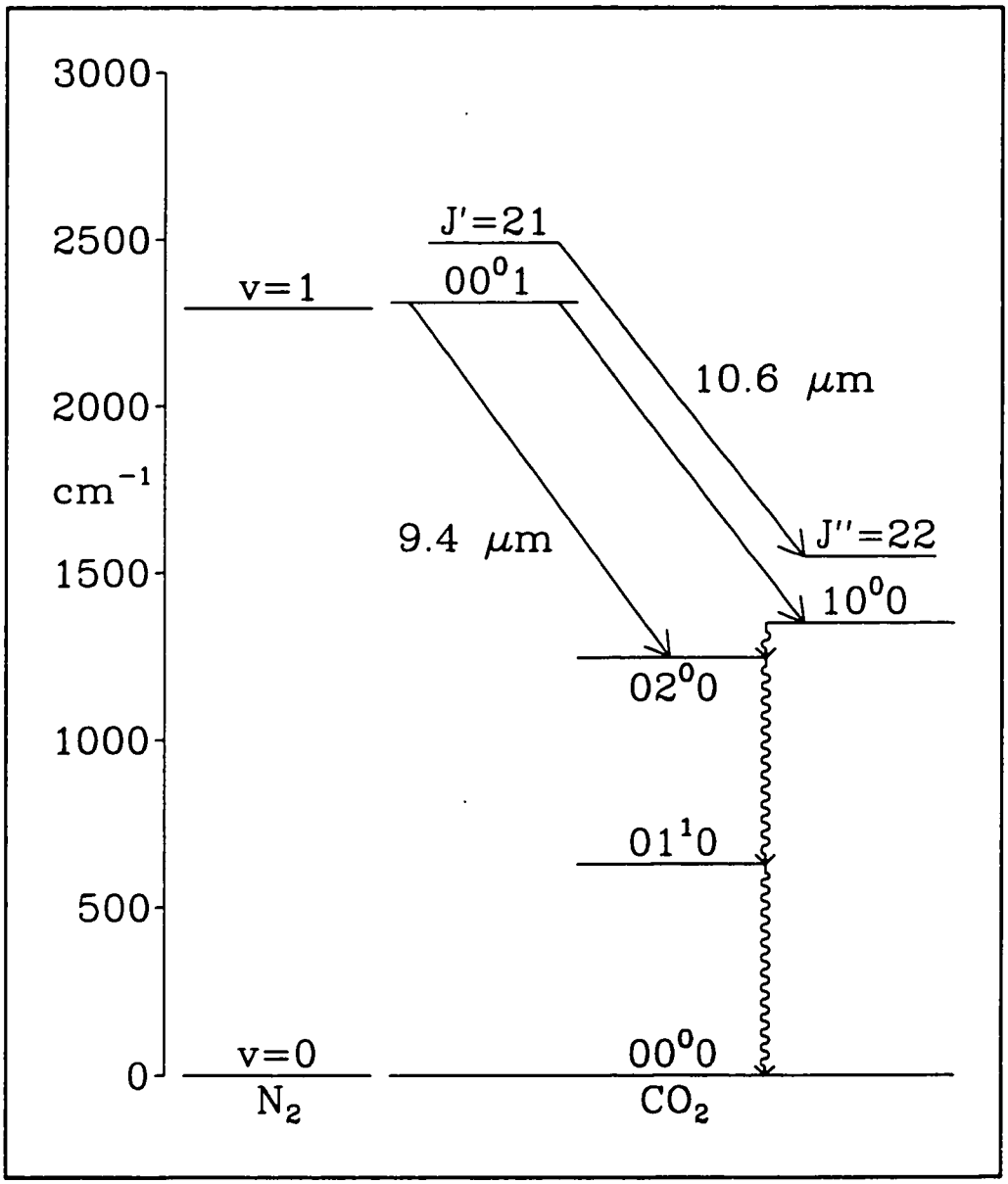

Figure 2.4: The pertinent energy levels for the CO_2 laser. The radiative laser transitions are shown by diagonal arrows. See text for details on how the CO_2 (00^01) level becomes populated.

Because both laser transitions originate from the same state, the transition that is more likely to occur is the one that tends to dominate. Consequently, usually the CO_2 $(00^01) \rightarrow CO_2$ (10^00) transition only occurs. However, another transition can be selected by introducing a device which prevents unwanted transitions from being amplified in the laser cavity. The Lumonics series TEA-820 CO_2 laser achieves this selection by replacing the back reflecting mirror with a diffraction grating.

So far only transitions from one vibrational level to another have been considered, however, this description is not complete. In addition to the vibrational transitions, rotational transitions can also occur. The CO_2 (00^01) state is asymmetric and so only the rotational levels with odd values of the rotational quantum number J are populated whereas both CO_2 (10^00) and CO_2 (02^00) are symmetric and only have even rotational levels populated. Because the spacing between rotational levels is smaller than k_BT, several levels are populated and the laser transitions also need to specify the rotational level at the end of the transition and whether the molecule has come from a lower rotational level ($\Delta J = -1$) or from a higher level ($\Delta J = +1$). $\Delta J = +1$ transitions give rise to the R-branch and $\Delta J = -1$ transitions as the P-branch. Putting everything together, the shorthand notation 10P22 can be introduced to describe the photon originating from the following laser transition

$$CO_2(00^01, J' = 21) \rightarrow CO_2(10^00, J'' = 22) + h\nu_{10} \qquad (2.14)$$

where the prefix indicates the vibrational transition (the 10 μm transition or the 9

μm transition), either an "R" or a "P" to indicate $\Delta J = +1$ or $\Delta J = -1$ and then a numerical suffix indicating the rotational level of the lower state. 9R32 would refer to the following transition

$$CO_2(00^01, J' = 33) \rightarrow CO_2(02^00, J'' = 32) + h\nu_9 \tag{2.15}$$

and

$$CO_2(00^01, J' = 33) \rightarrow CO_2(02^00, J'' = 34) + h\nu_9 \tag{2.16}$$

is the transition for the 9P34 CO_2 laser line.

The Lumonics series TEA-820 CO_2 laser can be operated at a variety of different settings to control the output power of the laser. The gas regulators for the three components of the gain medium (CO_2, N_2 and He) were all set to 10 psig. The flow rate for CO_2 was set to a value of 7 on a Brooks 3.65B model flowmeter built into the CO_2 laser and corresponds to an approximate flow rate of 8 ft^3/hr (3.8 L/min). A setting of 3 on a Brooks 2.65B model flowmeter for N_2 correlates to a flow rate of 4 ft^3/hr (1.9 L/min). The helium atoms had a flow rate of approximately 40 ft^3/hr (19 L/min) through the laser cavity as indicated by the Brooks 4.65B model flowmeter setting of 12. The Lumonics series TEA-820 CO_2 laser also uses extra dry air for the spark gap assembly which is involved in generating the discharged electron. The regulator for the extra dry air was set to 16 psig to prevent erratic behaviour of the

spark gap and the gas flow rate had an approximate setting of 24 on a Brooks 4.65B model flowmeter (approximately 60 ft^3/hr or 28 L/min).

The other major parameter for the Lumonics series TEA-820 CO_2 laser is the high voltage to the charging capacitor which controls the output power of the laser. For this work, the output power of the CO_2 laser was measured with a Scientech model MC2500 meter set to display the average power rather than the cumulative energy output. For the wavelength dependent measurements in chapter 3, the voltage was adjusted to achieve an output power of 1.0 W. For the power dependent measurements, the voltage was set to the maximum of 40 kV and the output power of the CO_2 laser was decreased by placing sodium chloride window flats in the path of the laser beam. The largest attenuation occurred with the flats that had the most humidity damage to the surfaces of the windows.

The CO_2 laser was used to generate photofragments while the Nd:YAG laser photoionized the fragments but because both of these are pulsed lasers, it was necessary to synchronize the two lasers. Both lasers provide synchronization output pulses and can be triggered externally so one laser could be used to trigger the other laser. In order to improve the signal to noise of the mass spectra, signal averaging was performed with the LeCroy 9450 digital oscilloscope. Unfortunately, during the long data acquisition time of the signal averaging process (up to around half an hour), the sample pressure may drift which would result in a slight change in the molecular density for the second set of signal averaged mass spectra. To overcome this problem, the CO_2

laser was triggered on alternating Nd:YAG laser pulses. In this way, alternating mass spectra would involve the CO_2 laser to possibly photofragment the sample molecules.

The Nd:YAG laser provides a 2.2 V [72] pulse for synchronizing with the flash lamps but this falls short of the 2.5 V required to trigger the CO_2 laser [73]. The analog Nd:YAG laser flash lamp synchronization pulse was converted to a binary signal and every second pulse was used to generate a trigger pulse for the CO_2 laser. This half frequency digitized pulse (designated as F/2 in figures 2.1 and 2.2) was also used with the full frequency pulse (F) as inputs for the analog switching box.

As previously mentioned, the time of flight mass spectrometer used for this work produces a mass spectrum in 40 μs which can be captured by the LeCroy 9450 digital oscilloscope. However, alternating mass spectra correspond to first just photoionizing the sample and then both photofragmenting and photoionization. The analog switching box separates the alternating mass spectra into two output traces. This was done by sending the current mass spectrum as an output for one trace while the other analog signal output trace was set to ground. The digitized full frequency pulse from the synchronization trigger box switches the mass spectrum from one output trace to the other output trace while the output trace that does not correspond to the mass spectrum was set to ground. In this fashion, the LeCroy 9450 digital oscilloscope was able to signal average two separate sets of mass spectra, one corresponding to only photoionizing the molecules and another one when the sample was photofragmented and photoionized. A total of one thousand traces were signal averaged for each output

trace, 500 mass spectra and 500 ground signal traces. The resultant averaged traces were downloaded to an 80386 microcomputer for permanent storage and subsequent processing.

2.5 Mass Spectra Post-Processing

In order to further improve the signal to noise of the mass spectra, four sets of data files were recorded for each pair of mass spectra (eight in total). The four data files were averaged to produce a single mass spectrum. The ion signal intensity was converted from millivolts to counts because this value was required for the determination of the error bars associated with the ion signal. It was observed that a single ion generated an ion signal of approximately 50 mV and so the averaged signal intensity was divided by this number and then multiplied by one thousand (corresponding to the total number of traces that the LeCroy 9450 digital oscilloscope would have averaged for) to get an approximate number of ion counts at a specific flight time.

Since an ion of a certain mass could arrive at the detector over a small range of flight times, the true ion count must include the counts for this whole range. For simplicity, the range for mass m was taken to be the time half-way between the time for mass $m-1$ and mass m to the time half-way between mass m and mass $m+1$.

First consider the range endpoint. The time difference is

$$t_{m+1} - t_m = \left[\frac{t_{m+1}}{t_m} - 1\right] t_m. \tag{2.17}$$

From equation 2.5 on page 56, the flight time is proportional to the square root of the mass so the ratio of the flight time of the two different masses is just the ratio of the square root of the masses. Thus, the time difference becomes

$$\begin{aligned} t_{m+1} - t_m &= \left[\left(\frac{m+1}{m}\right)^{1/2} - 1\right] t_m & (2.18)\\ &= \left[\left(1 + \frac{1}{m}\right)^{1/2} - 1\right] t_m. & (2.19) \end{aligned}$$

The binomial series expansion for $(1 + x)^{1/2}$ yields

$$\begin{aligned} t_{m+1} - t_m &= \left[1 + \frac{1}{2m} - \frac{1}{8m^2} + \cdots - 1\right] t_m & (2.20)\\ &\approx \frac{t_m}{2m}. & (2.21) \end{aligned}$$

One half of the time difference is $t_m/4m$. Although the series expansion is only valid for large masses, it was observed that this approximation was adequate for a mass of 6 amu because the time range did not overlap with the range for 5 amu.

The simplified picture described in the previous paragraph is valid only when the separate masses are clearly resolved. Unfortunately, our apparatus could only clearly resolve successive masses up to 45 amu. For a single fragmentation species above this

mass, the total area was partitioned according to the relative intensities of the corresponding higher isotope mass ions. When two fragmentation species had adjacent masses, the total area was de-convoluted by fitting the appropriate region of the time of flight mass spectrum to two curves that had the same lineshape as the resolved masses. The area for each fragmentation species was then partitioned according to the relative intensities of the corresponding higher isotope mass ions. Because of the uncertainty of the intensities from the de-convolution procedure, fragmentation species that were unresolved in the time of flight mass spectra were generally avoided in the discussion of the experimental results. The lone exception was for the butene, butyl and butane ions from *sec*-butyl methyl sulfoxide which were included because it was incorrectly believed that the species were resolved.

Although examining the various mass spectra does provide some useful information, it was more beneficial to be able to compare the different mass spectra in some manner. It was assumed that the signal intensity of the parent molecular ion in the photoionization mass spectrum was an indication of the sample pressure at the time the mass spectra were recorded. Minor fluctuations in the pressure could be accounted for by normalizing the intensities in the photoionization and photofragmentation / photoionization mass spectra to the counts for the parent molecular ion in the photoionization mass spectrum. All of the stick mass spectra in the photofragmentation / photoionization experiments in chapter 3 have been normalized to the intensity of the parent molecular ion in the corresponding photoionization mass spectrum.

Chapter 3

Experimental Results

The main objective of the present work was to study the infrared multiple-photon dissociation of some small organic sulfoxide molecules. Before presenting these results, it is necessary to explain why only three molecules were investigated with the CO_2 laser. This is done in the first section dealing with the mass spectra of seven small organic sulfoxide molecules. The infrared multiple-photon dissociation study of the suitable sulfoxide molecules (dimethyl sulfoxide, methyl phenyl sulfoxide and *sec*-butyl methyl sulfoxide) is divided into two subsections to represent the two aspects of the investigation. First, the CO_2 laser photolysis wavelength was varied to determine which laser line would generate the most fragmentation for a certain output power. Next, the output power was varied at this CO_2 laser line. It should be pointed out that not all of the experimental mass spectra were presented in this chapter, only a representative sample has been selected and discussed.

3.1 Electron Impact Ionization and Photoionization Mass Spectra

Ideally, the mass spectrum of a molecular ion should be independent of the method of ionization. Whether sufficient energy to ionize the molecule is transferred from an energized electron or is the result of the absorption of a photon of light, the final result is the same: a molecule with enough internal energy to lose an electron.

The more energy absorbed by the molecule, the greater the number of different pathways that could be followed which corresponds to an increase in the number of fragmentation channels available to the energetically excited molecule. To minimize the fragmentation, one needs to minimize the energy absorbed by the molecule. With electron impact ionization, this is achieved by lowering the kinetic energy of the electron so that the collision with the electron transfers less energy to the molecule. With photoionization, increasing the wavelength of the light decreases the energy of a photon.

Electron impact ionization typically involves utilizing 70 eV electrons which is enough energy to remove an electron from most orbitals in the molecule. In addition to ionization, extensive fragmentation can also occur as the excess energy can be used to break some bonds in the molecule. This results in a somewhat complicated mass spectrum when one uses 70 eV electron impact ionization.

In principle, one could use a variable wavelength source to tune the frequency of

the light such that the molecule is ionized but not fragmented. In practice, however, a fixed wavelength is usually utilized. The drawback to this approach is that not all molecules have the same first ionization potential. A molecule with a lower ionization potential will have more excess energy available for fragmentation than another molecule which has an ionization potential closer to the energy of the photon.

3.1.1 Dimethyl Sulfoxide

The 70 eV electron impact and 10.5 eV photoionization mass spectra of dimethyl sulfoxide are presented in figure 3.1 on page 71. The photoionization time of flight mass spectrum was obtained at a sample pressure of 3.1×10^{-6} Torr. The spectra have been normalized to the intensity of the dimethyl sulfoxide peak. The bottom spectrum is the photoionization time of flight mass spectrum where the abscissa has been transformed from flight time to mass. The middle spectrum is the corresponding stick spectrum for the photoionization time of flight mass spectrum. The top spectrum is the electron impact ionization mass spectrum.

It is quite clear that the electron impact mass spectrum contains more fragmentation species than the photoionization mass spectrum. In particular, the species at 63 amu has almost the same intensity as the parent ion. Bowie *et al.* identify this peak as occurring from the loss of a $[CH_3]^\bullet$ group from the parent with supporting evidence by the presence of the appropriate metastable peak [45]. The further loss of H_2O from 63 amu results in the peak at 45 amu. The loss of an OH group from the

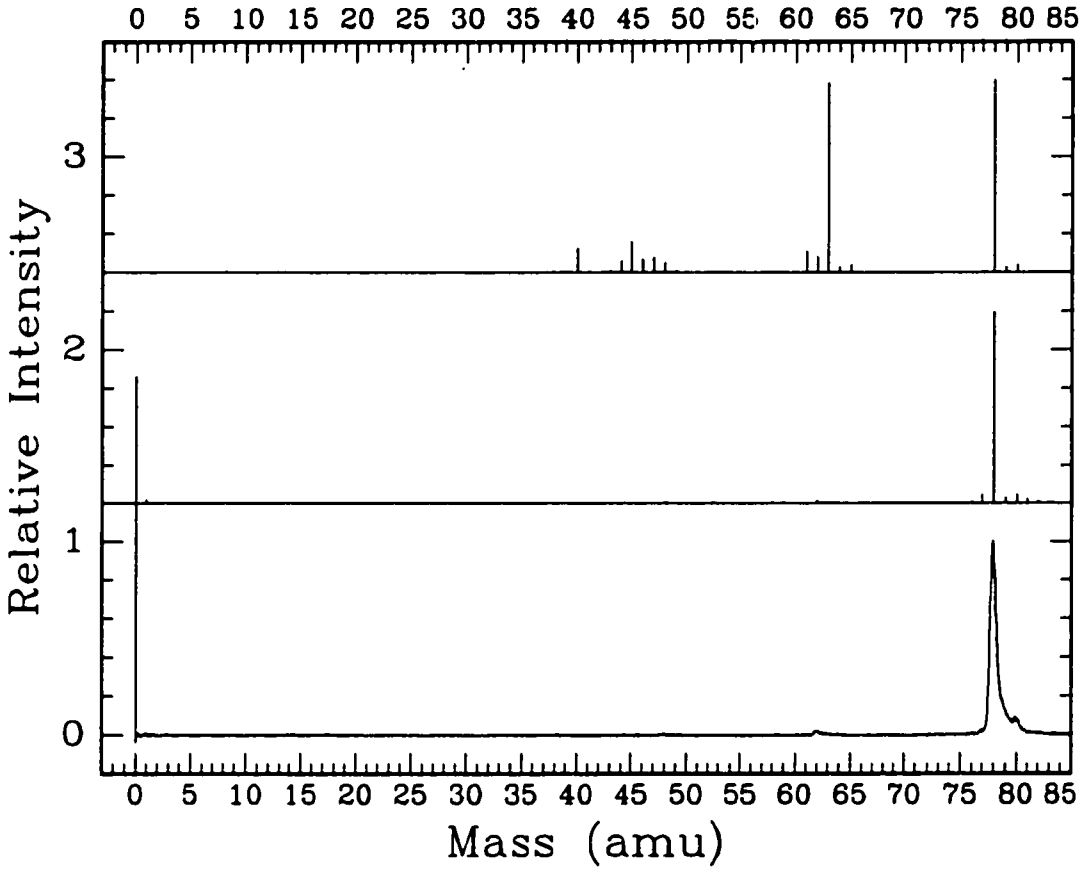

Figure 3.1: The photoionization and electron impact mass spectra of dimethyl sulfoxide. The bottom spectrum is the time of flight mass spectrum (converted from flight time to mass) up to 85 amu recorded at 3.1×10^{-6} Torr. The middle spectrum is a stick spectrum generated from the time of flight mass spectrum by integrating the area corresponding to each mass. The top spectrum is an electron impact mass spectrum obtained with an electron energy of 70 eV. The various spectra have been separately normalized to the intensity of the parent molecular ion at 78 amu.

parent results in a peak at 61 amu.

The peak at 40 amu does not appear in the electron impact mass spectrum of dimethyl sulfoxide presented by Bowie *et al.* [45]. The identity of this peak is a mystery because the presence of a sulfur atom seems unlikely since the necessary eight hydrogen atoms are not present in the parent molecule and so the only remaining candidate is one with the molecular formula given by $[C_2O]^{+\bullet}$.

One minor peak in the electron impact mass spectrum which should be mentioned occurs at 47 amu. This species has a molecular formula given by $[H_3CS]^+$. Amos *et al.* also observed the 47 amu species as well as a minor peak at 31 amu which would suggest that the complementary pair (H_3CS and OCH_3) occur after the migration of a methyl group to the oxygen atom followed by cleavage of the sulfur-oxygen bond [47]. This cleavage will generate one ion and one radical so either $[H_3CS]^+$ and $[OCH_3]^\bullet$ or $[H_3CS]^\bullet$ and $[OCH_3]^+$ will be formed.

A comparison of the electron impact mass spectrum of dimethyl sulfoxide (top spectrum) with the photoionization mass spectrum (bottom or middle spectrum) in figure 3.1 clearly shows that virtually no fragmentation of the parent molecular ion was observed in the photoionization mass spectrum. The only fragmentation species that exhibited any significant intensity occurred at 62 amu. With this species being 16 amu below the mass of dimethyl sulfoxide, this corresponds to either the loss of an oxygen atom from the parent ion or the loss of methane (more likely as a hydrogen atom and a methyl group). The photofragment translational spectroscopy

work performed by Zhao *et al.* did not observe the formation of any oxygen atoms [64] and the species with mass equal to 62 amu was attributed to the loss of a methyl group and a hydrogen atom from dimethyl sulfoxide.

3.1.2 Diethyl Sulfoxide

The most striking feature in the mass spectra of diethyl sulfoxide (figure 3.2 on page 74) is the low signal-to-noise in the photoionization time of flight mass spectrum (bottom of the figure). One contributing factor is the low volatility of diethyl sulfoxide as indicated by the lower sample pressure (2.1×10^{-6} Torr) despite the sample inlet valve being open the same amount as for the other molecules. The sample pressure for methyl phenyl sulfoxide was only 0.6×10^{-6} Torr and the photoionization mass spectrum in figure 3.3 on page 76 has a much better signal-to-noise ratio than was observed with diethyl sulfoxide. Thus, the performance of the time of flight mass spectrometer on the day that the diethyl sulfoxide spectra were collected must have been far from ideal.

Regardless of these problems, the main points worth noting about the mass spectra of diethyl sulfoxide are still valid. Several fragmentation species were observed at an abundance which exceeded the background level in both the electron impact (top spectrum) and the photoionization mass spectra (bottom). One peak of interest occurred at 78 amu and has the same molecular formula as dimethyl sulfoxide.

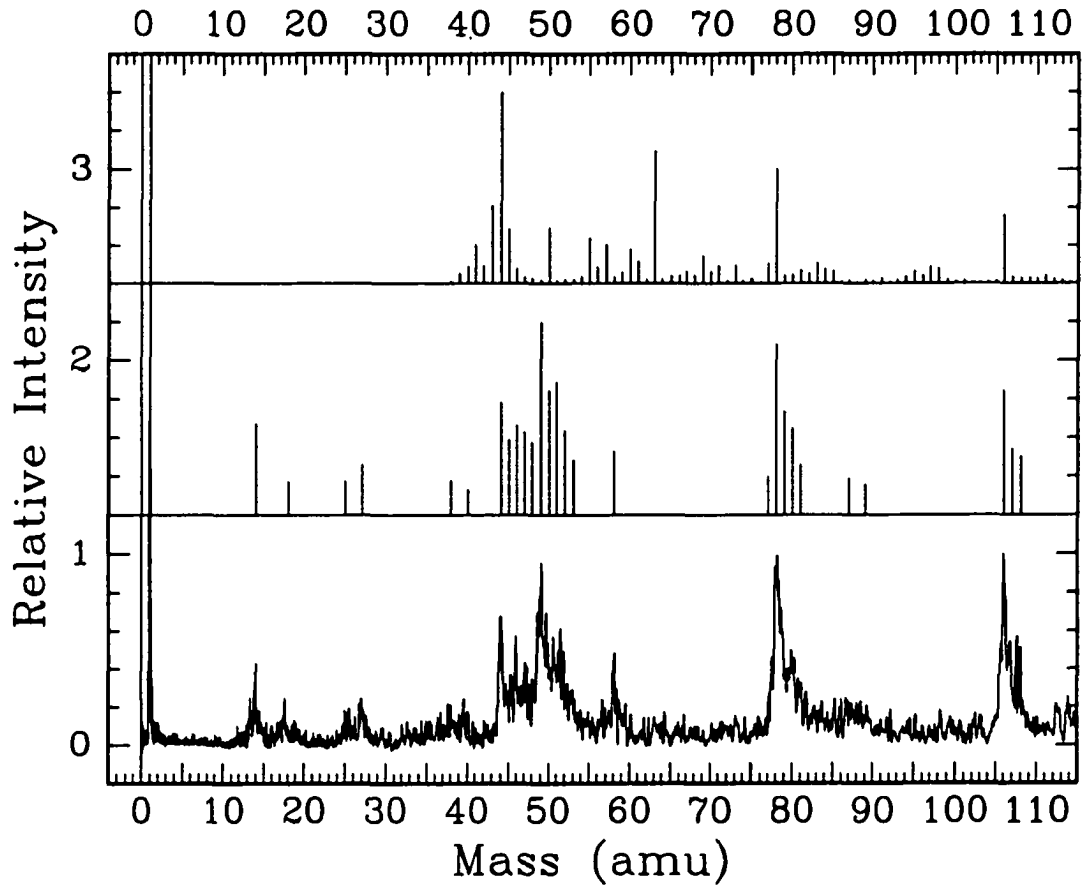

Figure 3.2: The photoionization and electron impact mass spectra of diethyl sulfoxide. The bottom spectrum is the time of flight mass spectrum (converted from flight time to mass) up to 115 amu recorded at 2.1×10^{-6} Torr. The middle spectrum is a stick spectrum generated from the time of flight mass spectrum by integrating the area corresponding to each mass. The top spectrum is an electron impact mass spectrum obtained with an electron energy of 70 eV. The various spectra have been separately normalized to the abundance of the most intense peak in the spectrum.

3.1.3 Methyl Phenyl Sulfoxide

The electron impact mass spectrum of methyl phenyl sulfoxide exhibits more fragmentation than the photoionization mass spectrum (figure 3.3 on page 76). The peak at 125 amu corresponds to the loss of a methyl group while the peak at 77 amu was attributed to a phenyl ion which has broken away from the parent molecular ion.

An interesting feature of the electron impact mass spectrum was the presence of the additional peaks which correspond to extensive rearrangements in the energized molecular ion. In particular, the peak at 97 amu was identified by Bowie *et al.* as having the molecular formula $[C_5H_5S]^+$ [45]. The presence of a metastable peak at the appropriate mass indicates that the $[C_5H_5S]^+$ species originated as $[C_6H_5SO]^+$ but then lost CO. Another peak observed by Bowie *et al.* was at 51 amu which also appeared in the electron impact mass spectrum in figure 3.3 and the mass corresponds to a molecular formula given by $[C_4H_3]^+$. The two peaks at 44 amu ($[CS]^{+\bullet}$) and 40 amu ($[C_3H_4]^{+\bullet}$) do not appear in the electron impact mass spectrum of Bowie *et al.* [45].

The photoionization time of flight mass spectrum of methyl phenyl sulfoxide contained fewer fragmentation species than the electron impact mass spectrum. The peak at 124 amu in the photoionization mass spectrum is 16 amu below the mass of the parent molecular ion. Although the loss of a methyl group is not surprising, the additional loss of a hydrogen atom was somewhat unexpected because the phenyl group is believed to be fairly stable.

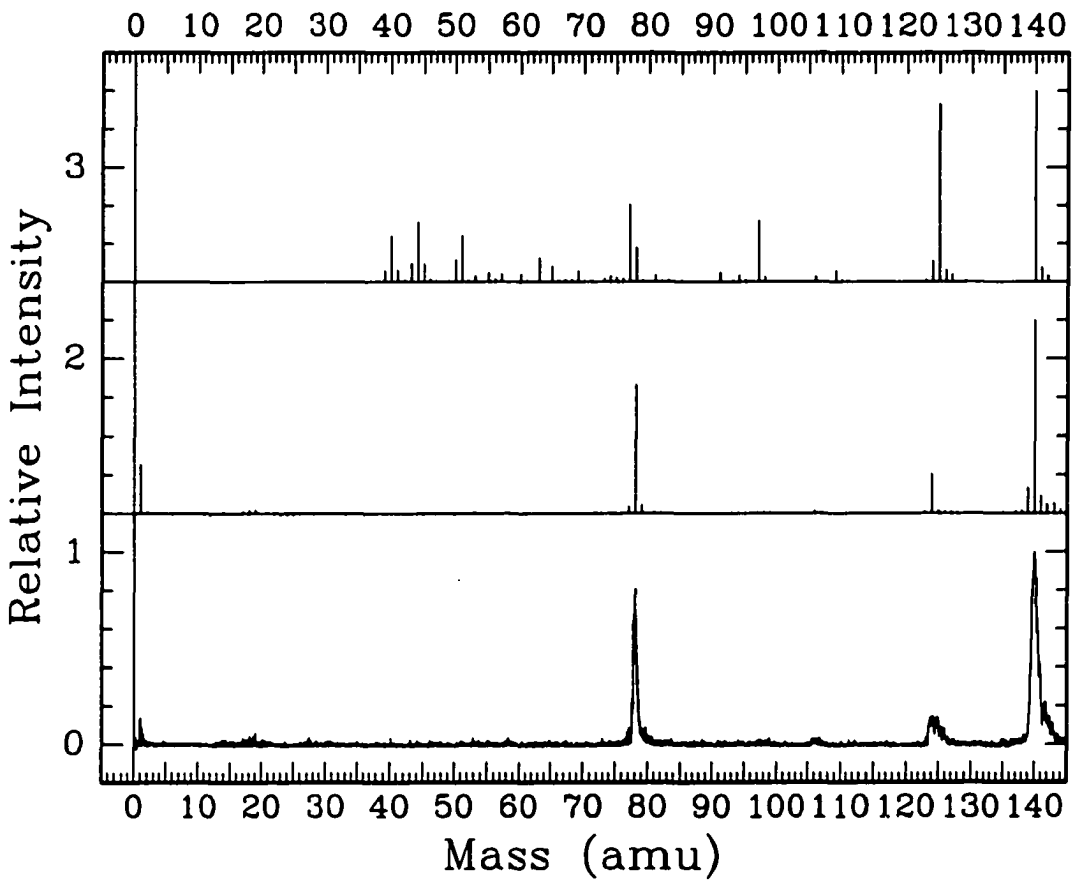

Figure 3.3: The photoionization and electron impact mass spectra of methyl phenyl sulfoxide. The bottom spectrum is the time of flight mass spectrum (converted from flight time to mass) up to 145 amu recorded at 0.6×10^{-6} Torr. The middle spectrum is a stick spectrum generated from the time of flight mass spectrum by integrating the area corresponding to each mass. The top spectrum is an electron impact mass spectrum obtained with an electron energy of 70 eV. The various spectra have been separately normalized to the intensity of the parent molecular ion at 140 amu.

Another unexpected feature of the photoionization mass spectrum was the rather intense peak at 78 amu. This mass corresponds to both $[C_6H_6]^{+\bullet}$ and $[C_2H_6SO]^{+\bullet}$ and so could be an impurity in the methyl phenyl sulfoxide sample. A proton NMR spectrum determined that the only impurity present in the methyl phenyl sulfoxide sample was H_2O, and so the sample was not contaminated with some dimethyl sulfoxide. The formation of C_2H_6SO seems unlikely from a single methyl phenyl sulfoxide molecule because of the extensive rearrangements necessary to form the second methyl group. A more likely explanation seems to involve the migration of a hydrogen atom from the methyl group to the phenyl group and cleavage to form the $[C_6H_6]^{+\bullet}$ species.

3.1.4 Ethyl Phenyl Sulfoxide

The electron impact mass spectrum of ethyl phenyl sulfoxide shows extensive fragmentation and some anomalous features. The intense peak at 78 amu in the mass spectra of ethyl phenyl sulfoxide presented in figure 3.4 on page 78 raised a question concerning the purity of the ethyl phenyl sulfoxide sample. The second largest peak in the electron impact mass spectrum occurred at 126 amu which can be accounted for by the loss of CO from the parent molecular ion. The peaks at 97 amu and 51 amu also occur in the electron impact mass spectrum of methyl phenyl sulfoxide. Somewhat surprising was the presence of the two peaks at 45 amu and 39 amu because, although these two species do not appear in the electron impact mass spectrum of

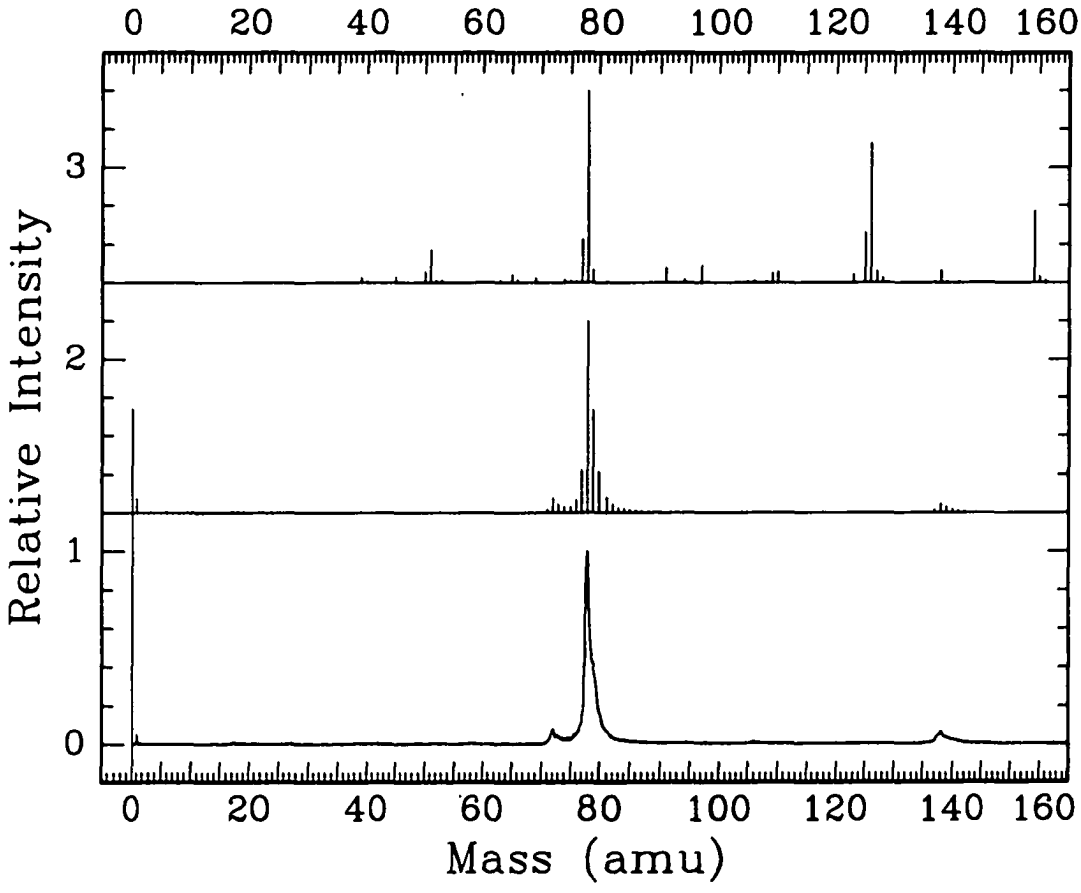

Figure 3.4: The photoionization and electron impact mass spectra of ethyl phenyl sulfoxide. The bottom spectrum is the time of flight mass spectrum (converted from flight time to mass) up to 160 amu recorded at 2.9×10^{-6} Torr. The middle spectrum is a stick spectrum generated from the time of flight mass spectrum by integrating the area corresponding to each mass. The top spectrum is an electron impact mass spectrum obtained with an electron energy of 70 eV. The various spectra have been separately normalized to the intensity of the ion at 78 amu.

methyl phenyl sulfoxide in figure 3.3 on page 76, they do appear in the mass spectrum of methyl phenyl sulfoxide reported by Bowie *et al.* [45].

Although the mass spectrum obtained by photoionizing the sample shows fewer fragmentation species than the electron impact mass spectrum, the photoionization mass spectrum does not have a peak at the mass of the parent molecular ion (154 amu). Besides the intense peak at 78 amu, two minor peaks were observed at 72 amu and at 138 amu. The first of this pair could have a molecular formula given by $[C_3H_4S]^{+\bullet}$ while the second species is the familiar loss of a methyl group and a hydrogen atom from the parent molecular ion.

3.1.5 *tert*-Butyl Methyl Sulfoxide

The electron impact mass spectrum of *tert*-butyl methyl sulfoxide in figure 3.5 on page 80 exhibited several fragmentation species. The electron impact mass spectrum had a rather intense peak at 41 amu which correlates to a molecular formula given by $[C_3H_5]^{+}$. The peak at 64 amu corresponds to a hydrogen migration to the sulfoxide group and a loss of the rest of the butyl group (i.e. loss of butene). The minor peak at 78 amu is $[C_2H_6SO]^{+\bullet}$ which arose by methyl migration from the butyl group to the sulfoxide group with a loss of the remaining C_3H_6 fragment.

The photoionization time of flight mass spectra of *tert*-butyl methyl sulfoxide presented in figure 3.5 was recorded at 4.5×10^{-6} Torr and shows very little fragmentation other than the generation of the butyl ion. In addition to the strong butyl ion peak

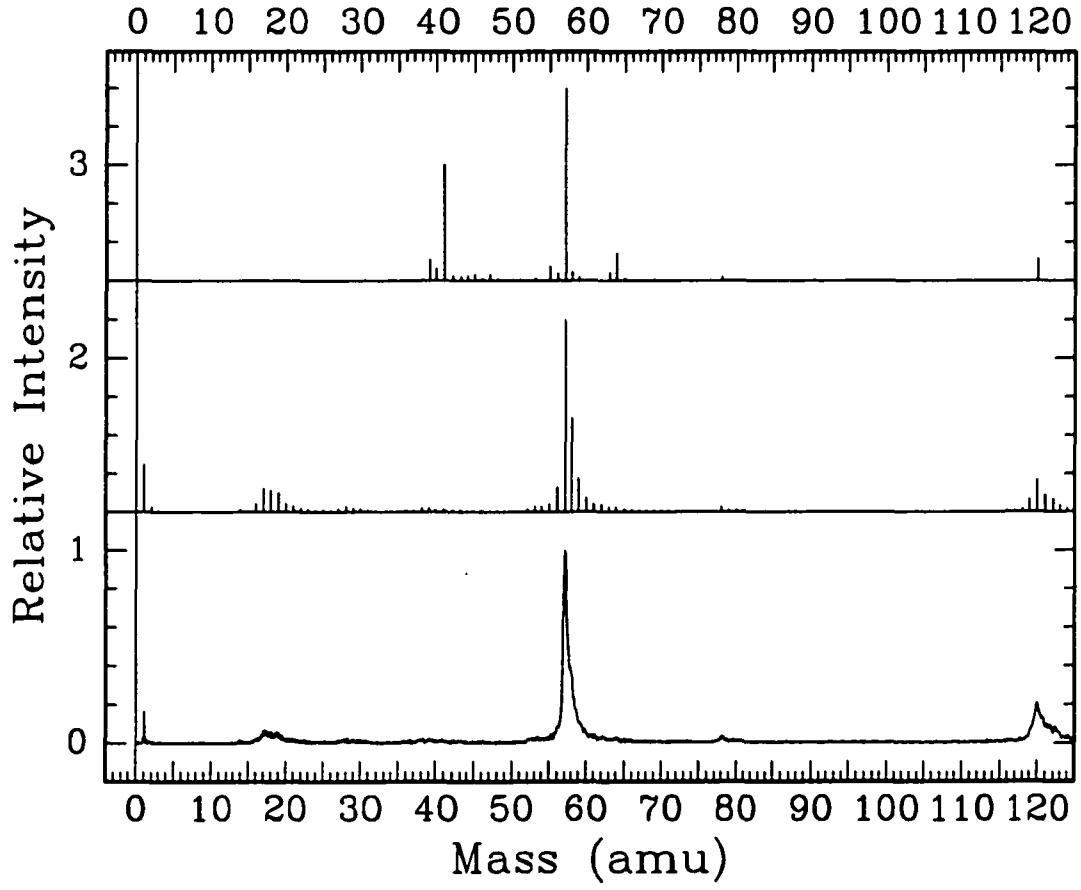

Figure 3.5: The photoionization and electron impact mass spectra of *tert*-butyl methyl sulfoxide. The bottom spectrum is the time of flight mass spectrum (converted from flight time to mass) up to 125 amu recorded at 4.5×10^{-6} Torr. The middle spectrum is a stick spectrum generated from the time of flight mass spectrum by integrating the area corresponding to each mass. The top spectrum is an electron impact mass spectrum obtained with an electron energy of 70 eV. The various spectra have been separately normalized to the intensity of the ion at 57 amu.

at 57 amu, the next largest peak was observed at 120 amu which is the mass of the parent molecular ion. The little blip in the mass spectrum at 78 amu corresponds to an ion with the molecular formula given by $[C_2H_6SO]^{+\bullet}$. The broad band around 18 amu is $[H_2O]^{+\bullet}$ which was present as an impurity in the *tert*-butyl methyl sulfoxide sample. The appearance of this species in the photoionization time of flight mass spectrum was somewhat surprising since the first ionization potential of water is 12.6 eV [74] which is above the photon energy of 10.5 eV and so should not have been ionized.

3.1.6 *sec*-Butyl Methyl Sulfoxide

The electron impact mass spectrum of *sec*-butyl methyl sulfoxide is illustrated in the top of figure 3.6 on page 83. The most intense peak has a mass of 64 amu which corresponds to $[H_3CSOH]^{+\bullet}$. Similar to *tert*-butyl methyl sulfoxide, a peak was observed at 41 amu which represents a fragmentation species from the butyl group in both molecules. Since the mass difference between the butyl ion and the species at 41 amu is also 16 amu, the butyl group has lost a hydrogen atom and a methyl group. The third largest peak in the electron impact mass spectrum of *sec*-butyl methyl sulfoxide appeared at 57 amu and was attributed to a butyl ion which has broken away from the parent molecular ion (mass of 120 amu). The peak at 55 amu corresponds to a molecular ion given by $[C_4H_7]^+$ and represents another species fragmenting from the butyl group. The peak at 44 amu is either $[C_3H_8]^{+\bullet}$ or

$[CS]^{+\bullet}$. In either case, extensive modifications occurred to the parent molecular ion to form either of these two species. Amongst the minor peaks, there was a small blip at 78 amu which has a molecular formula given by $[C_2H_6SO]^{+\bullet}$ and was formed by the ionization process of the parent molecule.

The photoionization time of flight mass spectrum of *sec*-butyl methyl sulfoxide in the bottom of figure 3.6 was recorded at a sample pressure of 2.9×10^{-6} Torr and contains some interesting features. Just like the electron impact mass spectrum, a peak was observed at 64 amu in the photoionization mass spectrum. The photoionization mass spectrum also contained a peak for the parent molecular ion at 120 amu and at 57 amu corresponding to a butyl ion species. A significant difference between the two mass spectra was that the photoionization mass spectrum contains more larger mass fragmentation species than the electron impact mass spectrum. The peak at 104 amu corresponds to the loss of a hydrogen atom and a methyl group from *sec*-butyl methyl sulfoxide.

The three peaks at 56, 57 and 58 amu represent an interesting group of fragmentation species. The most abundant peak is the butyl ion (57 amu) generated by simply breaking the bond between the sulfur atom and the butyl group in the parent molecular ion. The peak at 58 amu corresponds to the butyl group acquiring a hydrogen atom from the methyl group to form a butane ion. Hydrogen migration from the butyl moiety to the sulfoxide group in the parent molecular ion with cleavage of the bond connecting the butene group to the sulfur atom accounts for the appearance of

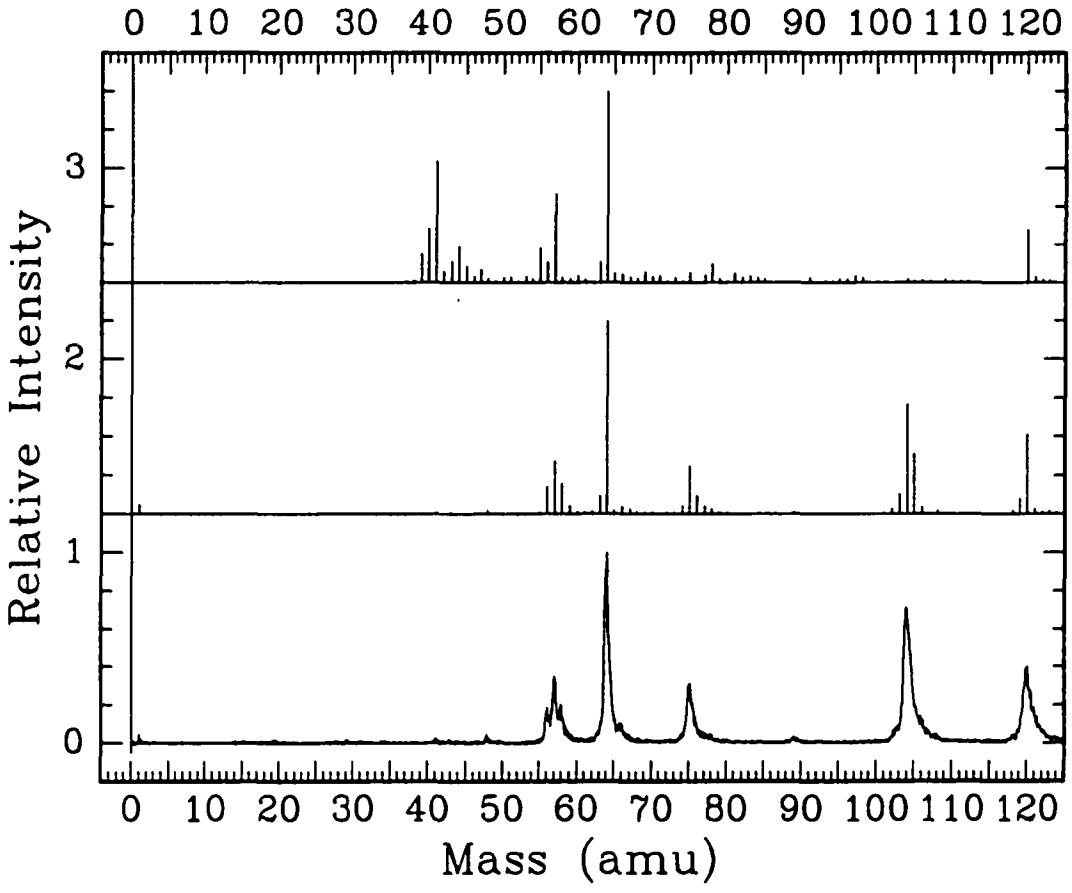

Figure 3.6: The photoionization and electron impact mass spectra of *sec*-butyl methyl sulfoxide. The bottom spectrum is the time of flight mass spectrum (converted from flight time to mass) up to 125 amu recorded at 2.9×10^{-6} Torr. The middle spectrum is a stick spectrum generated from the time of flight mass spectrum by integrating the area corresponding to each mass. The top spectrum is an electron impact mass spectrum obtained with an electron energy of 70 eV. The various spectra have been separately normalized to the intensity of the ion at 64 amu.

the $[C_4H_8]^{+\bullet}$ species.

One unexpected and rather surprising feature in the photoionization time of flight mass spectrum of *sec*-butyl methyl sulfoxide was the peak at 75 amu. A possible molecular formula for this peak is $[C_2H_3SO]^{+\bullet}$. Recall that the butyl moiety is bonded to the sulfur atom at a secondary carbon so the butyl moiety itself contains two methyl groups. If the proposed molecular formula for the 75 amu species is correct, it would correspond to the *sec*-butyl methyl sulfoxide parent molecular ion losing all three methyl groups. This seems unlikely because it would be improbable that only the bonds to the three methyl groups would break while the rest of the molecule remained intact.

3.1.7 *sec*-Butyl Ethyl Sulfoxide

The most intense peak in the electron impact mass spectrum of *sec*-butyl ethyl sulfoxide in figure 3.7 on page 85 was observed at 78 amu. What appears to have happened is that a hydrogen atom from the butyl group has migrated to the sulfoxide group and the remnant butene group was lost by the parent molecular ion. The presence of this mass was not startling since it was observed in the electron impact mass spectra of the other sulfoxide molecules presented in figures 3.1 to 3.6. What was surprising was the intensity because the peak at 78 amu was by far the largest feature in the spectrum for *sec*-butyl ethyl sulfoxide.

Another peak which involved rearrangements in the parent molecular ion was

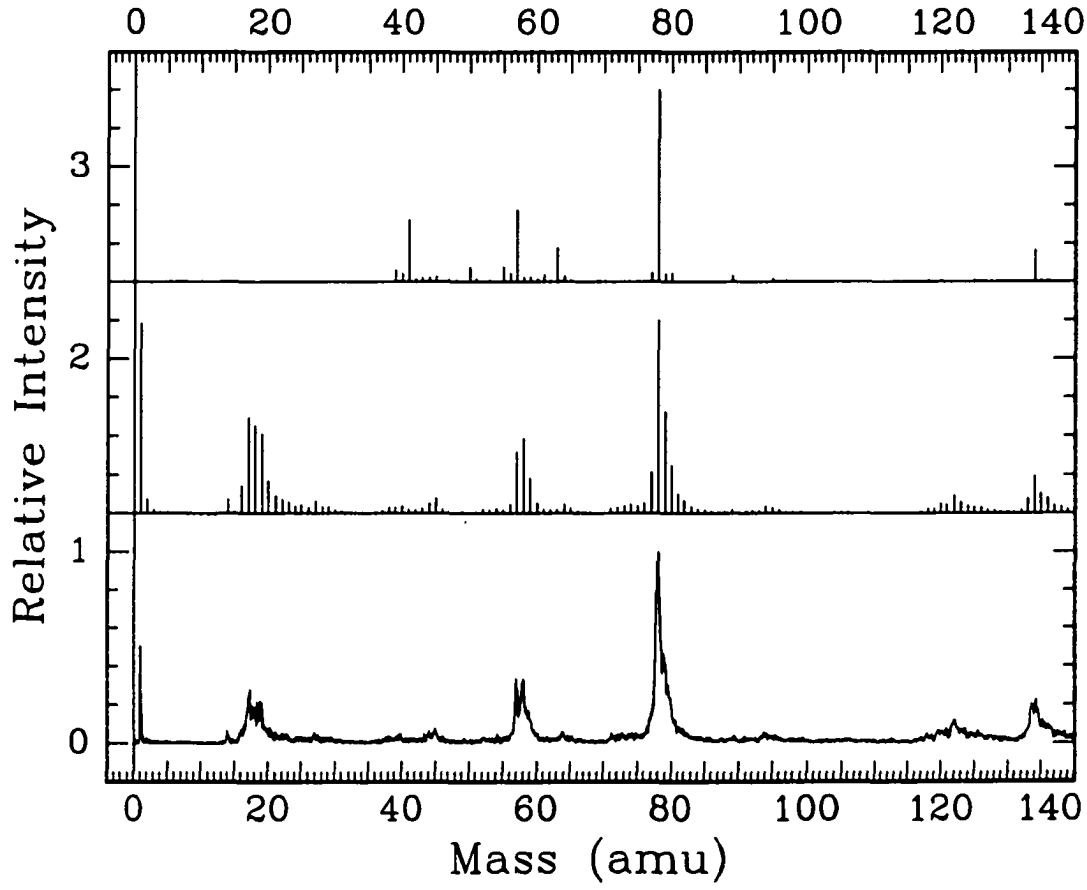

Figure 3.7: The photoionization and electron impact mass spectra of *sec*-butyl ethyl sulfoxide. The bottom spectrum is the time of flight mass spectrum (converted from flight time to mass) up to 140 amu recorded at 3.1×10^{-6} Torr. The middle spectrum is a stick spectrum generated from the time of flight mass spectrum by integrating the area corresponding to each mass. The top spectrum is an electron impact mass spectrum obtained with an electron energy of 70 eV. The various spectra have been separately normalized to the intensity of the ion at 78 amu.

observed at 63 amu and correlates to $[H_3CSO]^+$. Hydrogen migration to the sulfoxide group followed by the loss of the methyl group on the ethyl moiety and loss of the butene group would account for the species at 63 amu.

The second largest peak in the electron impact mass spectrum of *sec*-butyl ethyl sulfoxide appeared at 57 amu and corresponds to a butyl ion. The next largest peak was at 41 amu and corresponds to a molecular formula given by $[C_3H_5]^+$. These two ions also appeared in the electron impact mass spectra of *tert*-butyl methyl sulfoxide (figure 3.5 on page 80) and *sec*-butyl methyl sulfoxide (figure 3.6 on page 83) and are common fragmentation species of butyl groups.

The photoionization time of flight mass spectrum of *sec*-butyl ethyl sulfoxide presented in figure 3.7 was recorded at a sample pressure of 3.1×10^{-6} Torr and shows some interesting high mass features. The moderately intense peak at 134 amu corresponds to the parent molecular ion. The neighbouring peak at 122 amu was 12 amu below the mass of the parent molecular ion. This seems to suggest the rather surprising result that a *sec*-butyl ethyl sulfoxide ion has lost a single carbon atom and nothing else.

The electron impact mass spectrum of *sec*-butyl ethyl sulfoxide contained different fragmentation species than the photoionization mass spectrum. The major peak was also at 78 amu but the only other species with significant intensity was observed for the group around 57 amu. The $[C_4H_8]^{+\bullet}$, $[C_4H_9]^+$ and $[C_4H_{10}]^{+\bullet}$ group was also observed in the photoionization mass spectrum of *sec*-butyl methyl sulfoxide (figure 3.6 on

page 83).

3.1.8 Discussion

One common feature of the energetic excitation of the sulfoxides was the ease with which a hydrogen atom and/or a methyl group migrated to the sulfoxide group. The repeated appearance of a species at 78 amu seems to suggest that a common product was formed. In the case of diethyl sulfoxide and the butyl sulfoxides, this product was believed to be an ion with the same molecular formula as dimethyl sulfoxide. With methyl phenyl sulfoxide, the product seems more likely to be $[C_6H_6]^{+\bullet}$ because the extensive skeletal rearrangements necessary to form a methyl group from a phenyl ring rule out a species with a molecular formula given by $[C_2H_6SO]^{+\bullet}$. A fragmentation species of mass 78 amu could have occurred with ethyl phenyl sulfoxide by forming $[C_6H_6]^{+\bullet}$ like methyl phenyl sulfoxide or by forming $[C_2H_6SO]^{+\bullet}$ like diethyl sulfoxide.

The electron impact mass spectra of *tert*-butyl methyl sulfoxide (figure 3.5 on page 80), *sec*-butyl methyl sulfoxide (figure 3.6 on page 83) and *sec*-butyl ethyl sulfoxide (figure 3.7 on page 85) all show similar features. In particular, the formation of the butyl ion at 57 amu and the $[C_3H_5]^+$ species at 41 amu.

Although the investigation of the mass spectra for the various sulfoxide molecules was informative, the essential purpose of recording them was to determine the suitability of the molecule for the subsequent work in this chapter. The main goal of this work was to study the infrared multiple-photon dissociation of the sulfoxide molecules by

vibrational excitation with a CO_2 laser. Ideally, the photoionization process should not further fragment the product species from the infrared excitation. The more extensive the fragmentation due to the photoionization, the more complicated the analysis of the infrared dissociation products.

Inspection of the photoionization time of flight mass spectrum of dimethyl sulfoxide in figure 3.1 on page 71 shows that this molecule is a prime candidate for the infrared multiple-photon dissociation study to be performed in the next section. The problems already mentioned in section 3.1.2 on page 73 eliminate diethyl sulfoxide from this study.

The photoionization mass spectrum of methyl phenyl sulfoxide presented in figure 3.3 on page 76 is not ideal for the purposes of the infrared dissociation study, but the presence of a strong parent molecular ion peak and few fragmentation species make methyl phenyl sulfoxide a suitable candidate. Unfortunately, ethyl phenyl sulfoxide is not suitable because the photoionization time of flight mass spectrum in figure 3.4 on page 78 showed no peak associated with the parent molecular ion.

The weak intensity of the parent molecular ions for *tert*-butyl methyl sulfoxide (figure 3.5 on page 80), *sec*-butyl methyl sulfoxide (figure 3.6 on page 83) and *sec*-butyl ethyl sulfoxide (figure 3.7 on page 85) make this group unsuitable for the infrared multiple-photon dissociation study. However, the desirability of this group based on the investigation of the electron impact mass spectra necessitates that at least one of these three molecules be examined. The expected stability of the tertiary butyl group

eliminated *tert*-butyl methyl sulfoxide from consideration because few rearrangement reactions were expected to occur. In comparing *sec*-butyl methyl sulfoxide and *sec*-butyl ethyl sulfoxide, the relative intensity of the parent molecular ion favours *sec*-butyl methyl sulfoxide. Another factor supporting *sec*-butyl methyl sulfoxide is the higher signal-to-noise ratio of the parent molecular ion as indicated by the noise present in the baseline of the photoionization time of flight mass spectrum of *sec*-butyl ethyl sulfoxide (figure 3.7).

In summary, the suitable candidates for the infrared multiple-photon dissociation study were determined to be dimethyl sulfoxide, methyl phenyl sulfoxide and *sec*-butyl methyl sulfoxide. Dimethyl sulfoxide will be presented in the next section, methyl phenyl sulfoxide in section 3.3 which starts on page 116 and section 3.4 (page 145) deals with *sec*-butyl methyl sulfoxide.

3.2 Dimethyl Sulfoxide Infrared Photolysis

The infrared multiple-photon dissociation study of dimethyl sulfoxide involved varying the wavelength of the CO_2 laser and, as a separate investigation, changing the output power of the CO_2 laser at a fixed wavelength. The time-resolved detection of infrared multiple-photon dissociation reaction products for dimethyl sulfoxide investigated by Gross *et al.* stated that the maximum apparent static photolysis yield occurred at 1085.8 cm^{-1} (the 9R32 CO_2 laser line) [41]. Unfortunately, this line was the highest one that they could use so the precise location of the wavelength for maximum

dissociation could not be determined. In addition, a static gas sample cell might involve different mechanisms than with a flowing gas sample from an effusive source as was used in this work and so a wavelength dependent study seemed to be in order.

The first subsection deals with the CO_2 laser wavelength dependent investigation of dimethyl sulfoxide. The CO_2 laser was set to an output power of 1.0 W for each wavelength. The photon wavenumber was varied from a high of 1086.9 cm^{-1} (9R34 line) down to 1048.7 cm^{-1} (9P18 line) and a gap between 1069.0 (9R06 line) and 1057.3 cm^{-1} (9P08 line) because an output power of 1.0 W was not obtained for the transitions within this region. The sample pressure was approximately 3.3×10^{-6} Torr.

The next subsection involves the power dependent investigation at a single, fixed, wavelength and begins on page 104. The CO_2 laser was fixed at the 9R32 line and the output power varied from 1.6 W down to 0.0 W with a decrement of 0.1 W. The sample pressure was 3.0×10^{-6} Torr.

A summary of the photolysis results for dimethyl sulfoxide is displayed in table 3.1 on page 91. The details of the wavelength dependent study and the power dependent investigation can be found in the following two subsections. The table is presented at this point to provide a road map for the rest of this section.

3.2.1 Wavelength Dependence

Some interesting and rather unexpected results were observed in the wavelength dependent infrared multiple-photon dissociation investigation of dimethyl sulfoxide. In

Table 3.1: Fragment summary for species from dimethyl sulfoxide. The wavenumber maximum indicates the local maxima in the wavelength dependent CO_2 laser photolysis of dimethyl sulfoxide which generated the corresponding fragment. The power threshold refers to the CO_2 laser output power at 1085.8 cm^{-1} when the fragment first starts to appear. The maximum relative abundance is the power dependent measurement at 1.6 W compared to the amount of dimethyl sulfoxide in the corresponding photoionization mass spectrum and is presented in the fourth column. The last column indicates the relative abundance of the fragment in the 70 eV electron impact mass spectrum scaled to the amount of dimethyl sulfoxide.

Fragment	Wavenumber Maximum (cm^{-1})	Power Threshold (W)	Maximum Relative Abundance	Electron Impact Mass Spectrum Relative Abundance
$[H_3CSO]^+$	1085.8	0.4	0.161 ± 0.028	0.984
$[CH_3]^+$	1085.8	0.5	0.115 ± 0.024	
$[HCS]^+$	1085.8	1.2	0.027 ± 0.009	0.161
$[OCH_3]^+$	1085.8	1.4	0.024 ± 0.009	
$[H_3CS]^+$	1083.5	1.4	0.011 ± 0.006	0.080
$[SO]^{+\bullet}$	1082.3	0.0	0.013 ± 0.006	0.053

figure 3.8 on page 93, several photofragmentation species were observed. The bottom spectrum was obtained with only the photoionization laser beam interacting with the molecules. The middle spectrum was recorded with both the photofragmentation laser (i.e. CO_2 laser) and the photoionization laser (Nd:YAG laser) interacting with the molecules. The top spectrum represents the difference between the middle and bottom spectra. In essence, the top spectrum illustrates which species were produced by the use of the CO_2 laser (peaks pointing to the top of the page) and which were consumed (downward peaks).

Unfortunately, the presentation of time of flight mass spectra in terms of flight time is not very useful. The time of flight mass spectra in figure 3.8 were transformed from flight time to mass and the area associated with each mass was integrated as outlined in section 2.5 on page 65. The intensities were then normalized to the value for the parent molecular ion in the photoionization mass spectrum and are illustrated in figure 3.9 on page 94. The bottom three spectra correlate with the three spectra in figure 3.8.

The CO_2 laser production mass spectrum for the 9R32 line is presented at the top of figure 3.9. This spectrum represents the production of the various species due to the CO_2 laser and was obtained by subtracting a scaled amount of the photoionization mass spectrum (bottom) from the photofragmentation / photoionization mass spectrum (second from the bottom) to eliminate the parent molecular ion in the CO_2 laser production mass spectrum. This representation is beneficial when the

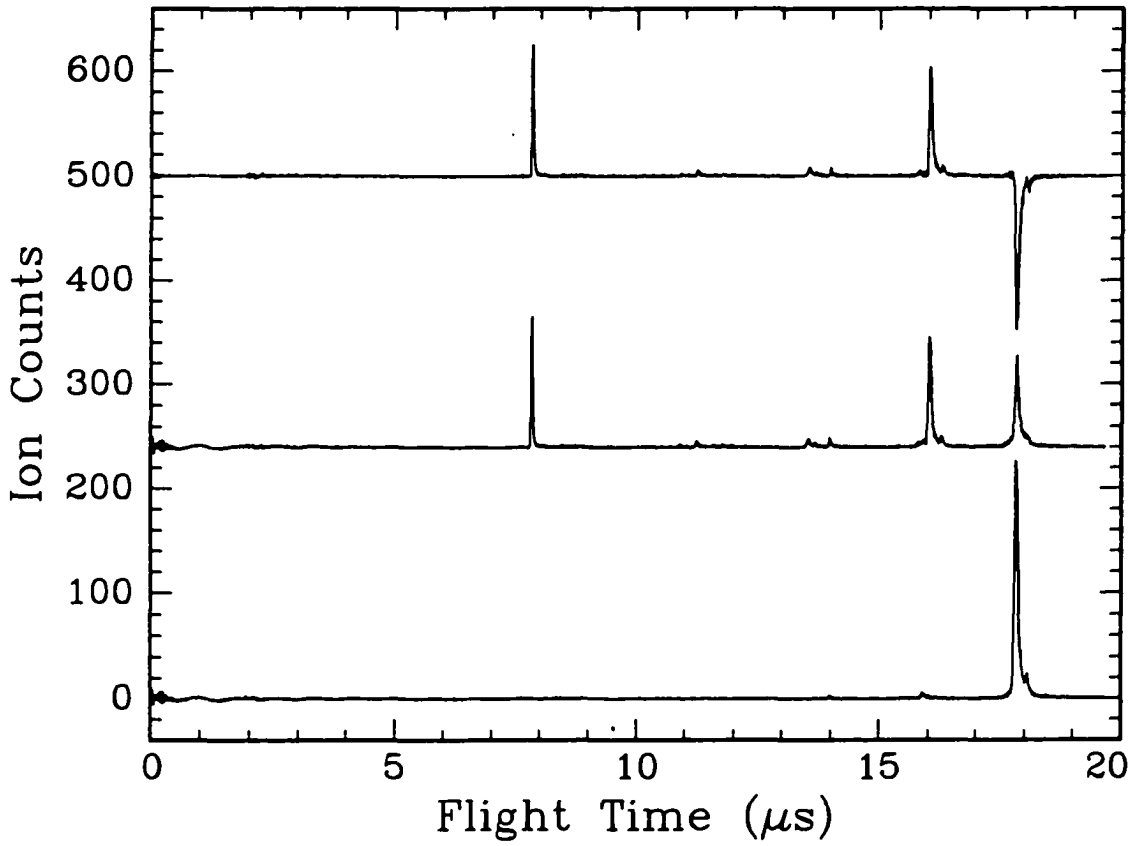

Figure 3.8: Dimethyl sulfoxide time of flight mass spectra (9R32 CO_2 laser line). The bottom spectrum was obtained with only the photoionization laser interacting with the molecule. The middle spectrum was obtained with first the CO_2 laser interacting with the sample followed by the photoionization laser. The top spectrum represents the difference between the two lower spectra. The sample pressure was 3.4×10^{-6} Torr.

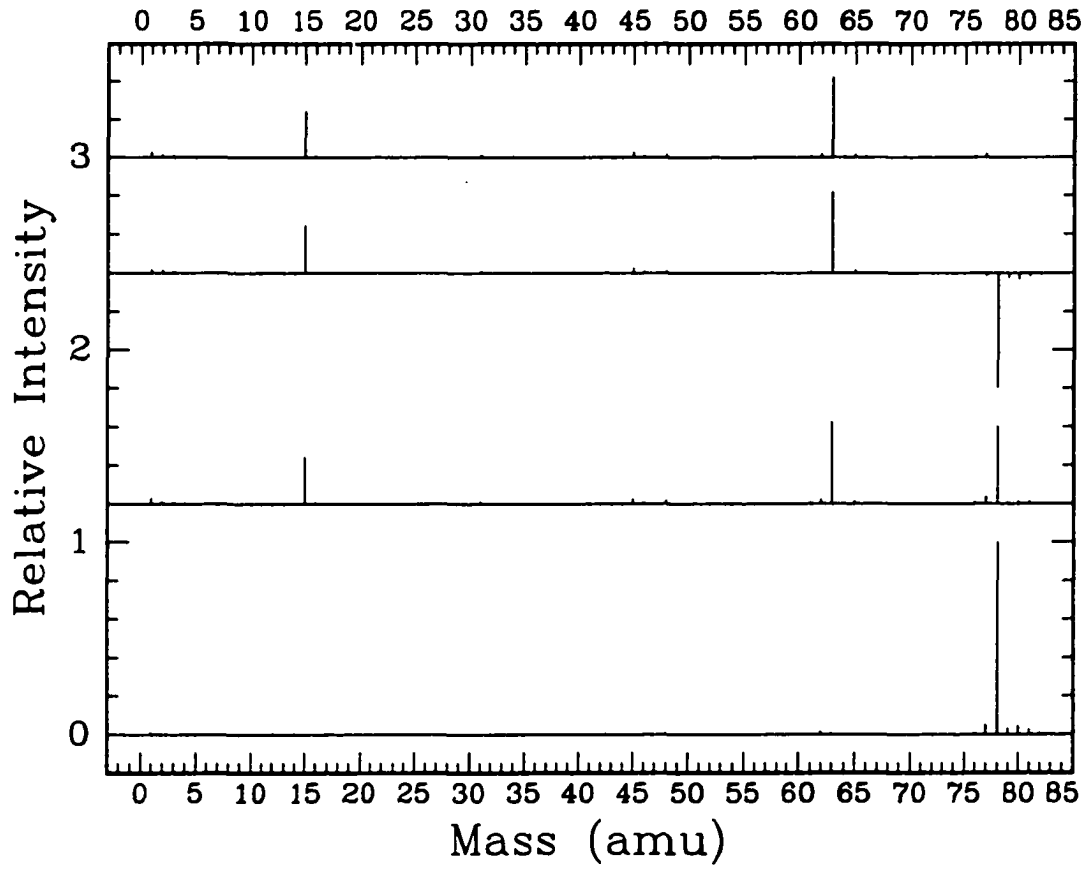

Figure 3.9: Dimethyl sulfoxide mass spectra (9R32 CO_2 laser line). The bottom spectrum is the corresponding stick mass spectrum to the photoionization mass spectrum in the previous figure (page 93). The second spectrum from the bottom correlates to the photofragmentation / photoionization mass spectrum in the previous figure. The second spectrum from the top represents the difference mass spectrum in the previous figure. The top spectrum indicates the photofragmentation species production due to the CO_2 laser. The intensities in all of the spectra were normalized to the value of the parent molecular ion at 78 amu in the photoionization mass spectrum.

photoionization mass spectrum contains extensive fragmentation species (as will be seen with methyl phenyl sulfoxide and *sec*-butyl methyl sulfoxide).

The major product species in figure 3.9 were $[H_3CSO]^+$ (63 amu) and $[CH_3]^+$ (15 amu). Although Gross *et al.* did observe the methyl radical, they did not observe the methyl sulfoxide species [41]. Instead, they detected the formation of SO which was attributed to the following two step reaction:

$$(H_3C)_2SO + n' h\nu_F \rightarrow H_3CSO + CH_3 \quad (3.1)$$

$$H_3CSO + n'' h\nu_F \rightarrow H_3C + SO. \quad (3.2)$$

A small blip in the photofragmentation mass spectrum appeared at 48 amu which indicates that some $[SO]^{+\bullet}$ was produced, but not nearly as much as the amount detected by Gross *et al.* where it was one of the primary products. This discrepancy can be attributed to the higher sample pressure (0.24 Torr) used by Gross *et al.* in a static gas cell which would involve collision induced fragmentation.

Additional minor product species in the 9R32 CO_2 laser line photolysis of dimethyl sulfoxide appeared at 31, 45 and 46 amu. Bowie *et al.* identified the peak at 45 amu as being $[HCS]^+$ [45] and so the species at 46 amu is $[H_2CS]^{+\bullet}$. The electron impact work on dimethyl sulfoxide performed by Amos *et al.* reported the relative intensities of $[H_3CS]^+$ (47 amu) and $[OCH_3]^+$ (31 amu) as 9.3% and 7.3% in their study [47]. Interestingly enough, the electron impact mass spectrum presented in figure 3.1 on

page 71 had a peak at 47 amu but not at 31 amu. The photofragmentation mass spectrum in figure 3.9, however, had a peak at 31 amu but not at 47 amu. It would appear that the electron impact process favours the formation of $[H_3CS]^+$ while the photofragmentation / photoionization process was biased towards forming $[OCH_3]^+$.

Even though several photofragmentation species were generated with the 9R32 CO_2 laser line (1085.8 cm^{-1}), the behaviour was found to be vastly different at other wavelengths. Figures 3.10 (page 97) and 3.11 (page 97) were recorded at 1050.4 cm^{-1} and correspond to the 9P16 CO_2 laser line. It was quite clear that very little photofragmentation was observed at this wavelength. One thing which was odd about these figures was the presence of a peak at 63 amu for the $[H_3CSO]^+$ species and the virtual absence of a peak at 15 amu corresponding to $[CH_3]^+$. It was expected that roughly equal amounts of the complementary pair species should occur since it was believed that $[H_3CSO]^+$ originated from the simple cleavage of a dimethyl sulfoxide molecule and photoionization of the methyl sulfoxide radical.

The wavelength dependence of the simple photofragmentation species is illustrated in figure 3.12 on page 99 and presented some interesting results. The intensity for an ion at a particular wavelength was obtained from the corresponding CO_2 laser production mass spectrum. The amount of the major photofragmentation products formed does depend on the CO_2 laser wavelength. In particular, a maximum was observed around 1085.8 cm^{-1} which is in agreement with the results of Gross *et al.* [41]. The different amounts of $[H_3CSO]^+$ and $[CH_3]^+$ seem to suggest that either the two

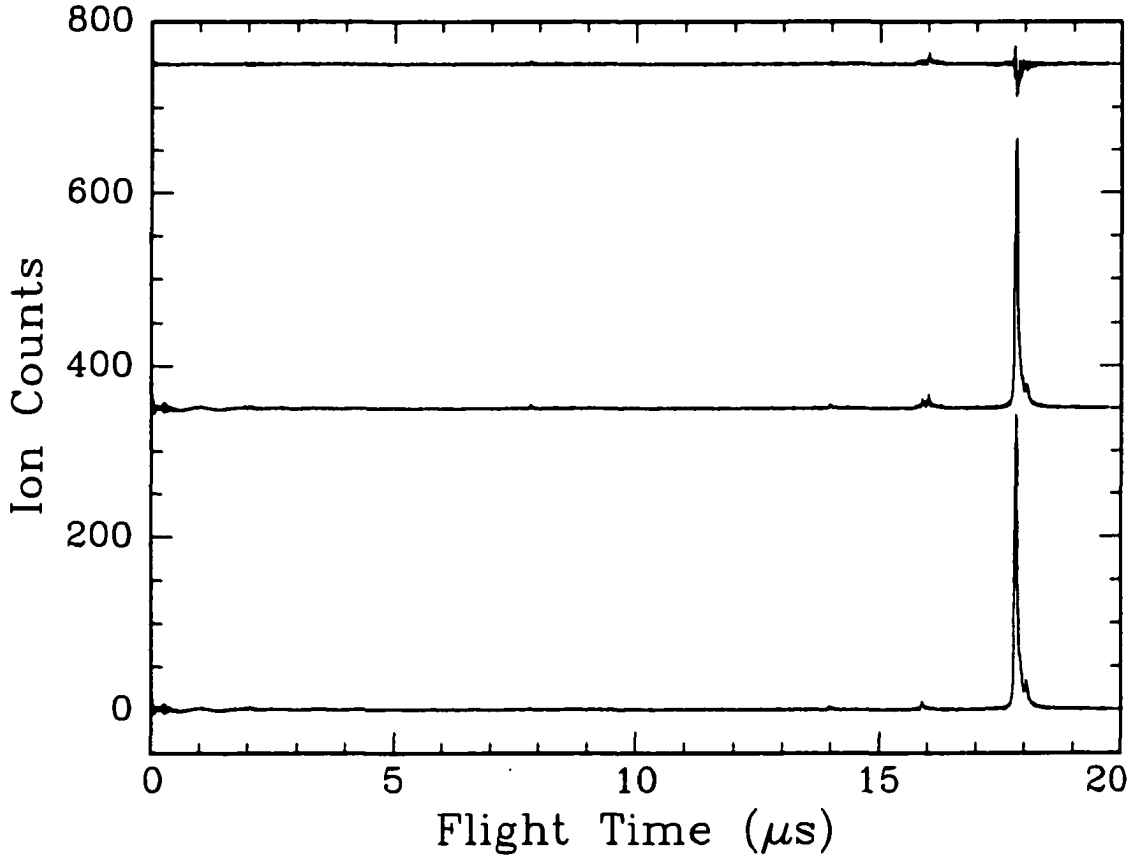

Figure 3.10: Dimethyl sulfoxide time of flight mass spectra (9P16 CO_2 laser line). The bottom spectrum was obtained with only the photoionization laser interacting with the molecule. The middle spectrum was obtained with first the CO_2 laser interacting with the sample followed by the photoionization laser. The top spectrum represents the difference between the two lower spectra. The sample pressure was 3.3×10^{-6} Torr.

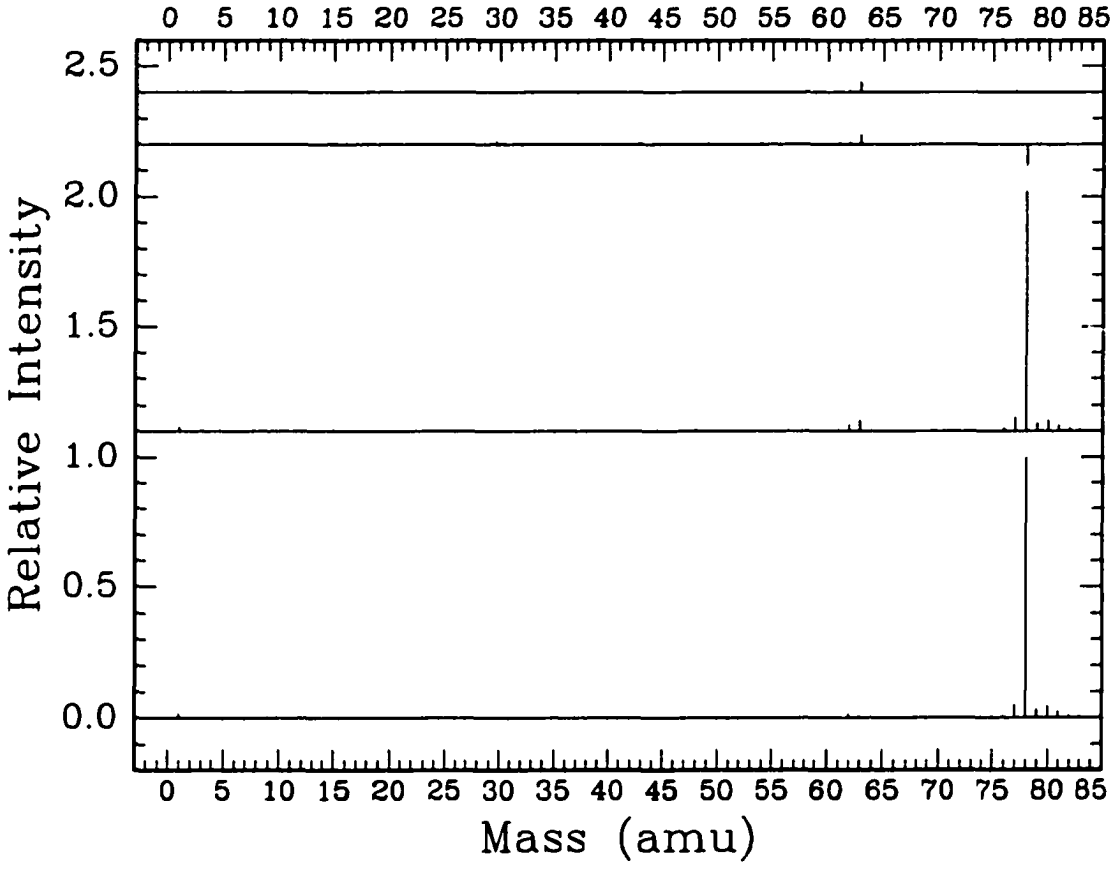

Figure 3.11: Dimethyl sulfoxide mass spectra (9P16 CO_2 laser line). The bottom spectrum is the corresponding stick mass spectrum to the photoionization mass spectrum in the previous figure (page 97). The second spectrum from the bottom correlates to the photofragmentation / photoionization mass spectrum in the previous figure. The second spectrum from the top represents the difference mass spectrum in the previous figure. The top spectrum indicates the photofragmentation species production due to the CO_2 laser. The intensities in all of the spectra were normalized to the value of the parent molecular ion at 78 amu in the photoionization mass spectrum.

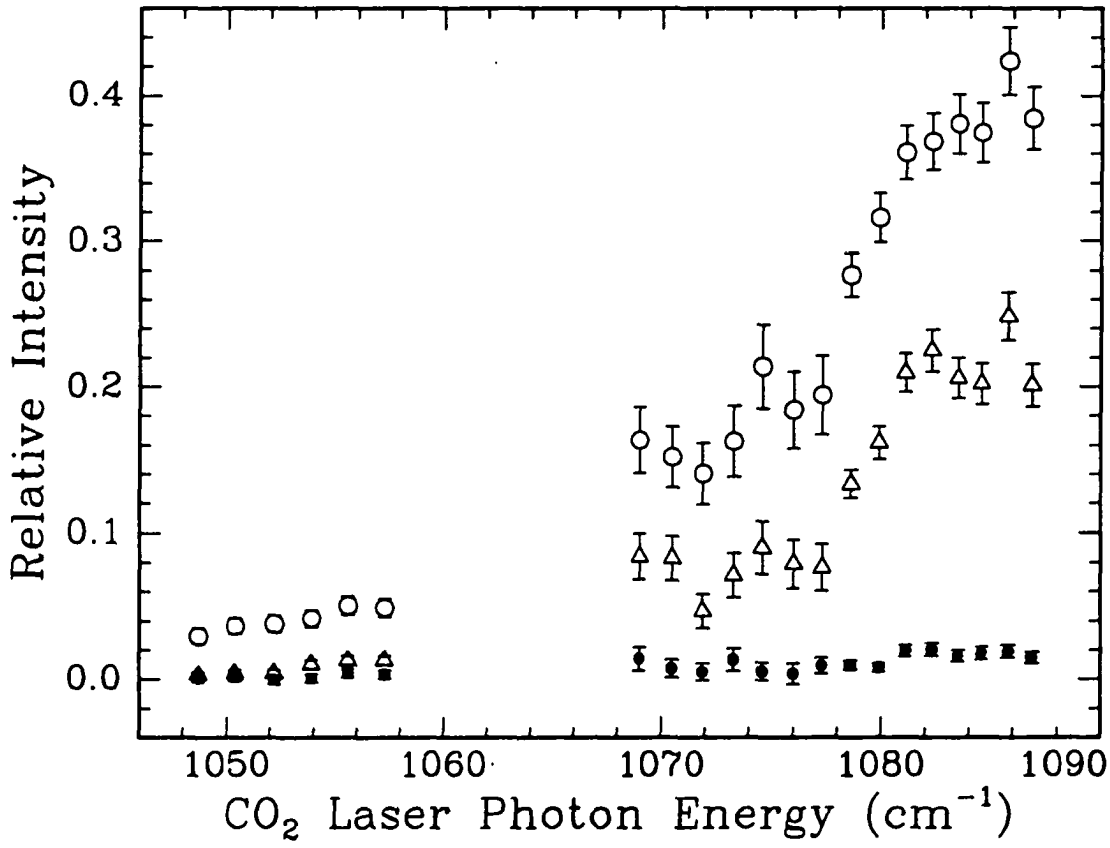

Figure 3.12: Dimethyl sulfoxide wavelength dependence for masses 63, 15 and 48 amu. The open circle data correspond to $[H_3CSO]^+$ (63 amu). The open triangles are for $[CH_3]^+$ (15 amu). The filled in circles correlate to $[SO]^{+\bullet}$ (48 amu). The intensities were obtained from the CO_2 laser production mass spectra and have been normalized to the abundance of the parent molecular ion at 78 amu in the corresponding photoionization mass spectra.

photofragmentation species have a different detection efficiency or that the photofragmentation step does not always fragment the parent molecule. At the 9R32 CO_2 laser line, the amount of dimethyl sulfoxide ion depleted was 0.597 ± 0.035 (relative to the amount of $[(H_3C)_2SO]^{+\bullet}$ in the photoionization mass spectrum) while the amount of $[H_3CSO]^+$ produced was 0.420 ± 0.022 and 0.248 ± 0.016 for $[CH_3]^+$. Because the sum of the produced species was greater than the amount depleted, the photofragmentation step must (in some cases) produce both $[H_3CSO]^\bullet$ and $[CH_3]^\bullet$ which were subsequently photoionized to form $[H_3CSO]^+$ and $[CH_3]^+$.

On the scale of figure 3.12, it was not obvious that the amount of $[SO]^{+\bullet}$ produced showed any dependence on the CO_2 laser wavelength and so an expanded view is provided in figure 3.13 on page 101. Although the amount produced was less than 0.02 (or 2%) of the amount of the dimethyl sulfoxide ion in the photoionization mass spectrum, it does show a slight increase as the CO_2 wavenumber approached 1085.8 cm^{-1}.

The wavelength dependence for the minor product at 45 amu is displayed in figure 3.14 on page 102. This mass corresponds to $[HCS]^+$ and must have originated through a somewhat complicated manner. The metastable species analysis provided by Bowie *et al.* suggests the following step [45]:

$$[H_3CSO]^+ \rightarrow H_2O + [HCS]^+. \tag{3.3}$$

Although the wavelength dependence does not parallel that for $[H_3CSO]^+$, both

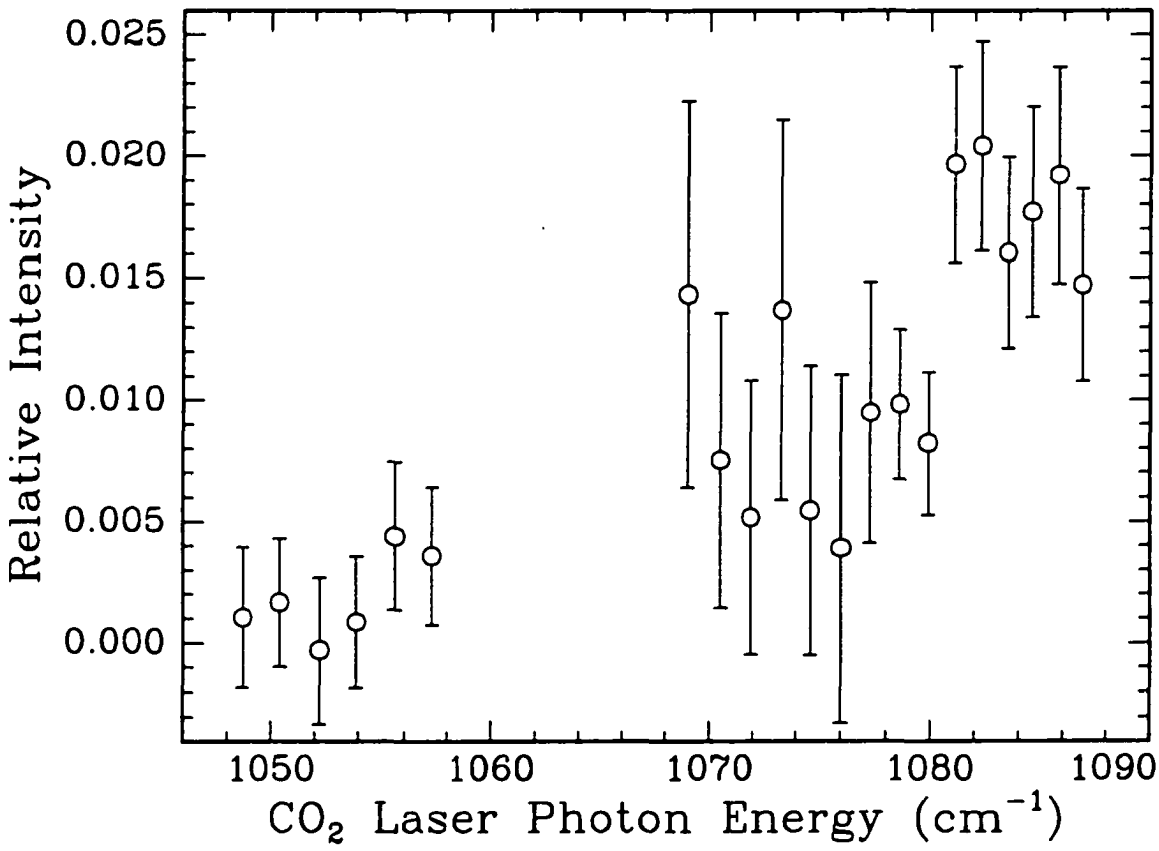

Figure 3.13: Dimethyl sulfoxide wavelength dependence for mass 48 amu ($[SO]^{+\bullet}$). The intensities were obtained from the CO_2 laser production mass spectra and have been normalized to the abundance of the parent molecular ion at 78 amu in the corresponding photoionization mass spectra.

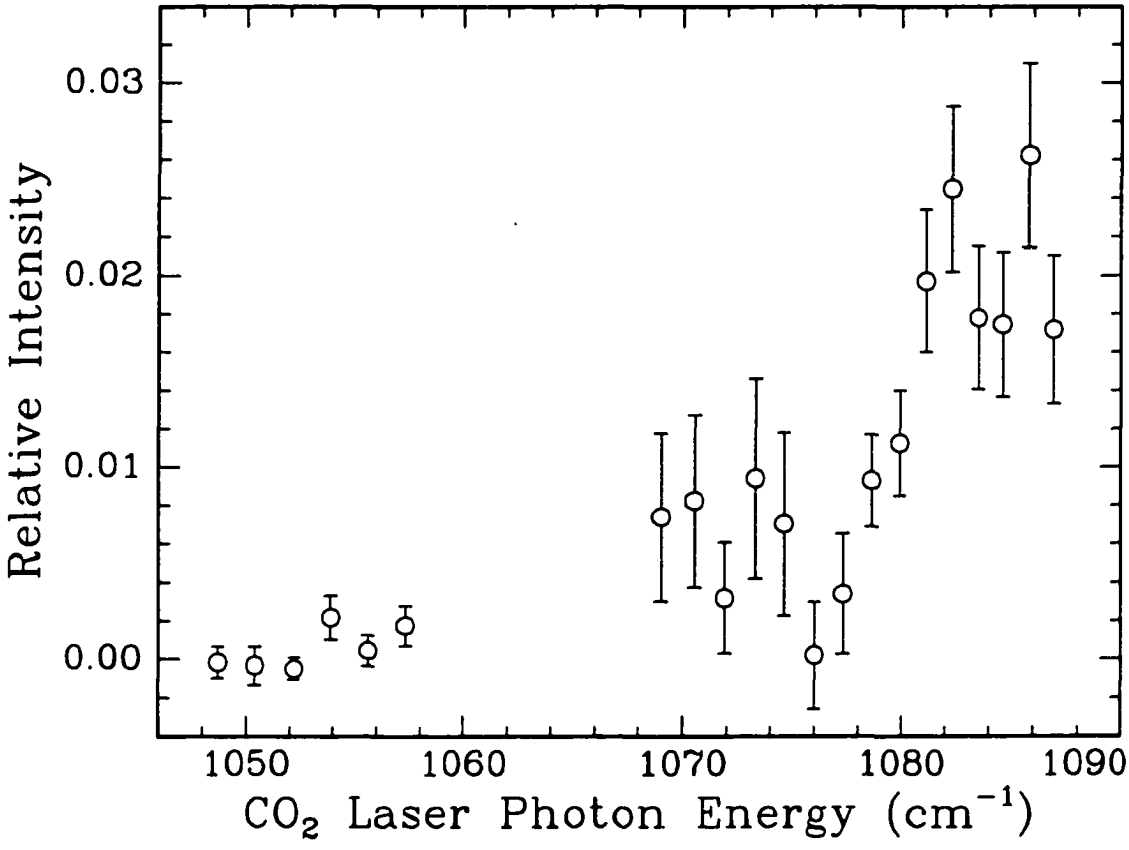

Figure 3.14: Dimethyl sulfoxide wavelength dependence for mass 45 amu ($[HCS]^+$). The intensities were obtained from the CO_2 laser production mass spectra and have been normalized to the abundance of the parent molecular ion at 78 amu in the corresponding photoionization mass spectra.

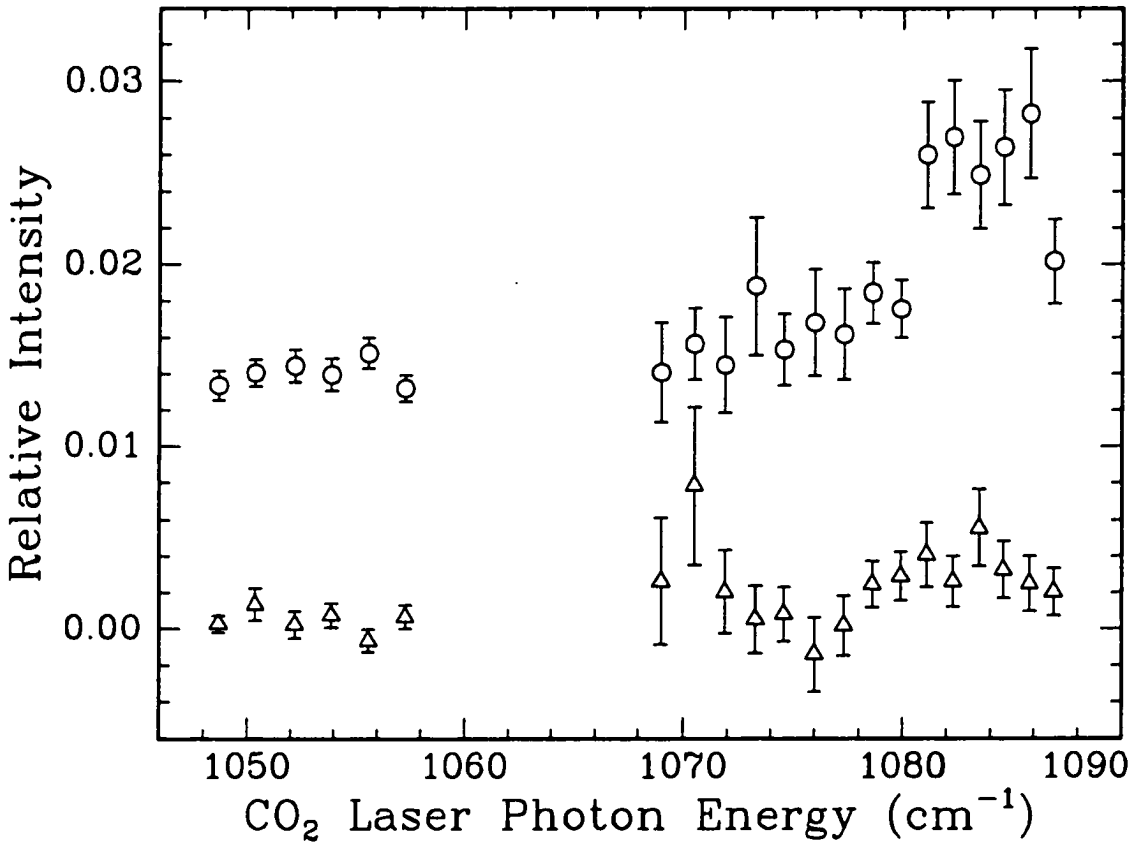

Figure 3.15: Dimethyl sulfoxide wavelength dependence for masses 31 and 47 amu. The open circle data correspond to $[OCH_3]^+$ (31 amu) and have been shifted up by 0.014. The open triangle data correlate to $[H_3CS]^+$ (47 amu). The intensities were obtained from the CO_2 laser production mass spectra and have been normalized to the abundance of the parent molecular ion at 78 amu in the corresponding photoionization mass spectra.

species do show a significant increase in abundance around 1080 cm^{-1}.

As previously mentioned, the $[H_3CO]^+$ / $[SCH_3]^+$ product pair does exhibit some unusual characteristics. The wavelength dependence for this pair is presented in figure 3.15 on page 103. For clarity, the data for the 31 amu species ($[H_3CO]^+$) have been shifted up by 0.014. Both species show an increase in the relative quantities produced as the CO_2 laser wavenumber approached 1090 cm^{-1}. However, $[H_3CO]^+$ showed a large increase around 1080 cm^{-1}. The sharp increase in abundance for $[H_3CO]^+$ occurred in the region that $[HCS]^+$ and $[H_3CSO]^+$ also increased and so the enhanced production of $[H_3CO]^+$ was also caused by the infrared excitation of the parent molecule.

3.2.2 Power Dependence

As the output power of the CO_2 laser is increased, the molecule will absorb more energy from the laser beam. As seen in the previous subsection, the wavelength of excitation was also important. Even if the CO_2 laser was set to the maximum output power, the molecule will not absorb as many photons if the wavelength was not correct as when the laser was tuned to the ideal wavelength. In figure 3.11 on page 98, very little photofragmentation was observed for the 9P16 CO_2 laser line while more photofragmentation species were generated in figure 3.9 on page 94 with the 9R32 line despite the output power of the CO_2 laser being identical for both laser lines. A variation in the output power at the 9R32 CO_2 laser line was expected

to be more informative than at the 9P16 line because more photofragmentation was observed at 1085.8 cm^{-1} than at 1050.4 cm^{-1}.

Figures 3.16 (page 106) and 3.17 (page 107) were recorded at the 9R32 CO_2 laser line set to an output power of 1.6 W and, unfortunately, the signal to noise ratio was a lot lower in these spectra than was observed in figure 3.8 on page 93. This could have been caused by a misalignment of the photoionization and photofragmentation laser beams with respect to the effusive molecular beam, a different amount of xenon in the tripling cell or some other (unknown) reason. Time constraints meant that the determination, and elimination, of this problem was not possible.

Although the mass spectra in figure 3.17 were recorded at a higher CO_2 laser output power than figure 3.9 (page 94), the fragmentation species were essentially the same in both cases. The major photofragmentation species were still $[H_3CSO]^+$ (63 amu) and $[CH_3]^+$ (15 amu). Rather disappointingly, the minor photofragmentation species showed almost the same intensity in figure 3.17 as in figure 3.9. The only possible exception was at 45 amu ($[HCS]^+$) but this can be attributed to the increased noise in figure 3.16. Two new and mysterious peaks appeared at 38 and 40 amu. An inspection of the corresponding region in the time of flight mass spectra (12.3 to 12.9 μs) revealed that these peaks represent noise in the spectra of figure 3.16 and are thus an artifact of the stick mass spectra generation procedure.

The photoionization mass spectrum (bottom) of dimethyl sulfoxide in figure 3.17 contained some different features than was observed in the photoionization mass spec-

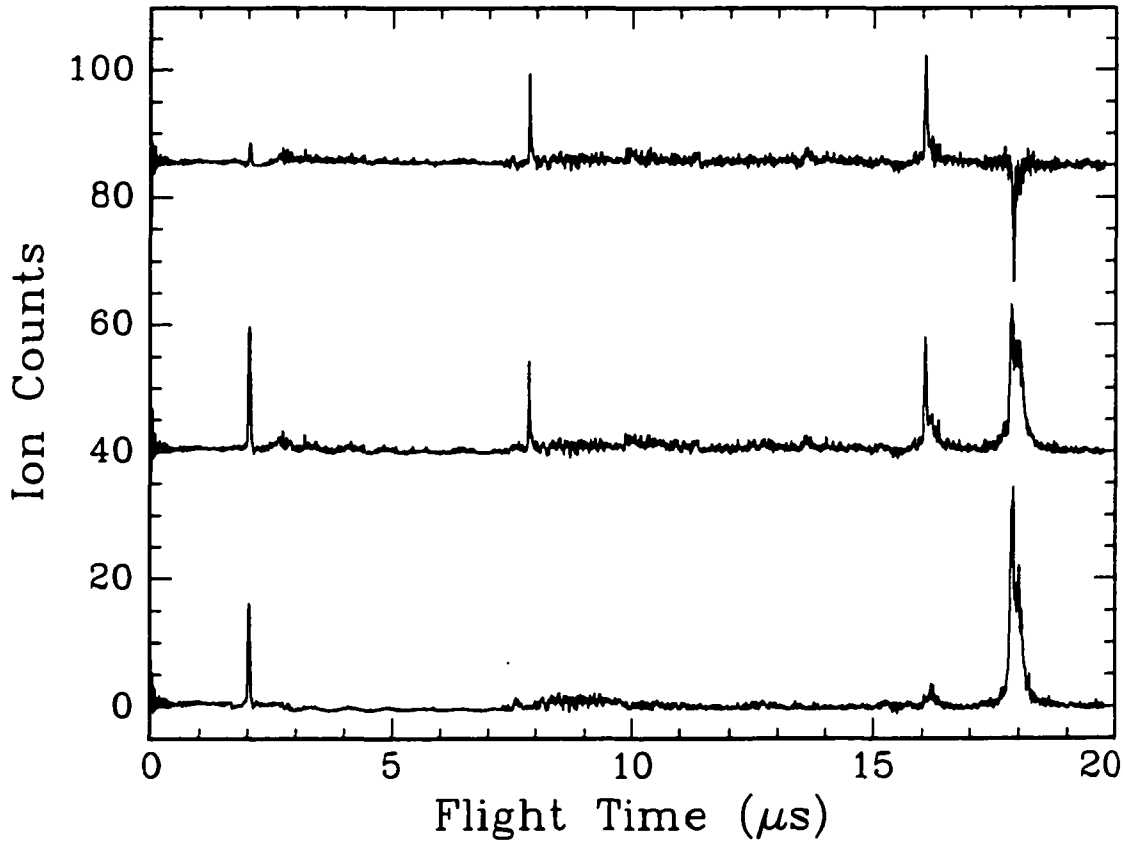

Figure 3.16: Dimethyl sulfoxide time of flight mass spectra (9R32 CO_2 laser line, 1.6 W). The bottom spectrum was obtained with only the photoionization laser interacting with the molecule. The middle spectrum was obtained with first the CO_2 laser interacting with the sample followed by the photoionization laser. The top spectrum represents the difference between the two lower spectra. The sample pressure was 3.0×10^{-6} Torr.

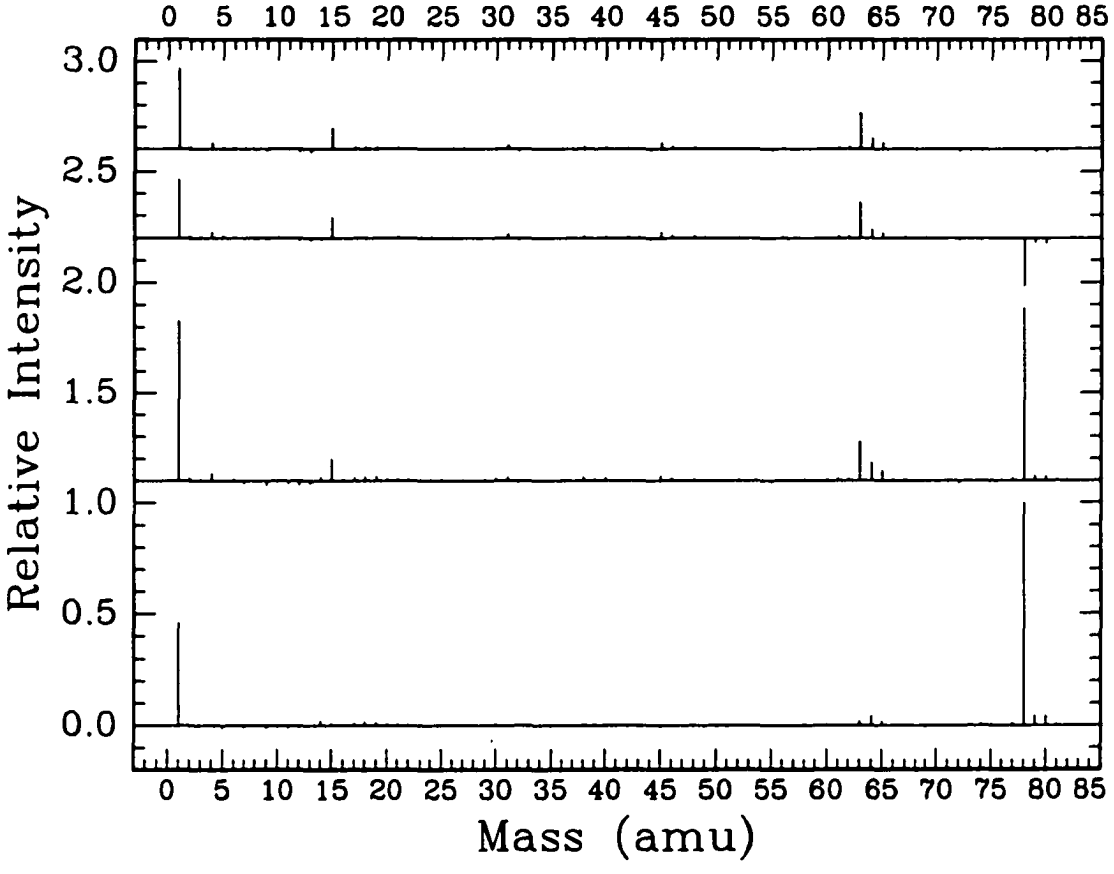

Figure 3.17: Dimethyl sulfoxide mass spectra (9R32 CO_2 laser line, 1.6 W). The bottom spectrum is the corresponding stick mass spectrum to the photoionization mass spectrum in the previous figure (page 106). The second spectrum from the bottom correlates to the photofragmentation / photoionization mass spectrum in the previous figure. The second spectrum from the top represents the difference mass spectrum in the previous figure. The top spectrum indicates the photofragmentation species production due to the CO_2 laser. The intensities in all of the spectra were normalized to the value of the parent molecular ion at 78 amu in the photoionization mass spectrum.

trum of dimethyl sulfoxide in figure 3.9 on page 94. In particular, the minor peak at 62 amu ($[H_2CSO]^{+\bullet}$) was not present but was replaced by a peak at 64 amu ($[H_3CSOH]^{+\bullet}$) and its complementary species at 14 amu ($[CH_2]^{+\bullet}$). What was particularly interesting about the 64 amu peak was that this shows that the hydrogen migration observed with the larger sulfoxide molecules in section 3.1 (starting on page 69) also occurred in dimethyl sulfoxide. It is now believed that the formation of the 63 amu species occurs by two different mechanisms [67, 76]. The first mechanism is just the simple cleavage of a methyl group and is represented by

$$[(H_3C)_2SO]^{+\bullet} \rightarrow [H_3CSO]^{+} + [CH_3]^{\bullet} \tag{3.4}$$

while the second mechanism involves hydrogen migration to the oxygen atom and then the fragmentation of this metastable species into $[H_2CSOH]^{+}$ and is illustrated in equations 3.5 and 3.6

$$[(H_3C)_2SO]^{+\bullet} \rightarrow [(H_3C)(H_2C)SOH]^{+\bullet} \tag{3.5}$$

$$[(H_3C)(H_2C)SOH]^{+\bullet} \rightarrow [H_2CSOH]^{+} + [CH_3]^{\bullet}. \tag{3.6}$$

The CO_2 laser low output power photolysis mass spectra for dimethyl sulfoxide are presented in figures 3.18 (page 109) and 3.19 (page 110) which were measured with an output power of 0.1 W for the 9R32 CO_2 laser line (1085.8 cm^{-1}). The CO_2 laser production mass spectrum (top of figure 3.19) showed virtually no photofragmentation

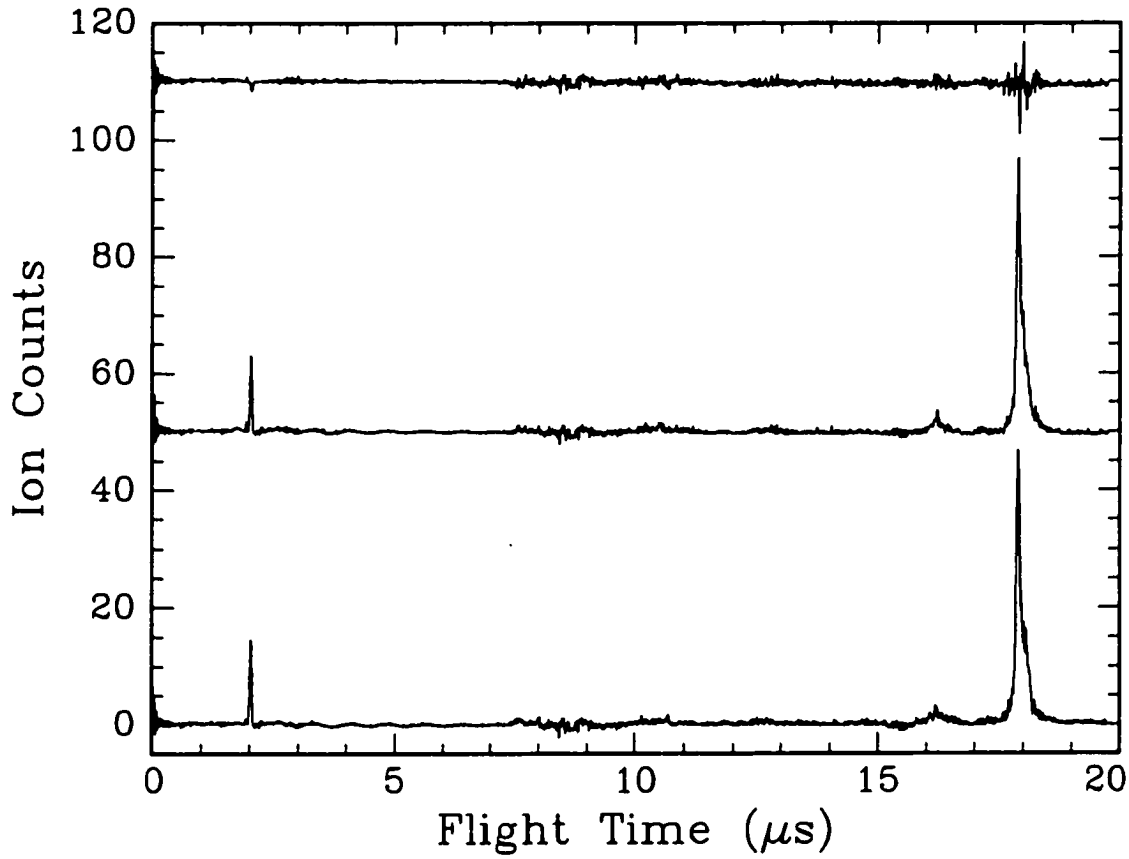

Figure 3.18: Dimethyl sulfoxide time of flight mass spectra (9R32 CO_2 laser line, 0.1 W). The bottom spectrum was obtained with only the photoionization laser interacting with the molecule. The middle spectrum was obtained with first the CO_2 laser interacting with the sample followed by the photoionization laser. The top spectrum represents the difference between the two lower spectra. The sample pressure was 3.0×10^{-6} Torr.

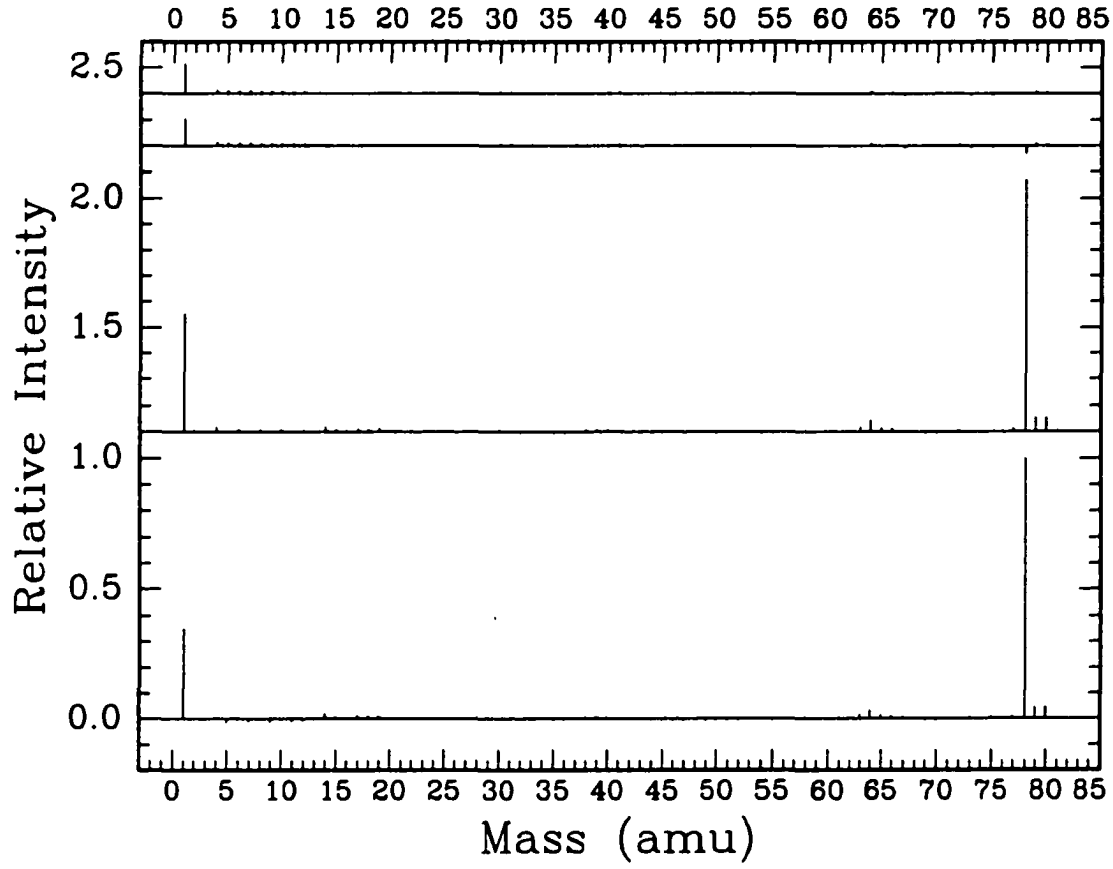

Figure 3.19: Dimethyl sulfoxide mass spectra (9R32 CO_2 laser line, 0.1 W). The bottom spectrum is the corresponding stick mass spectrum to the photoionization mass spectrum in the previous figure (page 109). The second spectrum from the bottom correlates to the photofragmentation / photoionization mass spectrum in the previous figure. The second spectrum from the top represents the difference mass spectrum in the previous figure. The top spectrum indicates the photofragmentation species production due to the CO_2 laser. The intensities in all of the spectra were normalized to the value of the parent molecular ion at 78 amu in the photoionization mass spectrum.

species.

Figure 3.20 on page 112 illustrates the 9R32 CO_2 laser line output power dependence for $[H_3CSO]^+$ and $[CH_3]^+$. For clarity, the data for $[H_3CSO]^+$ have been shifted up by 0.05. Both $[H_3CSO]^+$ and $[CH_3]^+$ had a threshold at 0.5 W. Below this output power, essentially no $[H_3CSO]^+$ and $[CH_3]^+$ were observed. Above this output power, the photolysis of dimethyl sulfoxide resulted in an increasing abundance of both $[H_3CSO]^+$ and $[CH_3]^+$.

The CO_2 laser output power dependent photolysis of dimethyl sulfoxide which generated $[SO]^{+\bullet}$ is presented in figure 3.21 on page 113. Even though the best fit line to the data has a positive slope, one could make the argument that increasing the output power did not significantly increase the abundance of $[SO]^{+\bullet}$ since the relative intensities are clustered around 0.005 or 0.5% of the dimethyl sulfoxide ion intensity in the photoionization mass spectrum.

The CO_2 laser output power dependence for the formation of the complementary pair $[H_3CS]^+$ and $[OCH_3]^+$ obtained by the photolysis of dimethyl sulfoxide is illustrated in figure 3.22 on page 114. The intensity data for $[H_3CS]^+$ have been shifted up by 0.04 for clarity. Both of these species were not observed with an output power below 1.3 to 1.4 W. Above this threshold, both fragmentation species increased in abundance. Figure 3.23 on page 115 presents the power dependence for $[HCS]^+$. The threshold appears at 1.2 W and the abundance increases as the CO_2 laser output power is increased above this value.

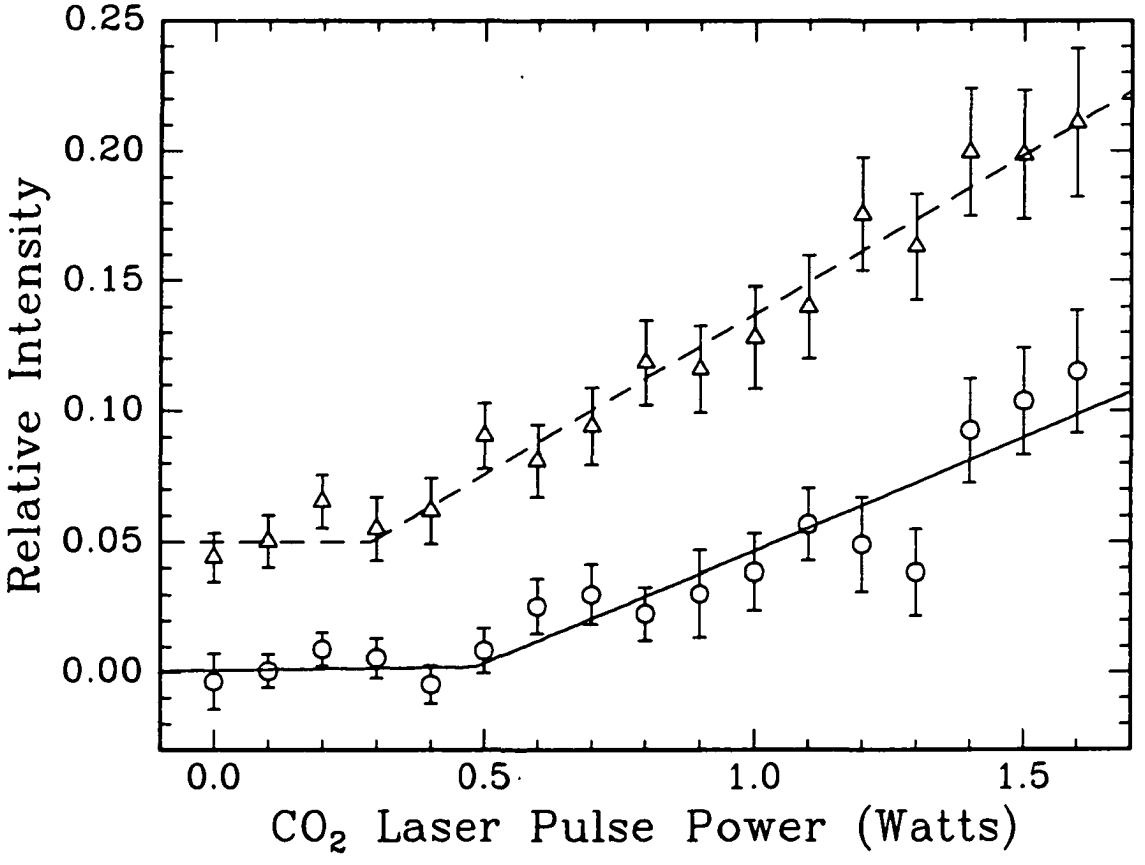

Figure 3.20: Dimethyl sulfoxide power dependence for masses 63 and 15 amu. The open triangles fitted by the dashed line are for $[H_3CSO]^+$ (63 amu) and have been shifted up in intensity by 0.05. The open circle data fitted by the solid line correspond to $[CH_3]^+$ (15 amu). The intensities were obtained from the CO_2 laser production mass spectra and have been normalized to the abundance of the parent molecular ion at 78 amu in the corresponding photoionization mass spectra.

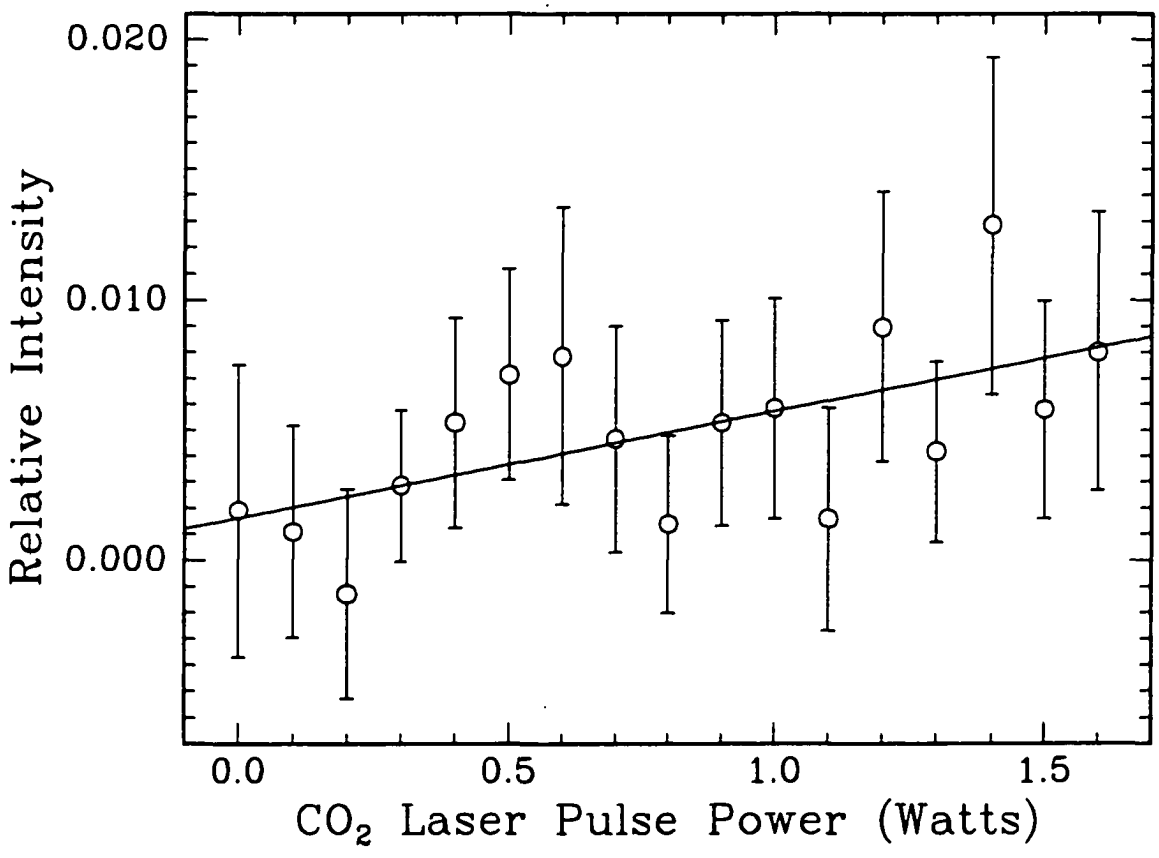

Figure 3.21: Dimethyl sulfoxide power dependence for mass 48 amu ($[SO]^{+\bullet}$). The intensities were obtained from the CO_2 laser production mass spectra and have been normalized to the abundance of the parent molecular ion at 78 amu in the corresponding photoionization mass spectra.

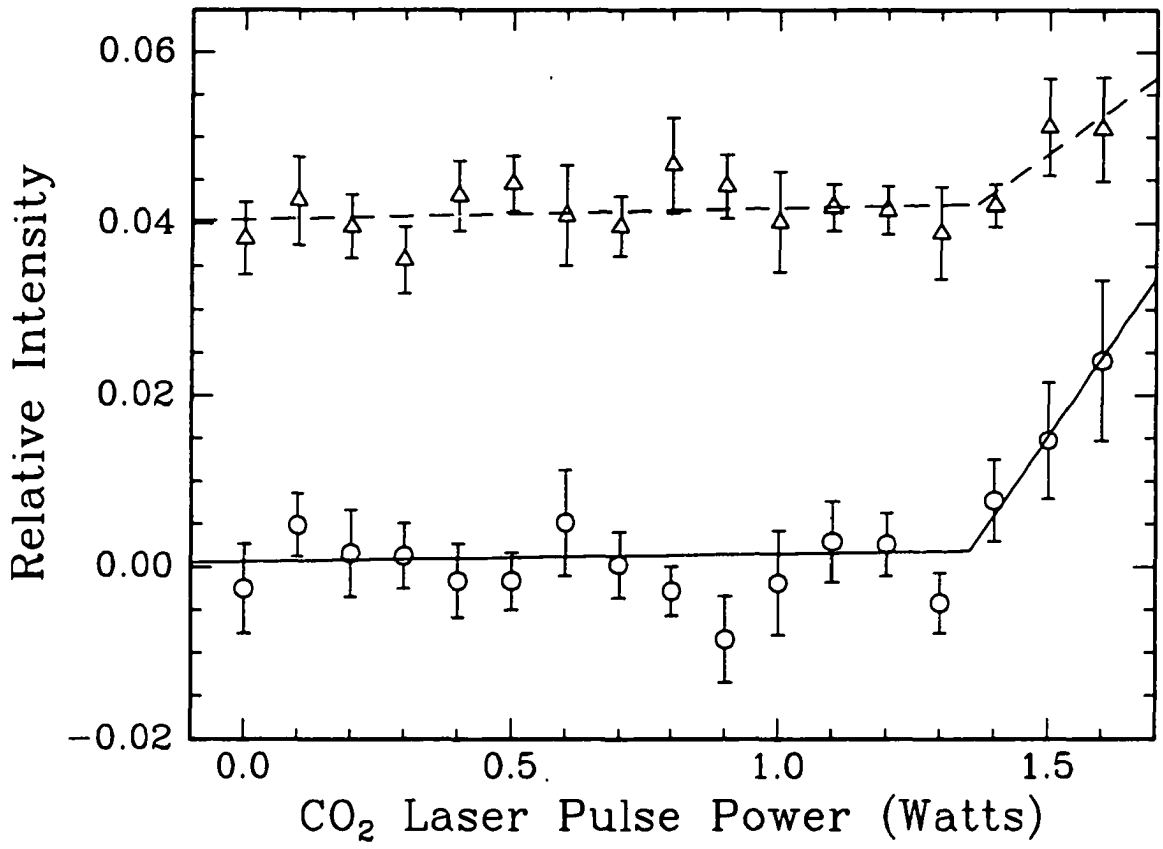

Figure 3.22: Dimethyl sulfoxide power dependence for masses 31 and 47 amu. The open circles fitted by the solid line correspond to $[OCH_3]^+$ (31 amu). The open triangles fitted by the dashed line correlate to $[H_3CS]^+$ (47 amu) and the intensity have been shifted up by 0.04. The intensities were obtained from the CO_2 laser production mass spectra and have been normalized to the abundance of the parent molecular ion at 78 amu in the corresponding photoionization mass spectra.

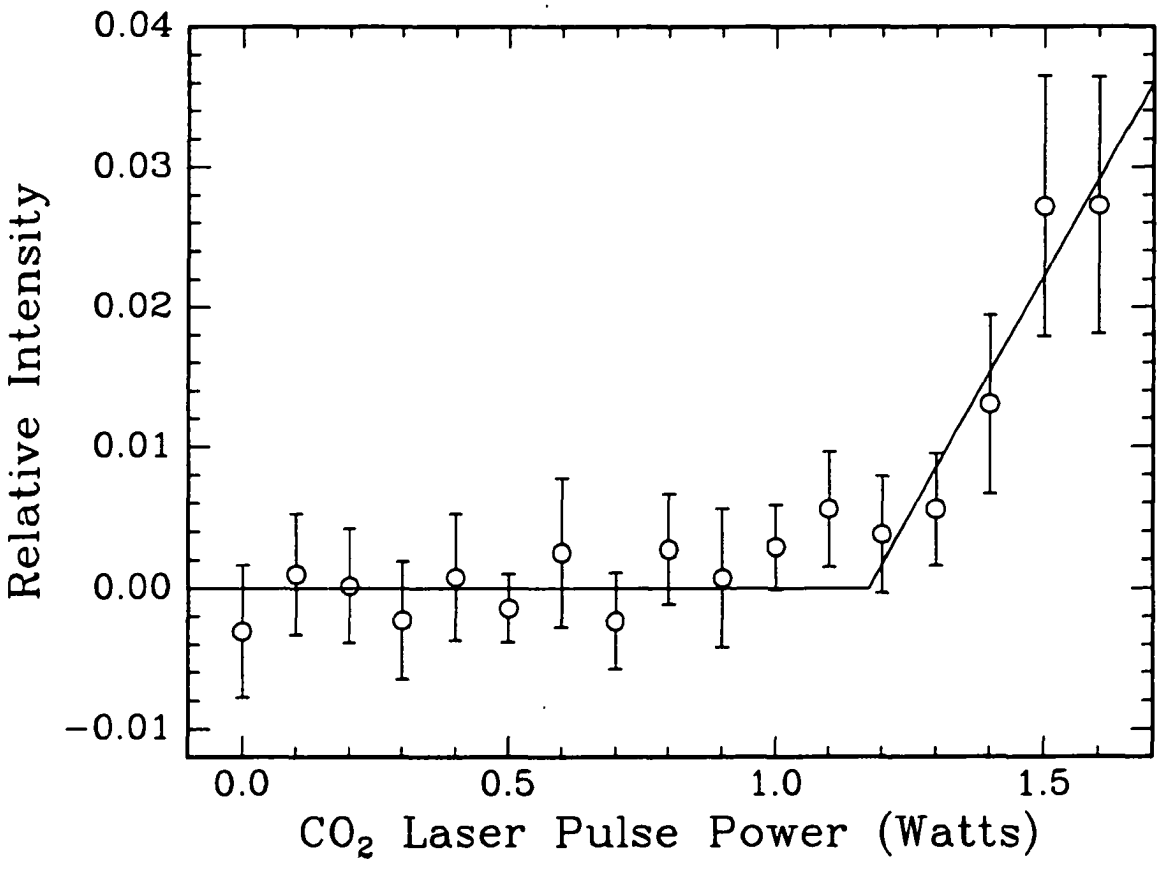

Figure 3.23: Dimethyl sulfoxide power dependence for mass 45 amu ($[HCS]^+$). The intensities were obtained from the CO_2 laser production mass spectra and have been normalized to the abundance of the parent molecular ion at 78 amu in the corresponding photoionization mass spectra.

3.3 Methyl Phenyl Sulfoxide Infrared Photolysis

The difference between methyl phenyl sulfoxide and dimethyl sulfoxide is that one of the methyl groups (CH_3) has been replaced by a phenyl group (C_6H_5 ring) and so the photolysis of methyl phenyl sulfoxide should lead to different photofragmentation species being formed. In addition, a comparison can be made between similar reactions that only differ by which side group (methyl or phenyl) was involved. Just like dimethyl sulfoxide, the infrared multiple-photon dissociation of methyl phenyl sulfoxide involved varying the wavelength of the CO_2 laser at a fixed output power of 1.0 W. This was followed by selecting a specific wavelength and then varying the output power of the CO_2 laser. The wavelength dependent measurements were recorded at a sample pressure of approximately 0.8×10^{-6} Torr and the regions 1087.9 cm^{-1} (9R36 laser line) to 1067.5 cm^{-1} (9R04 line) and 1058.9 cm^{-1} (9P06 line) to 1045.0 cm^{-1} (9P22 line). The power dependent measurements were recorded at a sample pressure of 2.5×10^{-6} Torr and a range of 1.6 to 0.0 W using the 9R32 CO_2 laser line (1085.8 cm^{-1}).

A summary of the photolysis results for methyl phenyl sulfoxide is displayed in table 3.2 on page 117. The details of the wavelength dependent study and the power dependent investigation can be found in the following two subsections. The table is presented at this point to provide a road map for the rest of this section.

Table 3.2: Fragment summary for species from methyl phenyl sulfoxide. The wavenumber maximum indicates the local maxima in the wavelength dependent CO_2 laser photolysis of methyl phenyl sulfoxide which generated the corresponding fragment. The power threshold refers to the CO_2 laser power at 1085.8 cm^{-1} when the fragment first starts to appear. The power plateau value corresponds to the CO_2 laser output power above which the relative abundance no longer increases. The maximum relative abundance is the power dependent measurement at 1.6 W compared to the amount of methyl phenyl sulfoxide in the corresponding photoionization mass spectrum or the relative abundance at the plateau power and is presented in the fifth column. The last column indicates the relative abundance of the fragment in the 70 eV electron impact mass spectrum scaled to the amount of methyl phenyl sulfoxide.

Fragment	Wavenumber Maximum (cm^{-1})	Power Threshold (W)	Power Plateau (W)	Maximum Relative Abundance	Electron Impact Mass Spectrum Relative Abundance
$[C_6H_5]^+$	1067.5	0.5		0.095 ± 0.013	0.408
$[OSCH_3]^+$	1087.9	0.5		0.071 ± 0.007	0.131
$[HCS]^+$	1082.3	0.7		0.016 ± 0.003	0.097
$[C_4H_5]^+$	1081.1	0.6		0.019 ± 0.003	0.036
$[C_4H_3]^+$	1077.3	0.6		0.012 ± 0.002	0.244
$[CH_3]^+$	1086.9	0.6		0.100 ± 0.007	
$[C_6H_5SO]^+$	1058.9	0.0	0.6	0.062 ± 0.014	0.932
$[C_5H_5S]^+$	1086.9	0.0	1.3	0.129 ± 0.010	0.321
$[C_6H_8S]^{+\bullet}$	1050.4	0.0	1.2	0.006 ± 0.002	

3.3.1 Wavelength Dependence

At the time the CO_2 laser wavelength dependent photofragmentation measurements were made on methyl phenyl sulfoxide, the results were first disappointing but then found to be very interesting. Figure 3.24 on page 119 illustrates the time of flight photoionization mass spectrum (bottom), the 9R32 CO_2 laser line (1085.8 cm^{-1}) photofragmentation / photoionization mass spectrum (middle) and difference spectrum (top). Since this investigation was started prior to recording the mass spectra presented in section 3.1, the presence of the strong peak at 18 μs was disappointing because it was assumed, somewhat naively, that the photoionization process would also only produce the parent molecular ion as was observed with dimethyl sulfoxide. However, the identification of the strong peak at 18 μs and the weak peak at 23.5 μs proved to be rather interesting because of the implications involved with the mechanisms necessary to generate these species and will be dealt with in the next paragraph.

The identification of the various species in the time of flight mass spectra presented in figure 3.24 was trivialized by the representation of the mass spectra in figure 3.25 on page 121. The mass spectra in figure 3.25 have been normalized to the intensity of the parent molecular ion (140 amu) in the photoionization mass spectrum (bottom). The strong peak in the time of flight photoionization mass spectrum at 18 μs corresponds to the species at 78 amu while the weak peak at 23.5 μs correlates to 124 amu. As previously mentioned in section 3.1.3 on page 75, the species at 78 amu could

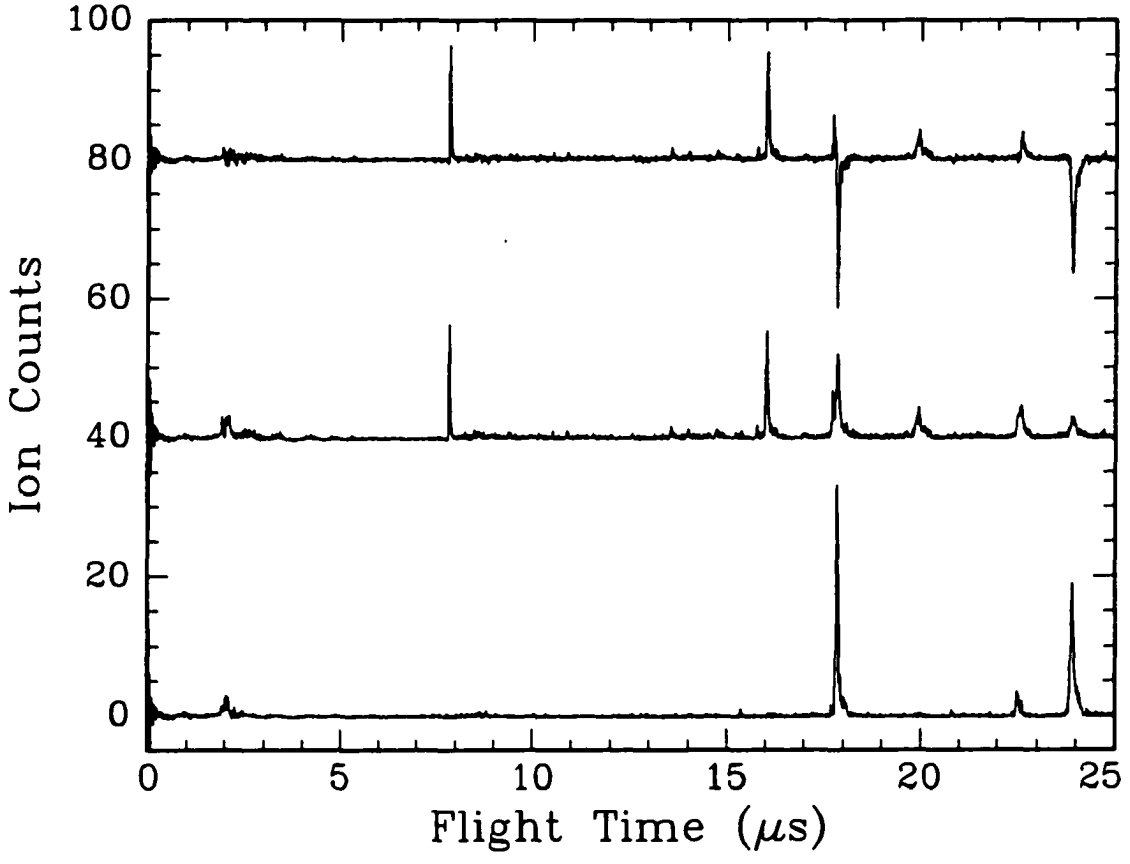

Figure 3.24: Methyl phenyl sulfoxide time of flight mass spectra (9R32 CO_2 laser line). The bottom spectrum was obtained with only the photoionization laser interacting with the molecule. The middle spectrum was obtained with first the CO_2 laser interacting with the sample followed by the photoionization laser. The top spectrum represents the difference between the two lower spectra. The sample pressure was 0.9×10^{-6} Torr.

either be $[C_2H_6SO]^{+\bullet}$ or $[C_6H_6]^{+\bullet}$. The presence of some dimethyl sulfoxide impurity in the methyl phenyl sulfoxide sample was ruled out since the only impurity was determined to be H_2O. The most likely explanation is that $[C_6H_6]^{+\bullet}$ was formed after the photoionization process by hydrogen migration from the methyl moiety to the phenyl group with cleavage of the bond between the sulfur atom and the C_6H_6 species

$$[(C_6H_5)(H_3C)SO]^{+\bullet} \rightarrow [(C_6H_6)]^{+\bullet} + H_2CSO. \tag{3.7}$$

The species at 124 amu corresponds to the loss of a methyl group and a hydrogen atom from the parent molecular ion and is represented as $[C_6H_4SO]^{+\bullet}$

$$[(C_6H_5)(H_3C)SO]^{+\bullet} \rightarrow [(C_6H_4)SO]^{+\bullet} + [CH_3]^{\bullet} + [H]^{\bullet}. \tag{3.8}$$

The 9R32 CO_2 laser line photofragmentation / photoionization mass spectrum in figure 3.25 presented some rather interesting product species. In particular, major product species were found at 15 ($[CH_3]^+$), 63 ($[OSCH_3]^+$), 77 ($[C_6H_5]^+$), 97 ($[C_5H_5S]^+$) and 125 amu ($[C_6H_5SO]^+$). With the exception of $[C_5H_5S]^+$, the rest of these represent simple cleavage products. The complementary pair $[C_6H_5SO]^+$ and $[CH_3]^+$ indicate cleavage of the bond between the sulfur atom and the methyl group in the parent molecular ion while the pair $[C_6H_5]^+$ and $[OSCH_3]^+$ involve breaking the bond between the phenyl group and the sulfur atom.

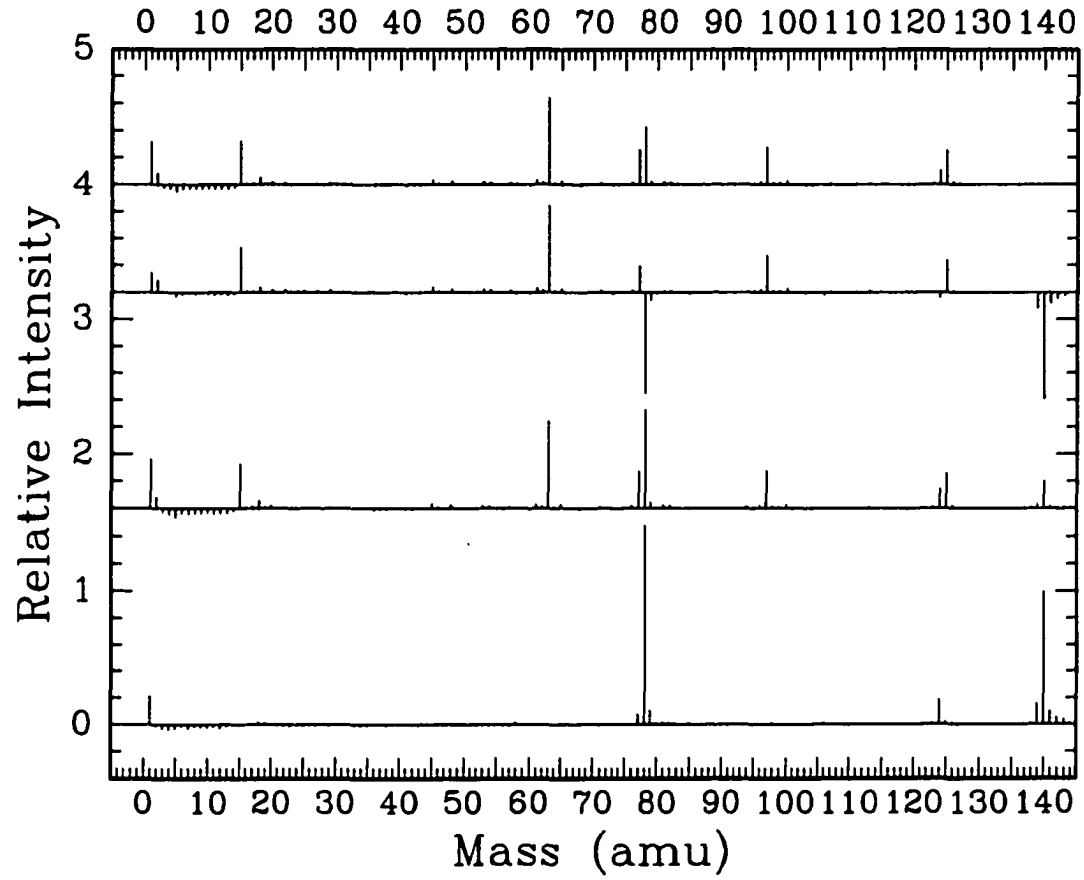

Figure 3.25: Methyl phenyl sulfoxide mass spectra (9R32 CO_2 laser line). The bottom spectrum is the corresponding stick mass spectrum to the photoionization mass spectrum in the previous figure (page 119). The second spectrum from the bottom correlates to the photofragmentation / photoionization mass spectrum in the previous figure. The second spectrum from the top represents the difference mass spectrum in the previous figure. The top spectrum indicates the photofragmentation species production due to the CO_2 laser. The intensities in all of the spectra were normalized to the value of the parent molecular ion at 140 amu in the photoionization mass spectrum.

The mechanism describing the formation of $[C_5H_5S]^+$ is more complicated than for the other major product species. The precursor to $[C_5H_5S]^+$ was determined to be $[C_6H_5OS]^+$ from the metastable species analysis of Bowie *et al.* [45]. The loss of CO seems to suggest that the oxygen atom was bonded to a carbon atom in this precursor molecular ion. From the ^{13}C isotope work performed by Siegel, the carbon atom bonded to the sulfur atom migrated to the oxygen atom [46]. A mechanism for the generation of $[C_5H_5S]^+$ starting from the parent molecular ion is as follows:

$$[(C_6H_5)(H_3C)SO]^{+\bullet} \rightarrow [H_3CSOC_6H_5]^{+\bullet} \quad (3.9)$$

$$[H_3CSOC_6H_5]^{+\bullet} \rightarrow [H_3C]^{\bullet} + [SOC_6H_5]^{+} \quad (3.10)$$

$$[SOC_6H_5]^{+} \rightarrow [OC_6H_5S]^{+} \quad (3.11)$$

$$[OC_6H_5S]^{+} \rightarrow CO + [C_5H_5S]^{+} \quad (3.12)$$

where $[OC_6H_5S]^+$ in equation 3.11 represents a migration of the sulfur atom from the oxygen atom to a carbon atom.

Several minor peaks also appear in the photofragmentation / photoionization mass spectrum of methyl phenyl sulfoxide presented in figure 3.25 on page 121. In particular, $[SO]^{+\bullet}$ (48 amu), $[C_4H_5]^+$ (53 amu) and $[HCS]^+$ (45 amu) are present in small amounts. These species, and a few others which were not as obvious, will be covered in more detail with the presentation of the CO_2 laser wavelength dependent results later in this section starting on page 126.

The benefit of the CO_2 laser production mass spectrum in figure 3.25 (top) on page 121 becomes apparent when $[C_6H_6]^{+\bullet}$ and $[C_6H_4SO]^{+\bullet}$ are considered. The difference mass spectrum (second from the top) seems to suggest that $[C_6H_6]^{+\bullet}$ and $[C_6H_4SO]^{+\bullet}$ were consumed when the CO_2 laser was introduced. However, by taking account of the presence of these species in the photoionization mass spectrum, the top mass spectrum shows that these species are also produced by the photofragmentation process.

The extensive photofragmentation observed in figures 3.24 (page 119) and 3.25 (page 121) was not maintained for all of the other CO_2 laser lines. Figures 3.26 (page 124) and 3.27 (page 125) were recorded at 1045.0 cm^{-1} (9P22 CO_2 laser line) and the only significant difference between the photoionization mass spectrum and the photofragmentation / photoionization mass spectrum was the presence of the peaks at 97, 112 and 125 amu. The peak at 125 amu ($[C_6H_5SO]^+$) from methyl phenyl sulfoxide corresponds with the peak at 63 amu ($[H_3CSO]^+$) from dimethyl sulfoxide observed in figure 3.11 on page 98 (i.e. the loss of a methyl group from the parent molecule). The fact that $[C_6H_5SO]^+$ appeared without the complementary pair species at $[CH_3]^+$ seems to suggest that the CO_2 laser generated an energetically excited parent molecule which was photoionized. The photoionization species fragmented to produce $[C_6H_5SO]^+$ and $[CH_3]^\bullet$.

The small number of different species in the CO_2 laser production mass spectrum (top spectrum) in figure 3.27 indicated that the parent molecule did not absorb as

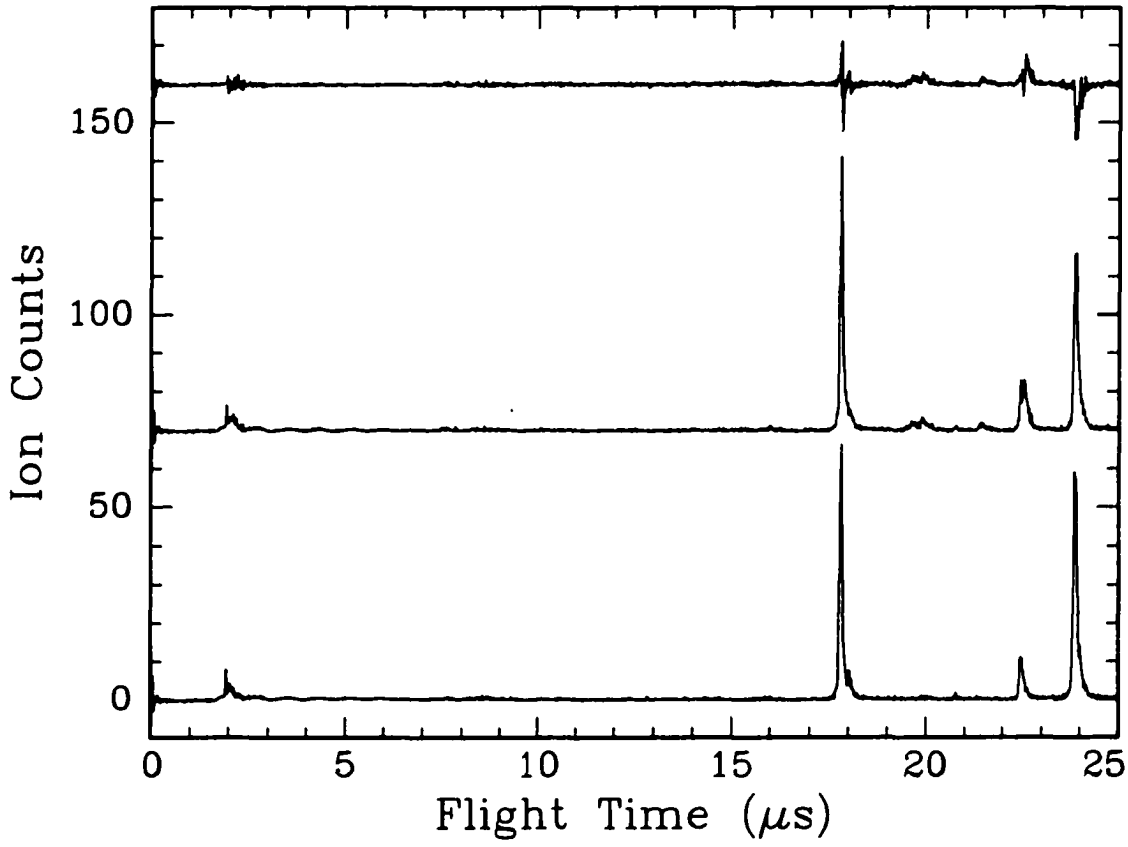

Figure 3.26: Methyl phenyl sulfoxide time of flight mass spectra (9P22 CO_2 laser line). The bottom spectrum was obtained with only the photoionization laser interacting with the molecule. The middle spectrum was obtained with first the CO_2 laser interacting with the sample followed by the photoionization laser. The top spectrum represents the difference between the two lower spectra. The sample pressure was 0.6×10^{-6} Torr.

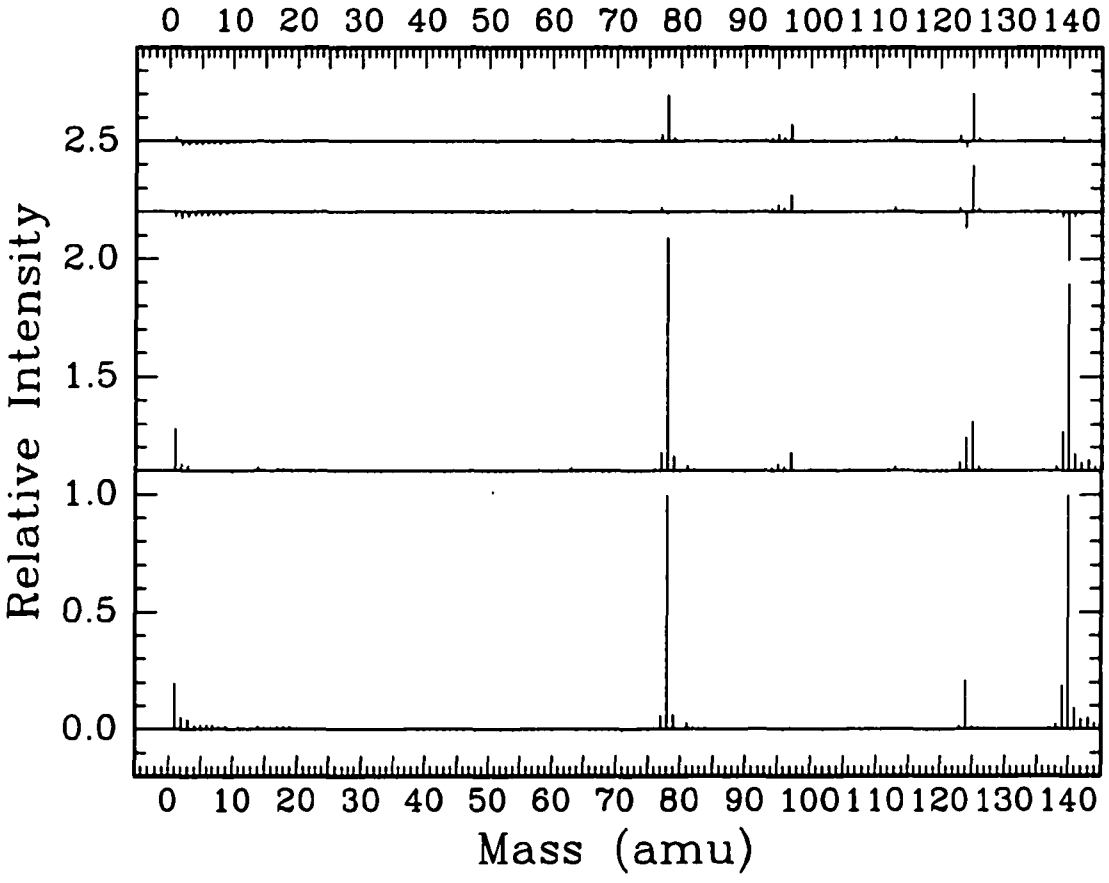

Figure 3.27: Methyl phenyl sulfoxide mass spectra (9P22 CO_2 laser line). The bottom spectrum is the corresponding stick mass spectrum to the photoionization mass spectrum in the previous figure (page 124). The second spectrum from the bottom correlates to the photofragmentation / photoionization mass spectrum in the previous figure. The second spectrum from the top represents the difference mass spectrum in the previous figure. The top spectrum indicates the photofragmentation species production due to the CO_2 laser. The intensities in all of the spectra were normalized to the value of the parent molecular ion at 140 amu in the photoionization mass spectrum.

much energy from the CO_2 laser at the 9P22 line (1045.0 cm^{-1}) as at the 9R32 line (1085.9 cm^{-1}).

The wavelength dependence of $[OSCH_3]^+$ is presented in figure 3.28 on page 127 and shows an interesting behaviour. Below 1050 cm^{-1}, very little $[OSCH_3]^+$ was formed. Between 1050 and 1080 cm^{-1} there was a slight increase in intensity from less than 0.05 to almost 0.2. Above 1080 cm^{-1}, there appears to be a large increase in abundance ending near 0.7 at 1087.9 cm^{-1}. Unfortunately, limitations with the CO_2 laser prevented the measurement of mass spectra above this wavenumber. Clearly, $[OSCH_3]^+$ displayed a strong photolysis wavelength dependence.

Figure 3.29 on page 128 shows the wavelength dependence of $[CH_3]^+$ which exhibited a similar behaviour as $[OSCH_3]^+$ but with some differences. For the CO_2 laser 9P branch of wavelengths (1045.0 to 1058.0 cm^{-1}), there was a slight increase in abundance as the wavenumber increased, ending at about 0.17. For the start of the 9R branch, the abundance was essentially constant at about 0.19 up to a wavenumber of 1080 cm^{-1}. Above this value, there was a large increase in abundance ending near 0.5 at 1087.9 cm^{-1}. Although the increase in abundance was not as much as was observed for $[OSCH_3]^+$, $[CH_3]^+$ also exhibited a strong photolysis wavelength dependence. The increased abundance of $[CH_3]^+$ between 1050 and 1078 cm^{-1} was probably due to the mechanism(s) responsible for forming $[CH_3]^+$ being favoured over the mechanism(s) for $[OSCH_3]^+$ when the parent molecule did not absorb as much energy from the CO_2 laser beam as it did near 1088 cm^{-1}.

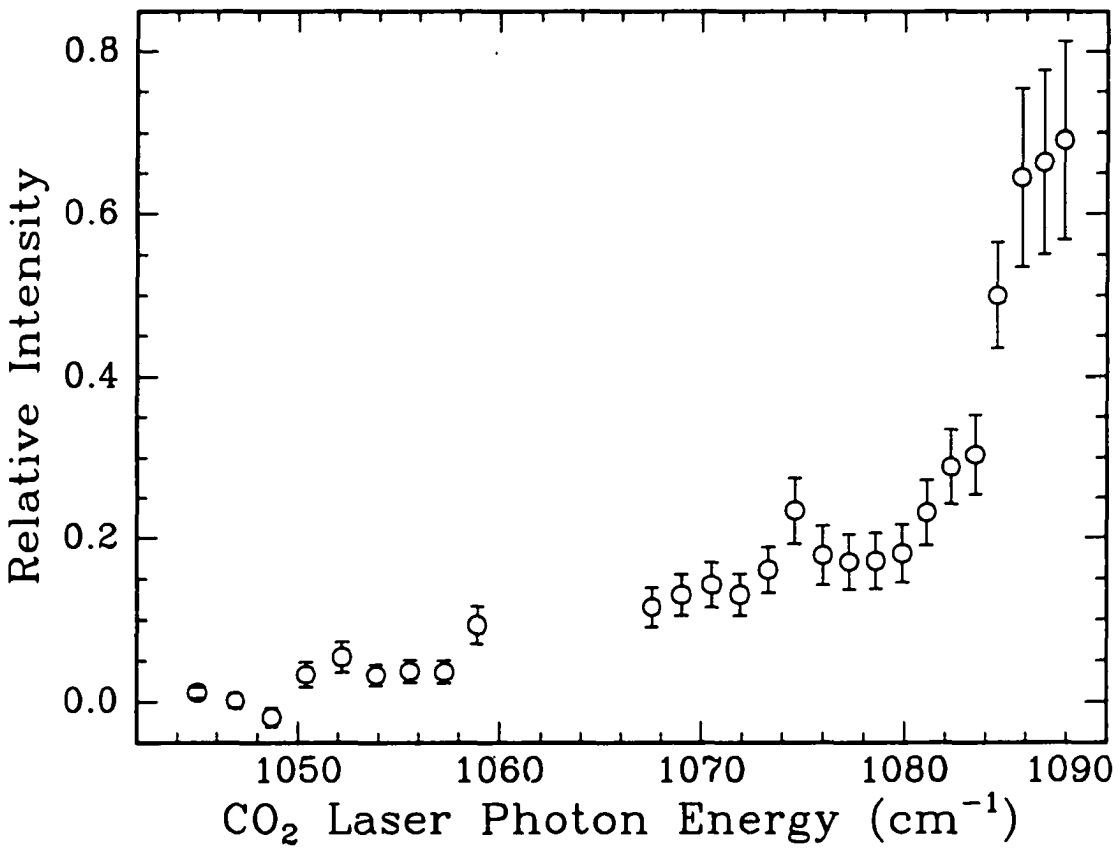

Figure 3.28: Methyl phenyl sulfoxide wavelength dependence for mass 63 amu ($[OSCH_3]^+$). The intensities were obtained from the CO_2 laser production mass spectra and have been normalized to the abundance of the parent molecular ion at 140 amu in the corresponding photoionization mass spectra.

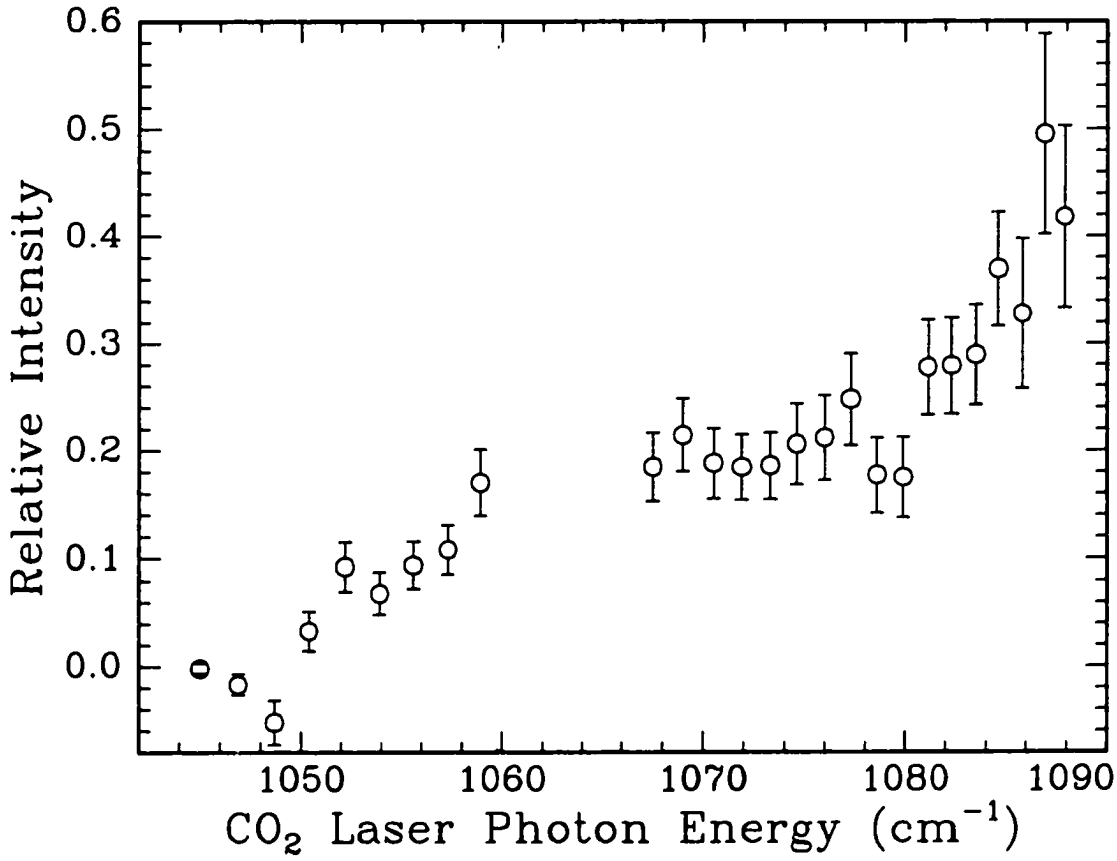

Figure 3.29: Methyl phenyl sulfoxide wavelength dependence for mass 15 amu ($[CH_3]^+$). The intensities were obtained from the CO_2 laser production mass spectra and have been normalized to the abundance of the parent molecular ion at 140 amu in the corresponding photoionization mass spectra.

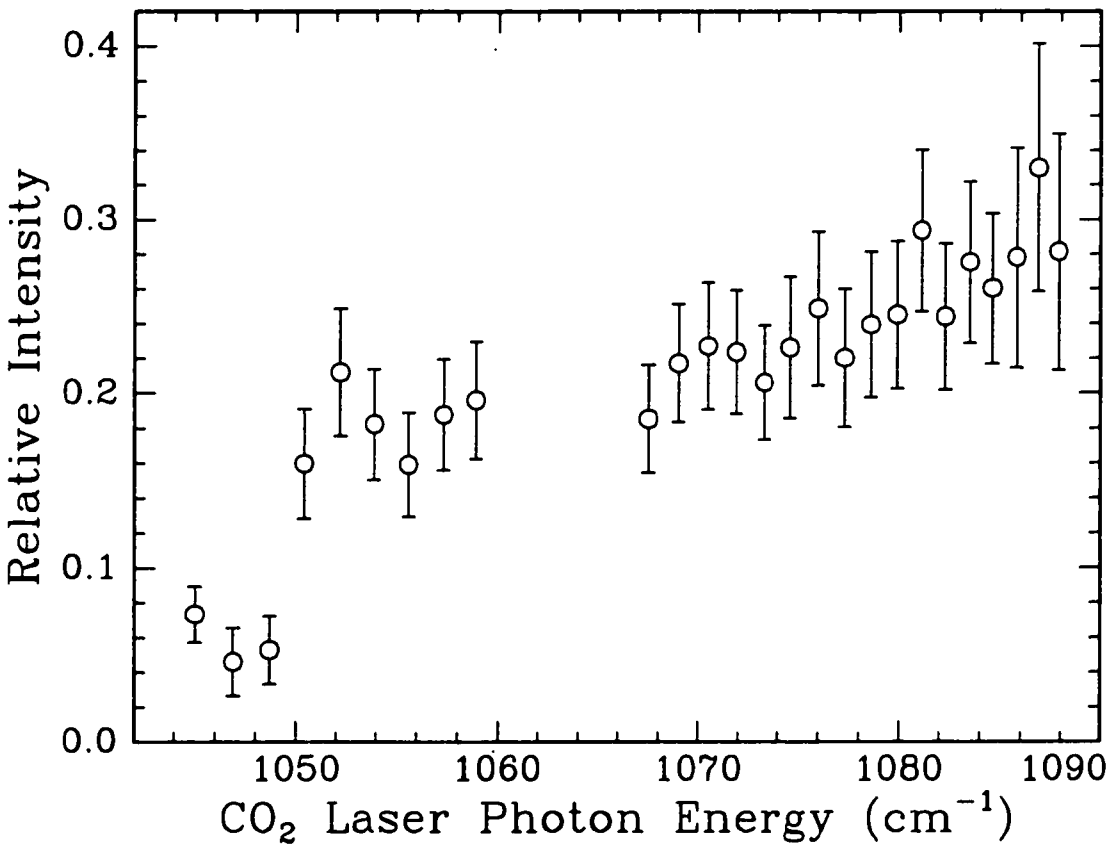

Figure 3.30: Methyl phenyl sulfoxide wavelength dependence for mass 97 amu ($[C_5H_5S]^+$). The intensities were obtained from the CO_2 laser production mass spectra and have been normalized to the abundance of the parent molecular ion at 140 amu in the corresponding photoionization mass spectra.

Even though $[C_5H_5S]^+$ is not a simple cleavage product like $[OSCH_3]^+$ and $[CH_3]^+$, it also had a strong photolysis wavelength dependence as seen in figure 3.30 on page 129. Below 1050 cm^{-1}, an abundance of less than 0.1 was observed. Above this wavenumber, however, the abundance suddenly doubled and slowly increased to around 0.3 at 1087.9 cm^{-1}. $[C_5H_5S]^+$ does show a photolysis wavelength dependence although not as strong as was observed with $[OSCH_3]^+$ and $[CH_3]^+$.

Figure 3.31 on page 131 illustrates the photolysis wavelength dependence for $[HCS]^+$ and $[C_4H_5]^+$ and both species exhibited a different behaviour from what was observed with the other fragmentation species. $[HCS]^+$ was also generated in the photolysis of dimethyl sulfoxide and the wavelength dependence was presented in figure 3.14 on page 102. In both cases, $[HCS]^+$ showed a wavelength dependence but the specific behaviour was different. In figure 3.31, the intensity increased as the wavenumber was increased to around 1084 cm^{-1}. Above this wavenumber, it appears that the abundance decreased. Since this was also the region that $[OSCH_3]^+$ showed a sharp increase (figure 3.28 on page 127), it would seem that a mechanism responsible for generating $[OSCH_3]^+$ was preventing the formation of $[HCS]^+$. One explanation is that above 1084 cm^{-1}, the parent molecule absorbed a sufficient amount of energy to quickly cleave the bond between the sulfur atom and the phenyl group and so few excited methyl phenyl sulfoxide molecules were left to create $[HCS]^+$. Below this wavenumber, the simple bond cleavage reaction did not readily occur and so more excited methyl phenyl sulfoxide molecules were able to explore the region of the

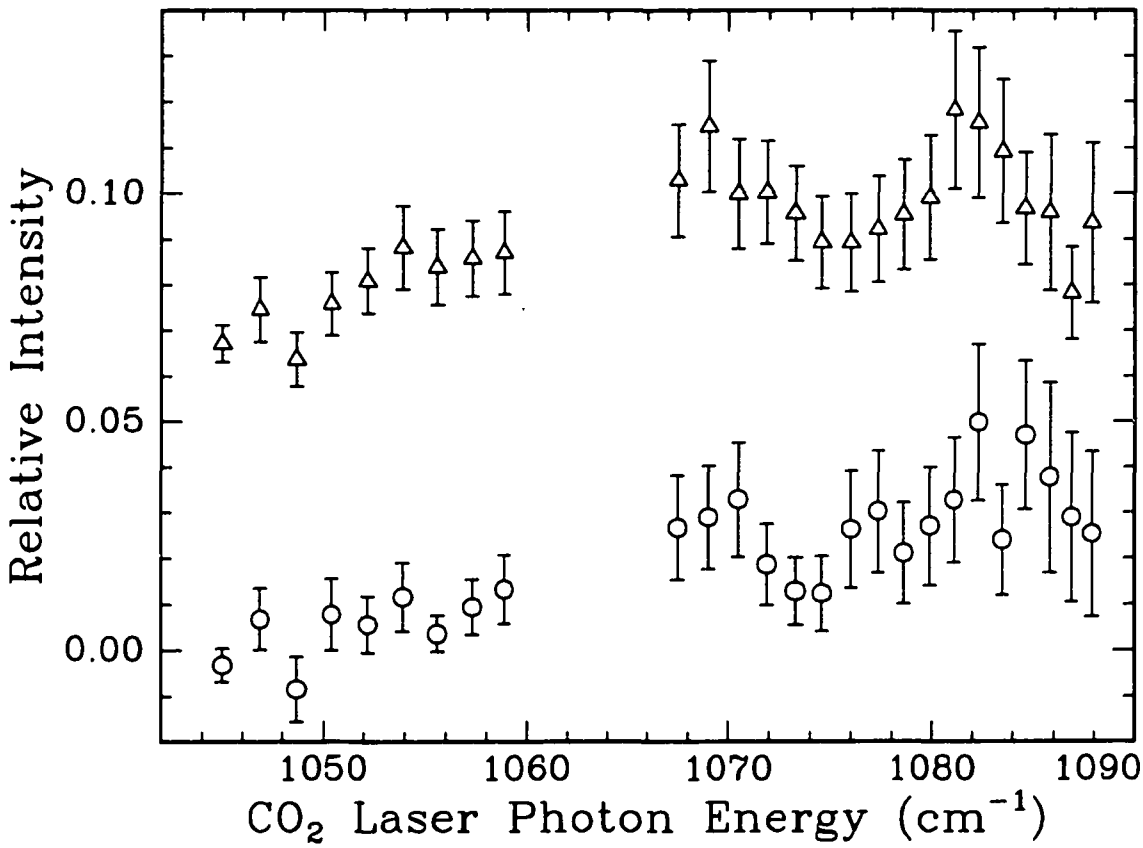

Figure 3.31: Methyl phenyl sulfoxide wavelength dependence for masses 45 and 53 amu. The open circle data represent $[HCS]^+$ (45 amu). The open triangle data correlate to $[C_4H_5]^+$ (53 amu) and have been shifted up by 0.07. The intensities were obtained from the CO_2 laser production mass spectra and have been normalized to the abundance of the parent molecular ion at 140 amu in the corresponding photoionization mass spectra.

potential energy surface which leads to the formation of $[HCS]^+$.

As previously mentioned, $[C_4H_5]^+$ displayed a similar behaviour to $[HCS]^+$ with one main difference. For clarity purposes, the intensity data for $[C_4H_5]^+$ have been shifted up by 0.07 in figure 3.31. $[C_4H_5]^+$ also showed a slight increase in abundance as the wavenumber was increased around 1080 cm^{-1} but then the abundance dropped as the wavenumber was increased above 1080 cm^{-1} which was a slightly different wavenumber than for $[HCS]^+$ (1084 cm^{-1}).

An interesting photolysis wavelength dependence occurred for $[C_6H_8S]^{+\bullet}$ and is presented in figure 3.32 on page 133. With this fragmentation species, the maximum intensity occurred at around 1050 cm^{-1}. It appears that above this wavenumber, the abundance decreased. Since the other wavelength dependent figures show maxima between 1080 and 1090 cm^{-1}, $[C_6H_8S]^{+\bullet}$ must represent an unfavourable product species. The product channel for $[C_6H_8S]^{+\bullet}$ is probably readily accessible energetically but is only entered when no other product channels are available for the excited molecule. This may be another example of a fragmentation species which is slow to develop. Bowie *et al.* identify this species as originating from the parent molecular ion with the loss of CO through the presence of the appropriate metastable peak [45]. This implies not only the migration of the phenyl group to the oxygen atom but also the migration of the sulfur atom (with the methyl group still attached) to a different carbon atom in the phenyl ring. With both migrations and the loss of the carbonyl group, it seems reasonable to assume that this fragmentation species would be slow

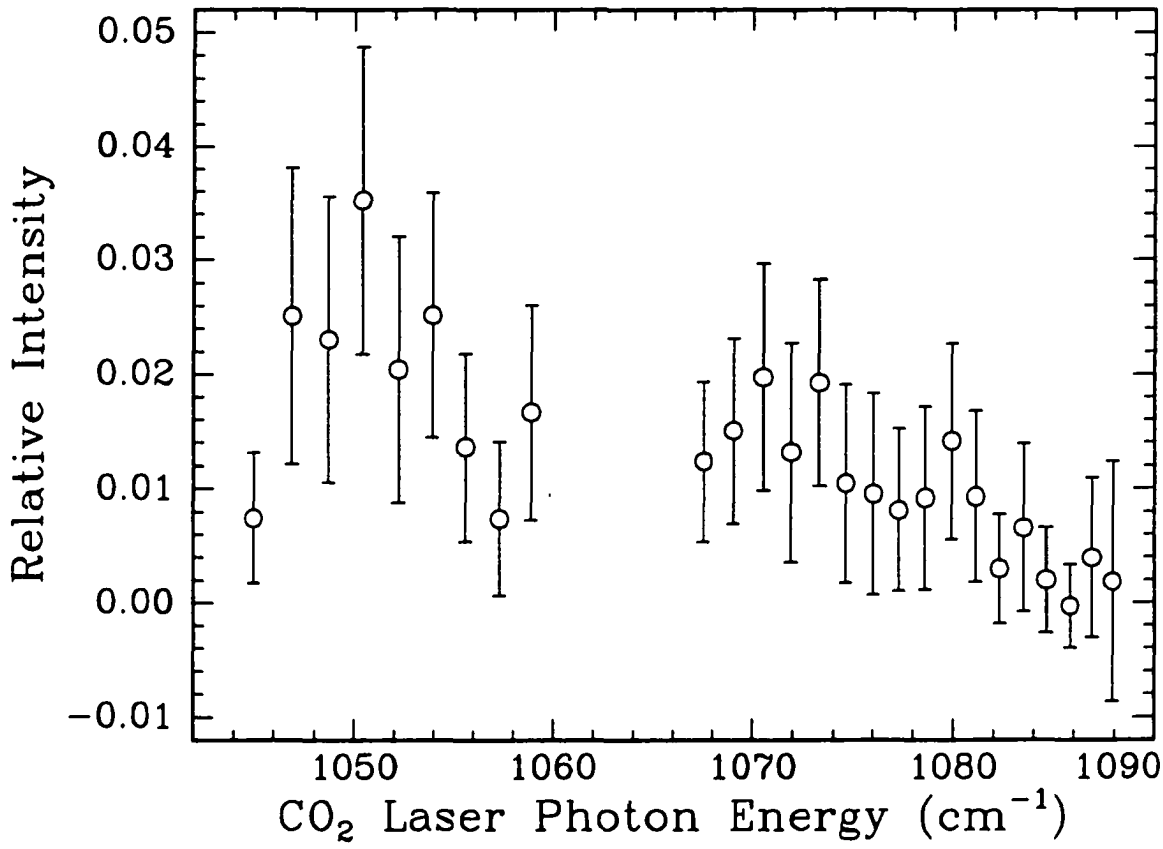

Figure 3.32: Methyl phenyl sulfoxide wavelength dependence for mass 112 amu ($[C_6H_8S]^{+\bullet}$). The intensities were obtained from the CO_2 laser production mass spectra and have been normalized to the abundance of the parent molecular ion at 140 amu in the corresponding photoionization mass spectra.

to develop.

3.3.2 Power Dependence

Increasing the output power of the CO_2 laser at the appropriate wavelength with dimethyl sulfoxide has already demonstrated the ability to increase the number and abundance of the photofragmentation products and the abundance of each species (section 3.2.2 starting on page 104) and so a similar investigation with methyl phenyl sulfoxide should also be beneficial. Figures 3.33 (page 136) and 3.34 (page 137) illustrate the time of flight mass spectra and regular mass spectra for methyl phenyl sulfoxide recorded at a sample pressure of 2.5×10^{-6} Torr with an output power of 1.6 W at the 9R32 CO_2 laser line (1085.8 cm^{-1}). Since the intensity maxima for $[HCS]^+$ and $[C_4H_5]^+$ occurred near this wavelength, varying the CO_2 laser output power when the laser was tuned to the 9R32 line should provide information on a variety of photofragmentation species. Selection of a higher wavenumber laser line would favour the major cleavage products at the expense of some of the less favourable reactions. A disadvantage with using a higher wavenumber was that the maximum output power at these higher lines is lower because of the lower relative population of the higher rotational levels for these CO_2 laser lines. Another advantage with selecting the 9R32 line was that it allows for a comparison with the power dependent study of dimethyl sulfoxide. At the time when the power dependent mass spectra were recorded, it was thought that the sample pressure for the wavelength dependent mass

spectra of methyl phenyl sulfoxide was almost the same as for dimethyl sulfoxide. Consequently, a much higher sample pressure was used with the power dependent mass spectra (2.5×10^{-6} Torr) than with the wavelength dependent mass spectra (0.8×10^{-6} Torr).

Although the amount of the parent molecular ion depleted was small, there was a large variety of photofragmentation species observed in the photofragmentation / photoionization mass spectrum of methyl phenyl sulfoxide with the 9R32 CO_2 laser line at an output power of 1.6 W (figure 3.34). The major product species were $[CH_3]^+$ (15 amu), $[OSCH_3]^+$ (63 amu), $[C_6H_5]^+$ (77 amu), $[C_6H_6]^{+\bullet}$ (78 amu), $[C_5H_5S]^+$ (97 amu), $[C_6H_4SO]^{+\bullet}$ (124 amu) and $[C_6H_5SO]^+$ (125 amu). Minor peaks were observed at 45 ($[HCS]^+$), 48 ($[SO]^{+\bullet}$), 51 ($[C_4H_3]^+$) and 53 amu ($[C_4H_5]^+$).

The time of flight mass spectra and regular mass spectra for methyl phenyl sulfoxide measured with the 9R32 CO_2 laser line (1085.8 cm^{-1}) and an output power of 0.1 W at a sample pressure of 2.5×10^{-6} Torr are presented in figures 3.35 (page 138) and 3.36 (page 139) and show very few photofragmentation species. Despite the anomalous result that the parent molecular ion intensity was larger in the photofragmentation / photoionization mass spectrum (second from the bottom) than in the photoionization mass spectrum (bottom), very few photofragmentation species were observed. A slight change in abundance was observed for the peaks at 77 ($[C_6H_5]^+$), 78 ($[C_6H_6]^{+\bullet}$) and 97 amu ($[C_5H_5S]^+$).

The CO_2 laser power dependence for the complementary pair 63 ($[OSCH_3]^+$) and

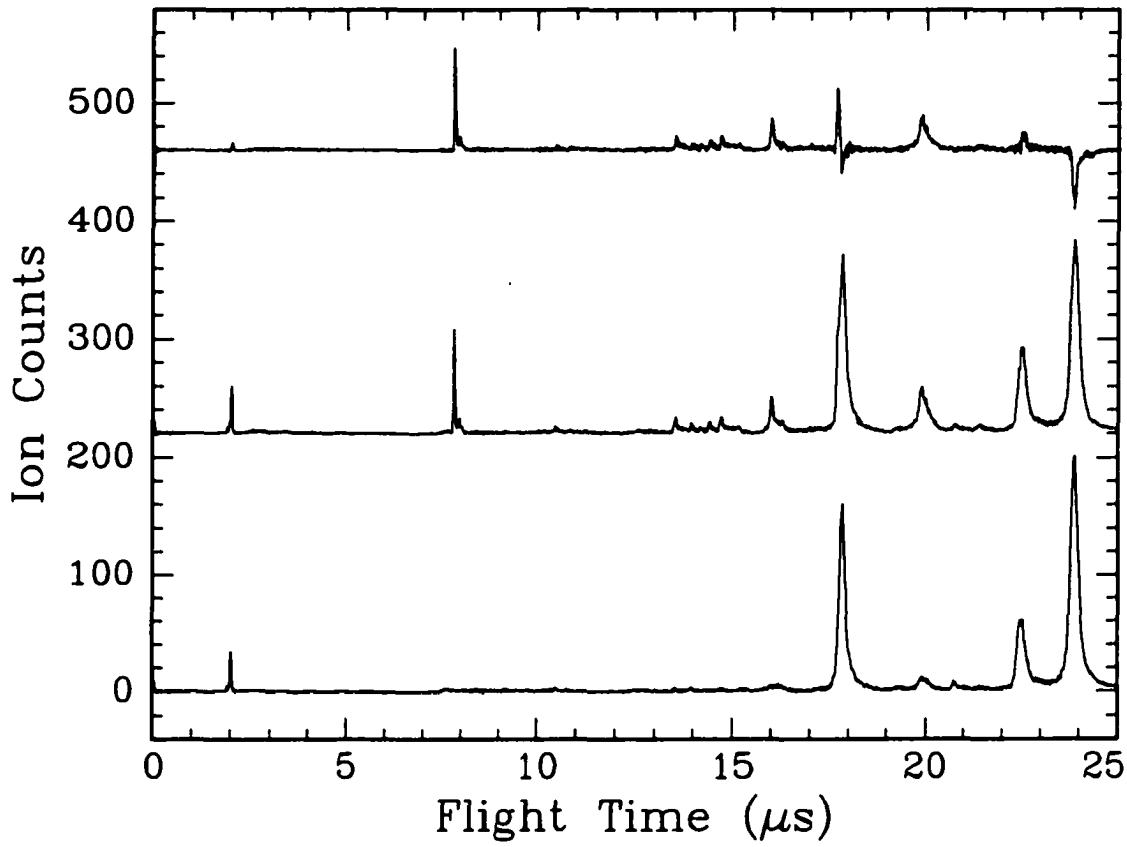

Figure 3.33: Methyl phenyl sulfoxide time of flight mass spectra (9R32 CO_2 laser line, 1.6 W). The bottom spectrum was obtained with only the photoionization laser interacting with the molecule. The middle spectrum was obtained with first the CO_2 laser interacting with the sample followed by the photoionization laser. The top spectrum represents the difference between the two lower spectra. The sample pressure was 2.5×10^{-6} Torr.

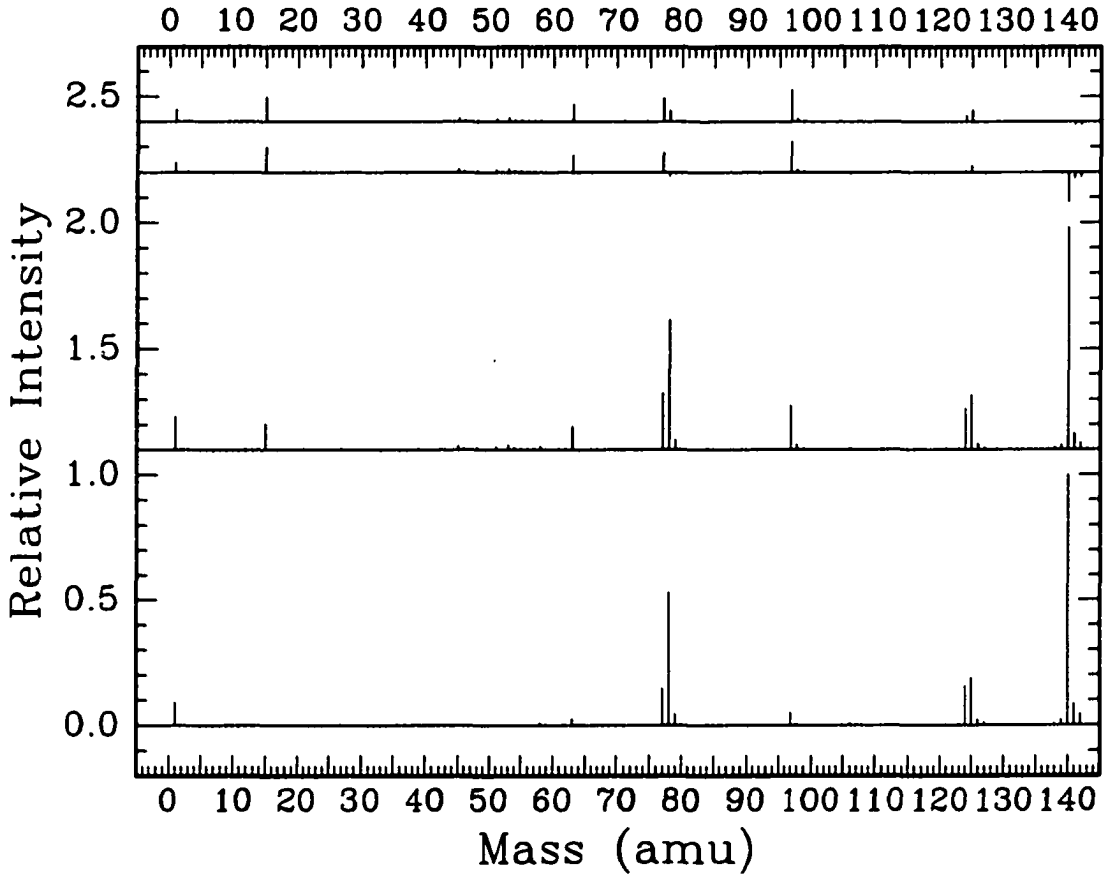

Figure 3.34: Methyl phenyl sulfoxide mass spectra (9R32 CO_2 laser line, 1.6 W). The bottom spectrum is the corresponding stick mass spectrum to the photoionization mass spectrum in the previous figure (page 136). The second spectrum from the bottom correlates to the photofragmentation / photoionization mass spectrum in the previous figure. The second spectrum from the top represents the difference mass spectrum in the previous figure. The top spectrum indicates the photofragmentation species production due to the CO_2 laser. The intensities in all of the spectra were normalized to the value of the parent molecular ion at 140 amu in the photoionization mass spectrum.

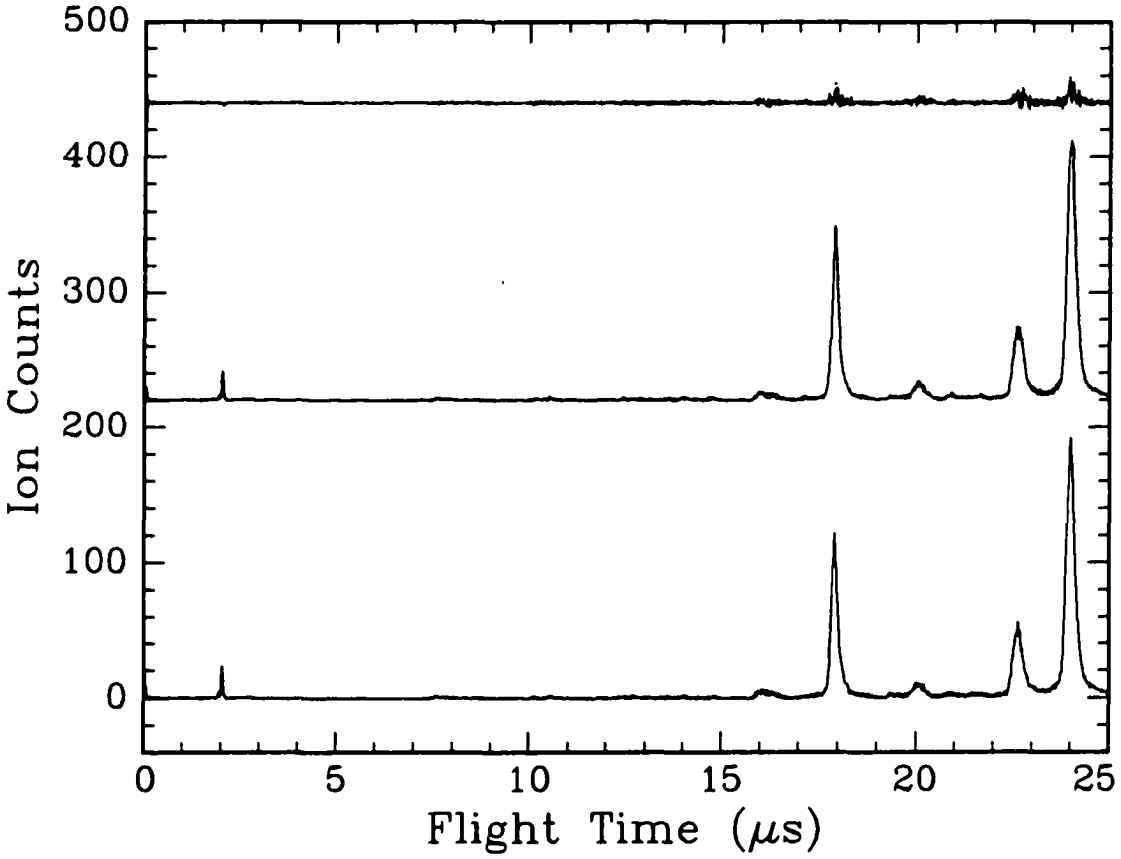

Figure 3.35: Methyl phenyl sulfoxide time of flight mass spectra (9R32 CO_2 laser line, 0.1 W). The bottom spectrum was obtained with only the photoionization laser interacting with the molecule. The middle spectrum was obtained with first the CO_2 laser interacting with the sample followed by the photoionization laser. The top spectrum represents the difference between the two lower spectra. The sample pressure was 2.5×10^{-6} Torr.

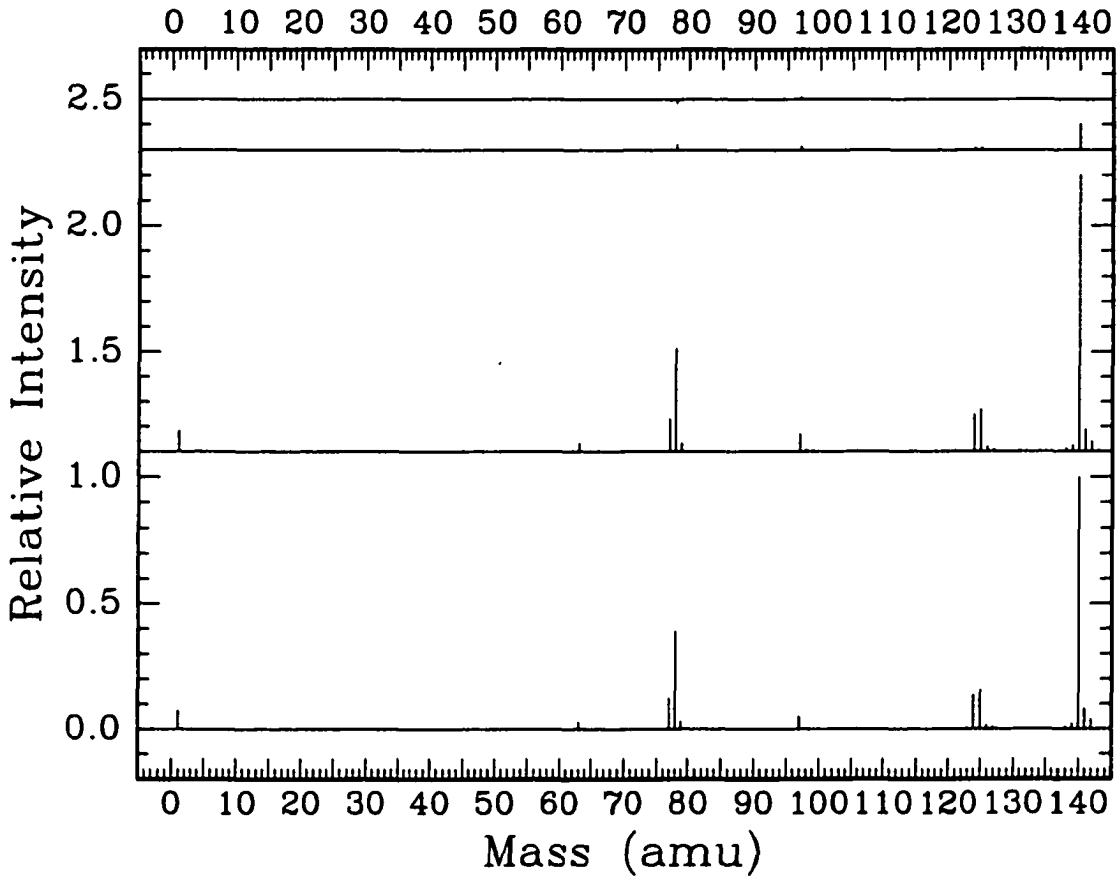

Figure 3.36: Methyl phenyl sulfoxide mass spectra (9R32 CO_2 laser line, 0.1 W). The bottom spectrum is the corresponding stick mass spectrum to the photoionization mass spectrum in the previous figure (page 138). The second spectrum from the bottom correlates to the photofragmentation / photoionization mass spectrum in the previous figure. The second spectrum from the top represents the difference mass spectrum in the previous figure. The top spectrum indicates the photofragmentation species production due to the CO_2 laser. The intensities in all of the spectra were normalized to the value of the parent molecular ion at 140 amu in the photoionization mass spectrum.

77 amu ($[C_6H_5]^+$) generated by the simple cleavage of the bond between the sulfur atom and the phenyl group is illustrated in figure 3.37 on page 141. For clarity purposes, the intensity data of the $[OSCH_3]^+$ species have been shifted up by 0.06. The power dependence for $[OSCH_3]^+$ represented in figure 3.37 is similar to what was observed for dimethyl sulfoxide in figure 3.20 on page 112. In both cases, below 0.5 W, there was virtually no $[OSCH_3]^+$ produced as the output power was increased from 0.0 to 0.5 W. At this threshold value, a jump in abundance was observed with an increased slope as the output power was increased to 1.6 W, the maximum power that could be used at the 9R32 CO_2 laser line. Even though the complementary species is different between dimethyl sulfoxide ($[H_3C]^+$) and methyl phenyl sulfoxide ($[C_6H_5]^+$), they both show a similar power dependence. Virtually no $[C_6H_5]^+$ was observed below 0.5 W, while above this threshold, the slope increased such that the abundance at 1.6 W was approximately 0.10.

Another noteworthy result presented in figure 3.37 is the significantly low intensities observed at a CO_2 laser output power of 1.0 and 1.1 W. Because the error bars represent the 95% confidence intervals, either the deviation from the best fit line is significant or a systematic error has occurred. A problem also occurs with figure 3.38 on page 142 and figure 3.39 on page 144. This means that a systematic error has occurred, most likely that the CO_2 laser intensity at the centre of the chamber was much weaker than the expected value. Unfortunately, time constraints meant that these measurements could not be repeated to correct this problem with the data.

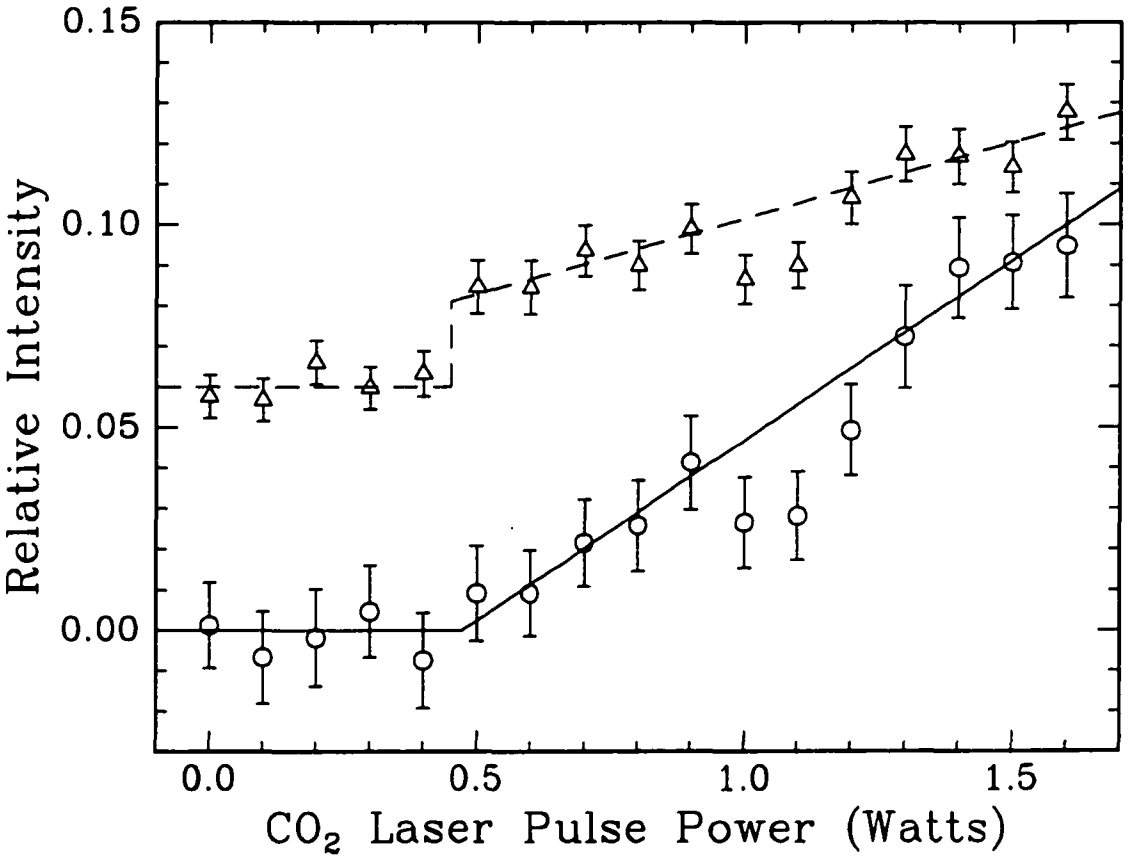

Figure 3.37: Methyl phenyl sulfoxide power dependence for masses 63 and 77 amu. The open triangle data fitted by the dashed line represent $[OSCH_3]^+$ (63 amu) and have been shifted up by 0.06. The open circle data fitted by the solid line correlate to $[C_6H_5]^+$ (77 amu). The intensities were obtained from the CO_2 laser production mass spectra and have been normalized to the abundance of the parent molecular ion at 140 amu in the corresponding photoionization mass spectra.

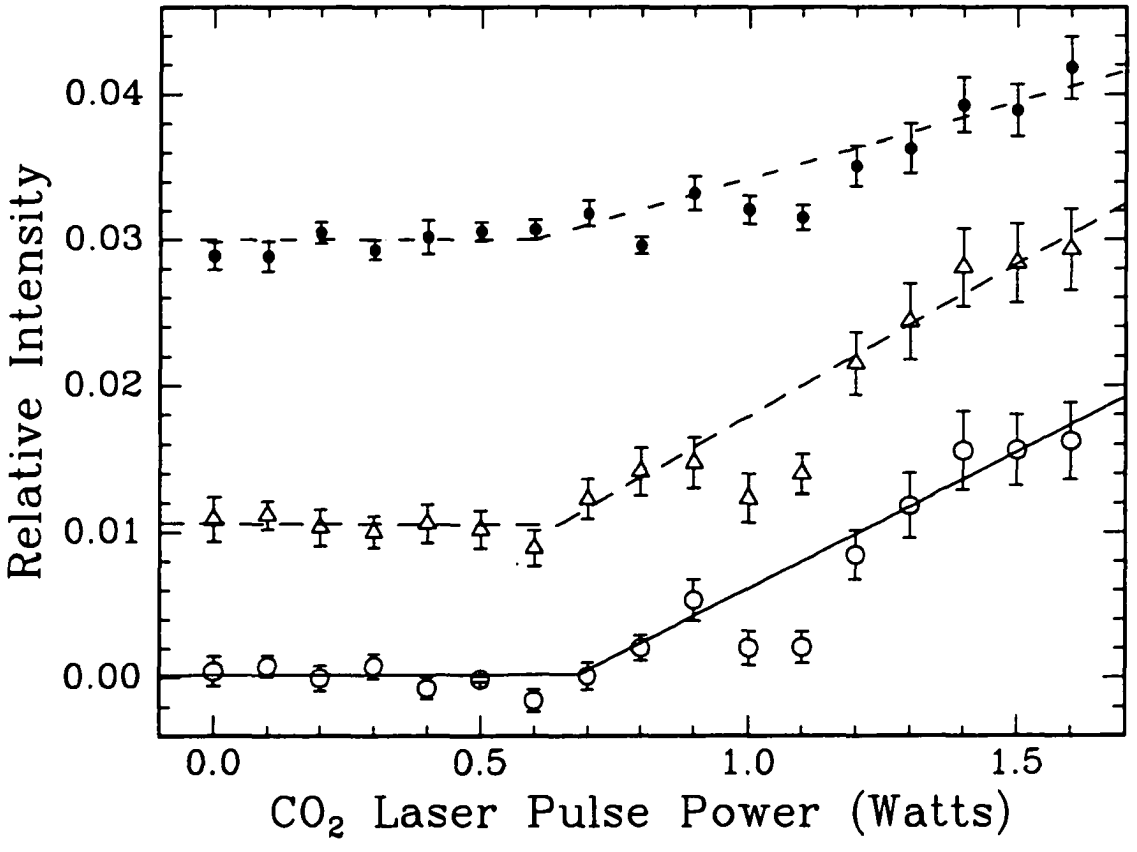

Figure 3.38: Methyl phenyl sulfoxide power dependence for masses 45, 53 and 51 amu. The open circle data fitted by the solid line correspond to $[HCS]^+$ (45 amu). The open triangle data fitted by the dashed line represent $[C_4H_5]^+$ (53 amu) and have been shifted up by 0.01. The filled in circle data fitted by the dot-dashed line are for $[C_4H_3]^+$ (51 amu) and have been shifted up by 0.03. The intensities were obtained from the CO_2 laser production mass spectra and have been normalized to the abundance of the parent molecular ion at 140 amu in the corresponding photoionization mass spectra.

A similar power dependence was observed for $[HCS]^+$ (45 amu), $[C_4H_5]^+$ (53 amu) and $[C_4H_3]^+$ (51 amu) and is presented in figure 3.38 on page 142. For clarity purposes, the intensity data for $[C_4H_5]^+$ have been shifted up by 0.01 while the data for $[C_4H_3]^+$ have been shifted up by 0.03. All three of these species show a threshold at around 0.6 W where a sharp increase in the slope occurred. Because these three species all represent products which are expected to involve mechanisms with several steps, a higher threshold power would be expected in order to form these three ions than for the simple cleavage product $[C_6H_5]^+$.

The power dependence of the second simple cleavage complementary product pair ($[C_6H_5SO]^+$ and $[CH_3]^+$) is illustrated in figure 3.39 on page 144 and one species showed the same behaviour as the other fragmentation species ($[CH_3]^+$) while the other displayed a somewhat different behaviour ($[C_6H_5SO]^+$). The intensity data for the $[C_6H_5SO]^+$ species have been shifted up by 0.06 for clarity. The abundance of $[C_6H_5SO]^+$ increased at low output power, but around 0.6 W it appeared to level off. Virtually no $[CH_3]^+$ was observed until the threshold value of approximately 0.6 W when the intensity increased in abundance up to about 0.10 at 1.6 W. It appears that once the threshold for generating $[CH_3]^+$ has been achieved, no additional $[C_6H_5SO]^+$ is formed and the abundance plateaus to the intensity at 0.6 W. A decrease in intensity could be accounted for by the large mass fragmentation species itself fragmenting into other product ions. The plateau would then be caused by a balance between an increase in the CO_2 laser output power generating more $[C_6H_5SO]^+$ and this species

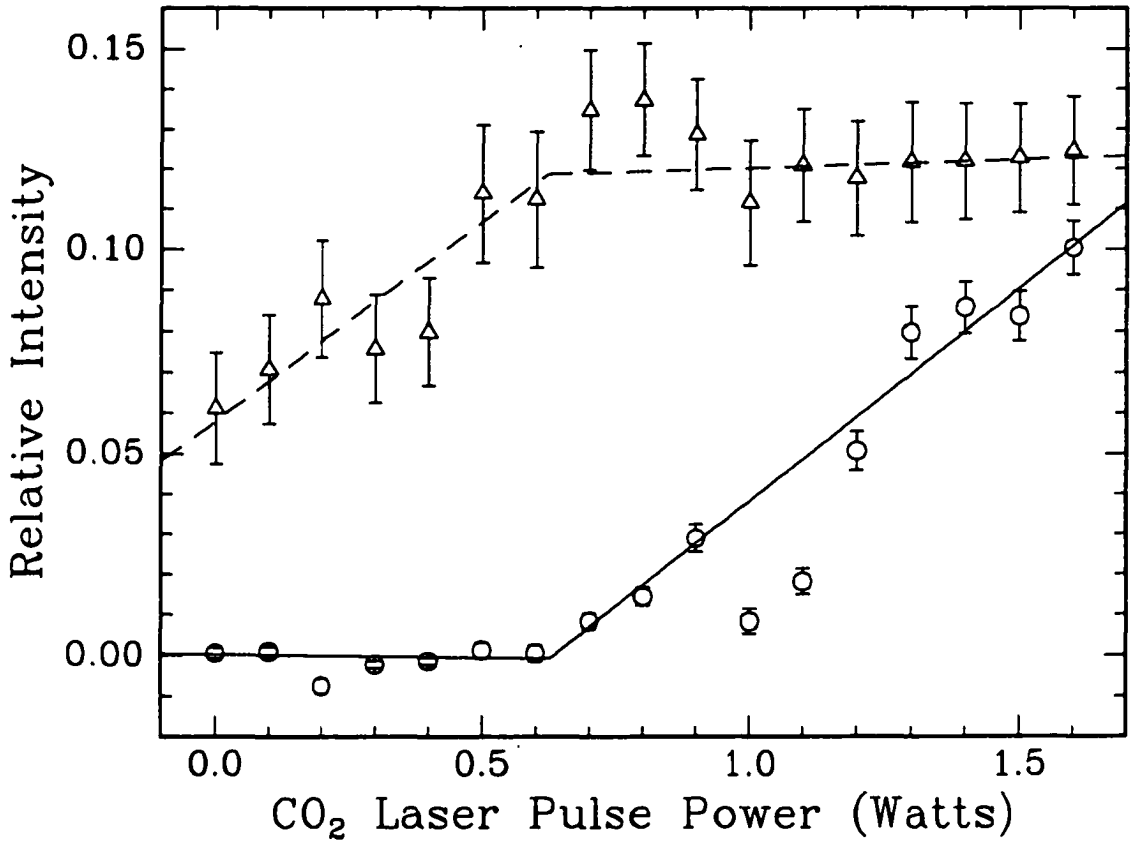

Figure 3.39: Methyl phenyl sulfoxide power dependence for masses 15 and 125 amu. The open circle data fitted by the solid line represent $[CH_3]^+$ (15 amu). The open triangle data fitted by the dashed line correspond to $[C_6H_5SO]^+$ (125 amu) and have been shifted up by 0.06. The intensities were obtained from the CO_2 laser production mass spectra and have been normalized to the abundance of the parent molecular ion at 140 amu in the corresponding photoionization mass spectra.

further fragmenting into other product ions.

The power dependence for two other large mass fragmentation species ($[C_5H_5S]^+$ and $[C_6H_8S]^{+\bullet}$) are presented in figures 3.40 (page 146) and 3.41 (page 147). In general, both $[C_5H_5S]^+$ (figure 3.40) and $[C_6H_8S]^{+\bullet}$ (figure 3.41) follow the same power dependent behaviour as $[C_6H_5SO]^+$ (figure 3.39 on page 144). Instead of plateauing at around 0.6 W, these two species level off at approximately 1.3 W. Regardless of the power at which the intensity plateau occurred, the decrease from the expected abundance can be explained by these relatively large mass species also further fragmenting into other product ions.

3.4 *sec*-Butyl Methyl Sulfoxide Infrared Photolysis

Although methyl phenyl sulfoxide yielded some interesting information towards providing an insight into the mechanisms involved with the fragmentation of simple sulfoxide molecules, replacing the phenyl group with a fully saturated hydrocarbon like a butyl group should produce some additional information. The butyl group in *sec*-butyl methyl sulfoxide is bonded to the sulfur atom at a secondary carbon and should provide a larger variety of fragmentation species than if the sulfur was bonded to a terminal carbon in the butyl chain because of the two different alkyl groups (methyl and ethyl) attached to the secondary carbon. The infrared multiple-photon dissociation study of *sec*-butyl methyl sulfoxide involved the same two parts as dimethyl sulfoxide and methyl phenyl sulfoxide. The first part varied the CO_2

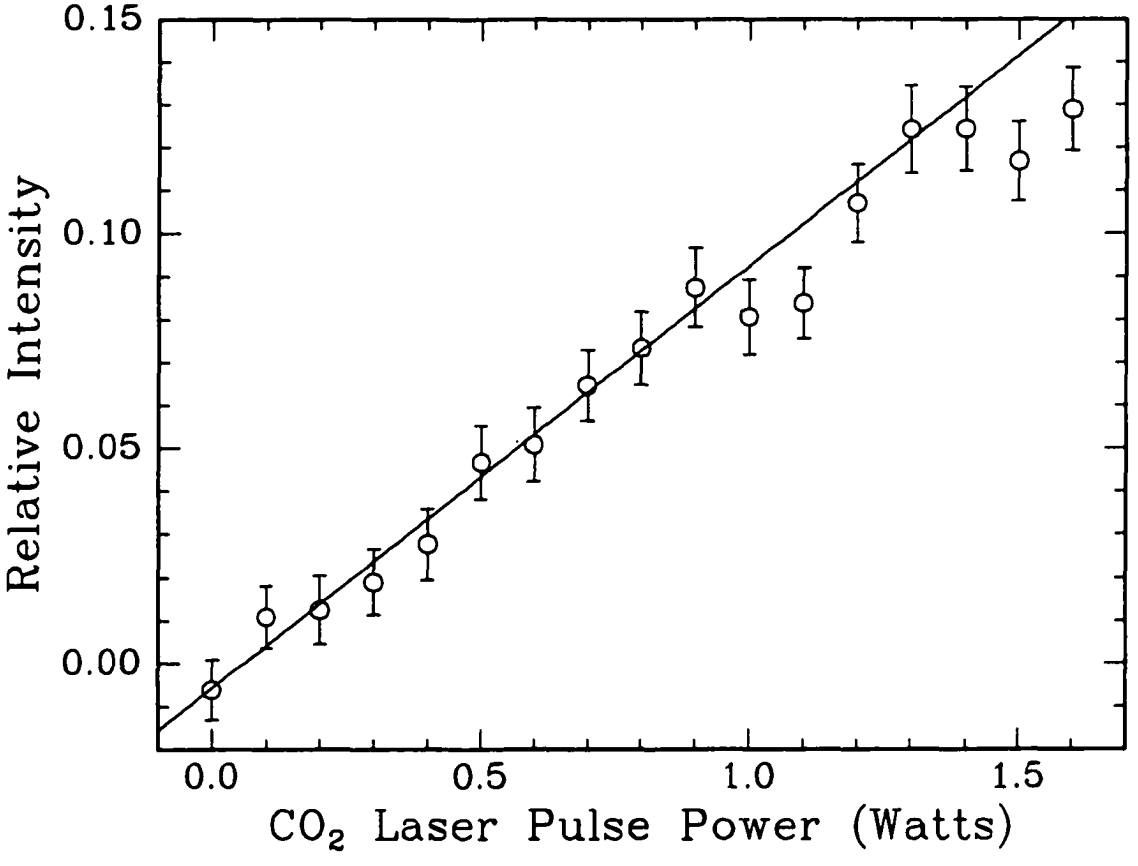

Figure 3.40: Methyl phenyl sulfoxide power dependence for mass 97 amu ($[C_5H_5S]^+$). The intensities were obtained from the CO_2 laser production mass spectra and have been normalized to the abundance of the parent molecular ion at 140 amu in the corresponding photoionization mass spectra.

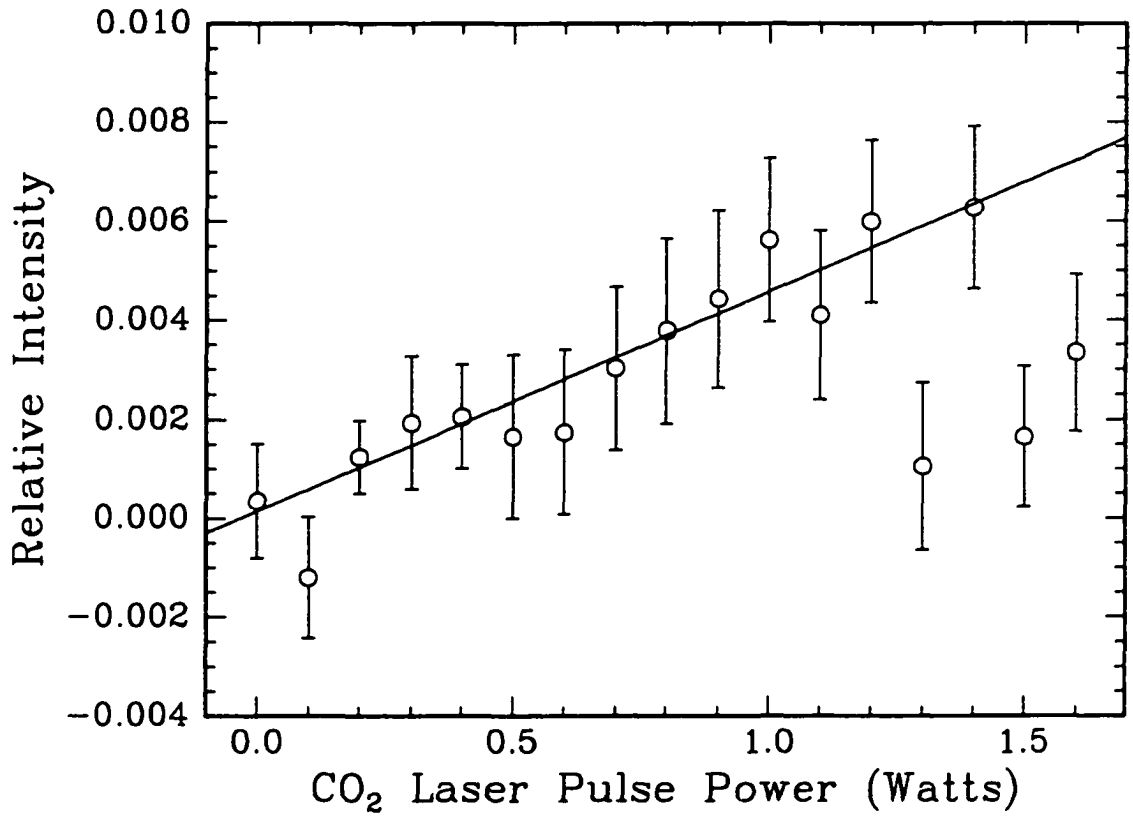

Figure 3.41: Methyl phenyl sulfoxide power dependence for mass 112 amu ($[C_6H_8S]^{+\bullet}$). The intensities were obtained from the CO_2 laser production mass spectra and have been normalized to the abundance of the parent molecular ion at 140 amu in the corresponding photoionization mass spectra.

laser wavenumber from 1087.9 cm^{-1} (9R36 line) to 1067.5 cm^{-1} (9R04 line) and 1058.9 cm^{-1} (9P06 line) to 1033.6 cm^{-1} (9P34 line). The CO_2 laser output power was set to 1.0 W for each laser line. The sample pressure was 3.3×10^{-6} Torr for the 9R36 line down to the 9P22 line (1045.0 cm^{-1}) and 2.2×10^{-6} Torr for the 9P24 (1042.9 cm^{-1}) to 9P34 line. The latter group were recorded on a separate day from the rest of the wavelength dependent mass spectra for *sec*-butyl methyl sulfoxide and it was not apparent at the time that the sample pressure was different from the day before. The CO_2 laser output power dependent measurements were recorded at a sample pressure of 2.1×10^{-6} Torr for the 9R32 laser line (1085.8 cm^{-1}) over a range of 1.6 down to 0.0 W.

A summary of the photolysis results for *sec*-butyl methyl sulfoxide is displayed in table 3.3 on page 149. The details of the wavelength dependent study and the power dependent investigation can be found in the following two subsections. The table is presented at this point to provide a road map for the rest of this section.

3.4.1 Wavelength Dependence

Despite the problems caused by the extensive fragmentation due to the photoionization process, the infrared multiple-photon dissociation investigation of *sec*-butyl methyl sulfoxide did yield some interesting results. Figure 3.42 on page 151 illustrates the time of flight mass spectra for *sec*-butyl methyl sulfoxide recorded at the 9R32 CO_2 laser line (1085.8 cm^{-1}) while the corresponding regular mass spectra are presented in

Table 3.3: Fragment summary from *sec*-butyl methyl sulfoxide. The wavenumber maximum indicates the maximum in the wavelength dependent CO_2 laser photolysis of *sec*-butyl methyl sulfoxide which generated the corresponding fragment. The power threshold refers to the CO_2 laser output power at 1085.8 cm^{-1} when the fragment first starts to appear. A second threshold value is listed for some species because the slope for the power dependence changed at a power above the first power threshold. The power plateau value corresponds to the CO_2 laser power above which the relative abundance no longer increased. The value for $[C_4H_9]^+$ is in parentheses to indicate that the relative abundance decreased above this power. The maximum relative abundance is the power dependent measurement at 1.6 W compared to the amount of *sec*-butyl methyl sulfoxide in the corresponding photoionization mass spectrum or the relative abundance at the plateau power and is presented in the fifth column. The last column indicates the relative abundance of the fragment normalized to the amount of $[HOSCH_3]^{+\bullet}$ in the 70 eV electron impact mass spectrum.

Fragment	Wavenumber Maximum (cm^{-1})	Power Threshold (W)	Power Plateau or Decline (W)	Maximum Relative Abundance	Electron Impact Mass Spectrum Relative Abundance
$[OSCH_3]^+$	1074.6	0.0		0.344 ± 0.044	0.110
$[C_4H_9]^+$	1074.6	0.0, 0.2	(0.7)	0.570 ± 0.063	0.468
$[C_4H_8]^{+\bullet}$	1074.6	0.2	1.0	0.470 ± 0.042	0.110
$[C_4H_{10}]^{+\bullet}$	1057.3	0.0, 0.2	1.1	0.260 ± 0.059	0.028
$[SCH_3]^+$	1086.9	0.8		0.178 ± 0.023	0.069
$[C_3H_8]^{+\bullet}$	1069.0	0.4		0.162 ± 0.021	0.059
$[C_3H_5]^+$	1073.3	0.4		0.265 ± 0.029	0.636
$[C_2H_5]^+$	1069.0	0.6		0.170 ± 0.023	
$[CH_3]^+$	1069.0	1.1		0.070 ± 0.013	

figure 3.43 on page 152. The peak intensities in figure 3.43 have been normalized to the intensity of the parent molecular ion (120 amu) in the photoionization mass spectrum (bottom of the figure). Some new low mass photofragmentation species appeared in the photofragmentation / photoionization mass spectrum which did not show up in the photoionization mass spectrum. These new species occurred at 15 ($[CH_3]^+$), 29 ($[C_2H_5]^+$), 41 ($[C_3H_5]^+$), 42 ($[C_3H_6]^{+\bullet}$) and 47 amu ($[SCH_3]^+$). In addition to these low mass product species, the CO_2 laser production mass spectrum (top spectrum in figure 3.43) exhibited strong peaks at 56 ($[C_4H_8]^{+\bullet}$), 57 ($[C_4H_9]^+$), 58 ($[C_4H_{10}]^{+\bullet}$), 63 ($[OSCH_3]^+$), 64 ($[HOSCH_3]^{+\bullet}$), 75 (possibly $[C_2H_3SO]^+$), 104 ($[C_4H_8SO]^{+\bullet}$) and 105 amu ($[C_4H_9SO]^+$).

A vastly different result was observed for the photolysis of *sec*-butyl methyl sulfoxide at other CO_2 laser wavelengths. Figures 3.44 (page 153) and 3.45 (page 154) illustrate the mass spectra for *sec*-butyl methyl sulfoxide measured at the 9P34 CO_2 laser line (1033.6 cm^{-1}). The only products which were present in the CO_2 laser production mass spectrum (top of the figure) were the intense peaks observed in figure 3.43 at the 9R32 CO_2 laser line (1085.8 cm^{-1}). In particular, 56 ($[C_4H_8]^{+\bullet}$), 57 ($[C_4H_9]^+$), 64 ($[HOSCH_3]^{+\bullet}$), 75 (possibly $[C_2H_3SO]^+$) and 104 amu ($[C_4H_8SO]^{+\bullet}$).

A study of the wavelength dependence for the formation of specific products provided some interesting results with *sec*-butyl methyl sulfoxide. The complementary pair $[C_4H_9]^+$ (57 amu) and $[OSCH_3]^+$ (63 amu) are presented in figure 3.46 on page 155. Unlike with dimethyl sulfoxide and methyl phenyl sulfoxide, the wavelength

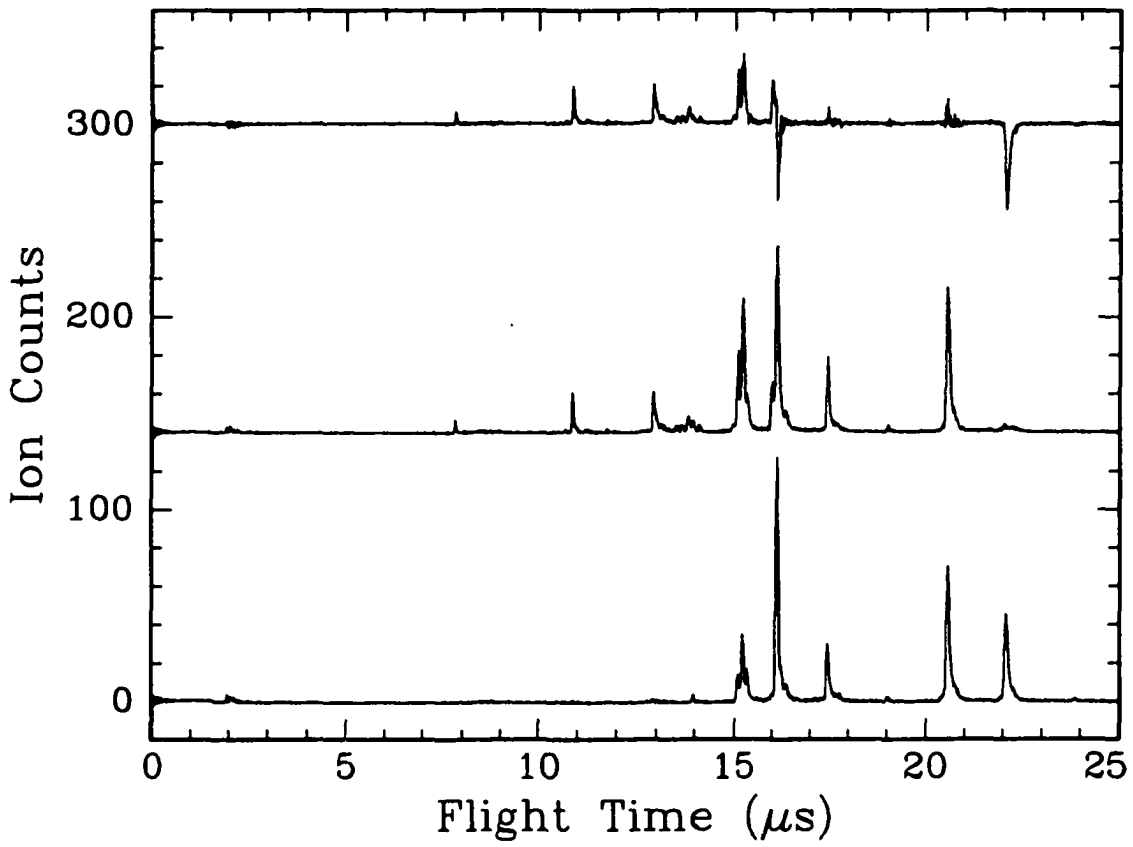

Figure 3.42: Time of flight mass spectra (9R32 CO_2 laser line) for *sec*-butyl methyl sulfoxide. The bottom spectrum was obtained with only the photoionization laser interacting with the molecule. The middle spectrum was obtained with first the CO_2 laser interacting with the sample followed by the photoionization laser. The top spectrum represents the difference between the two lower spectra. The sample pressure was 3.3×10^{-6} Torr.

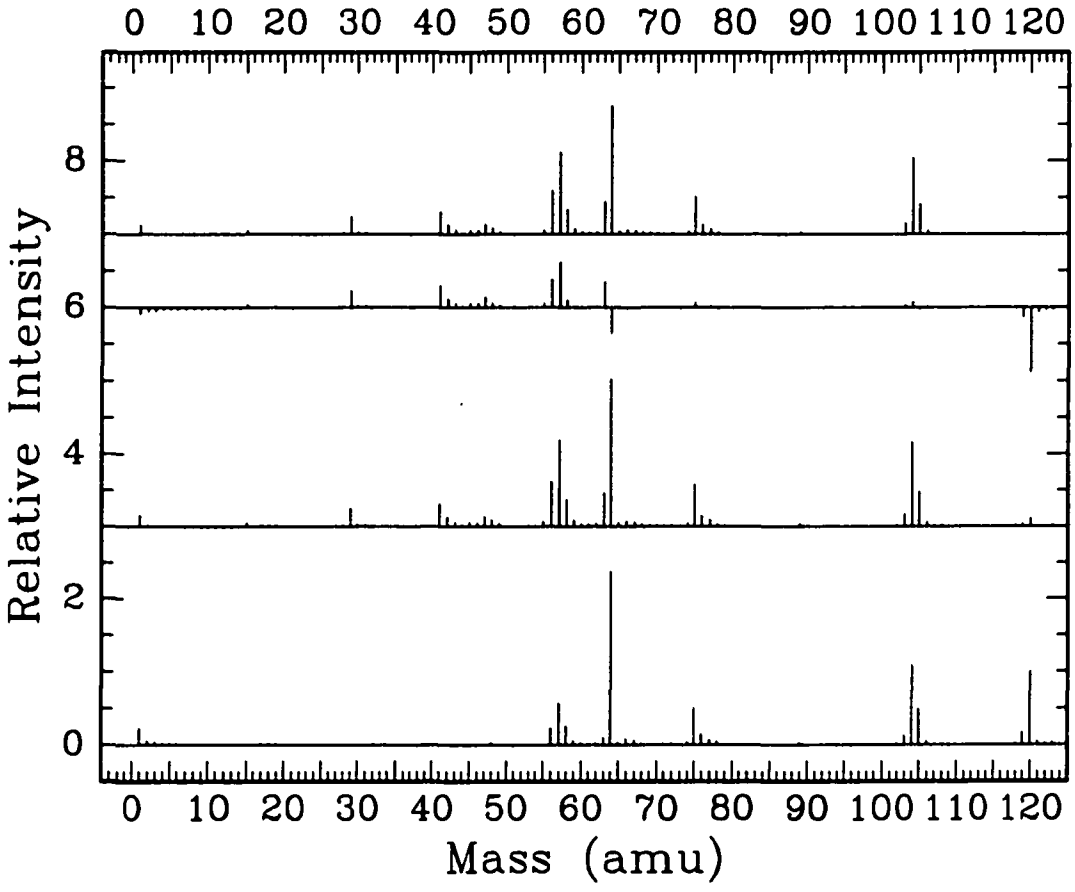

Figure 3.43: Mass spectra (9R32 CO_2 laser line) for *sec*-butyl methyl sulfoxide. The bottom spectrum is the corresponding stick mass spectrum to the photoionization mass spectrum in the previous figure (page 151). The second spectrum from the bottom correlates to the photofragmentation / photoionization mass spectrum in the previous figure. The second spectrum from the top represents the difference mass spectrum in the previous figure. The top spectrum indicates the photofragmentation species production due to the CO_2 laser. The intensities in all of the spectra were normalized to the value of the parent molecular ion at 120 amu in the photoionization mass spectrum.

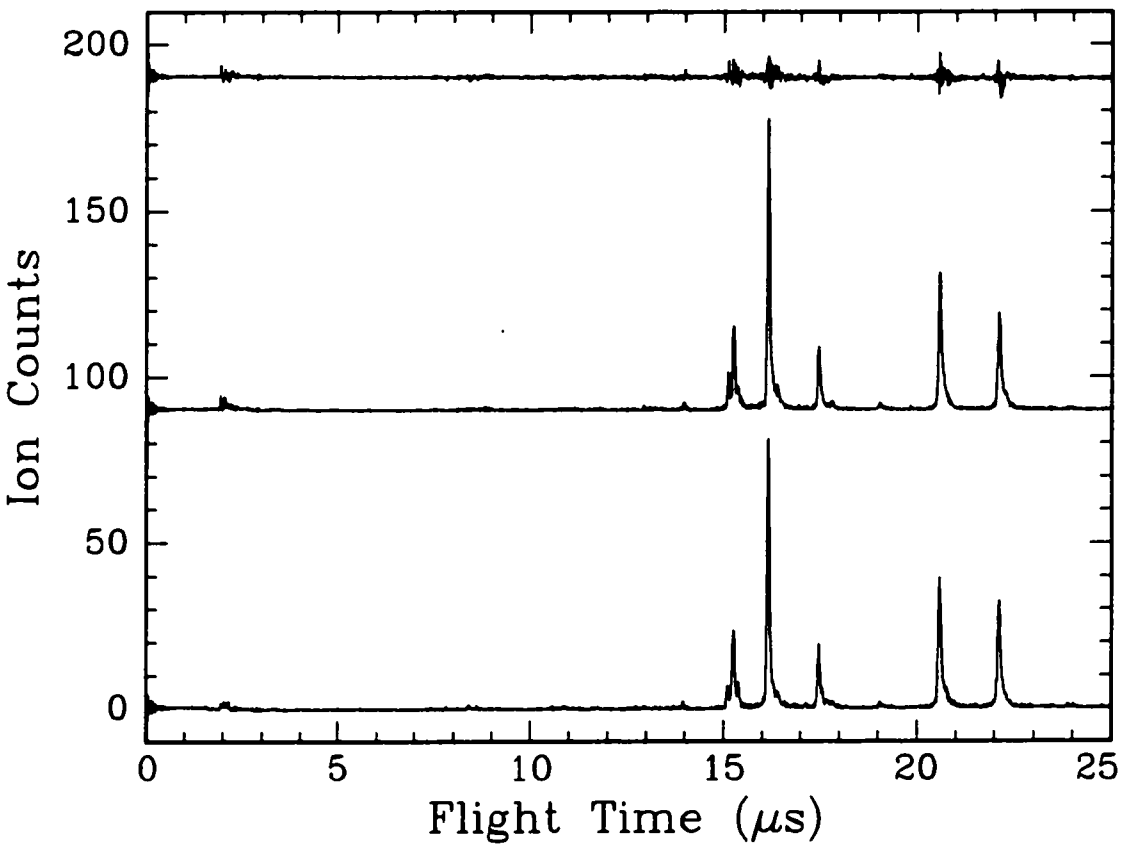

Figure 3.44: Time of flight mass spectra (9P34 CO_2 laser line) for *sec*-butyl methyl sulfoxide. The bottom spectrum was obtained with only the photoionization laser interacting with the molecule. The middle spectrum was obtained with first the CO_2 laser interacting with the sample followed by the photoionization laser. The top spectrum represents the difference between the two lower spectra. The sample pressure was 2.2×10^{-6} Torr.

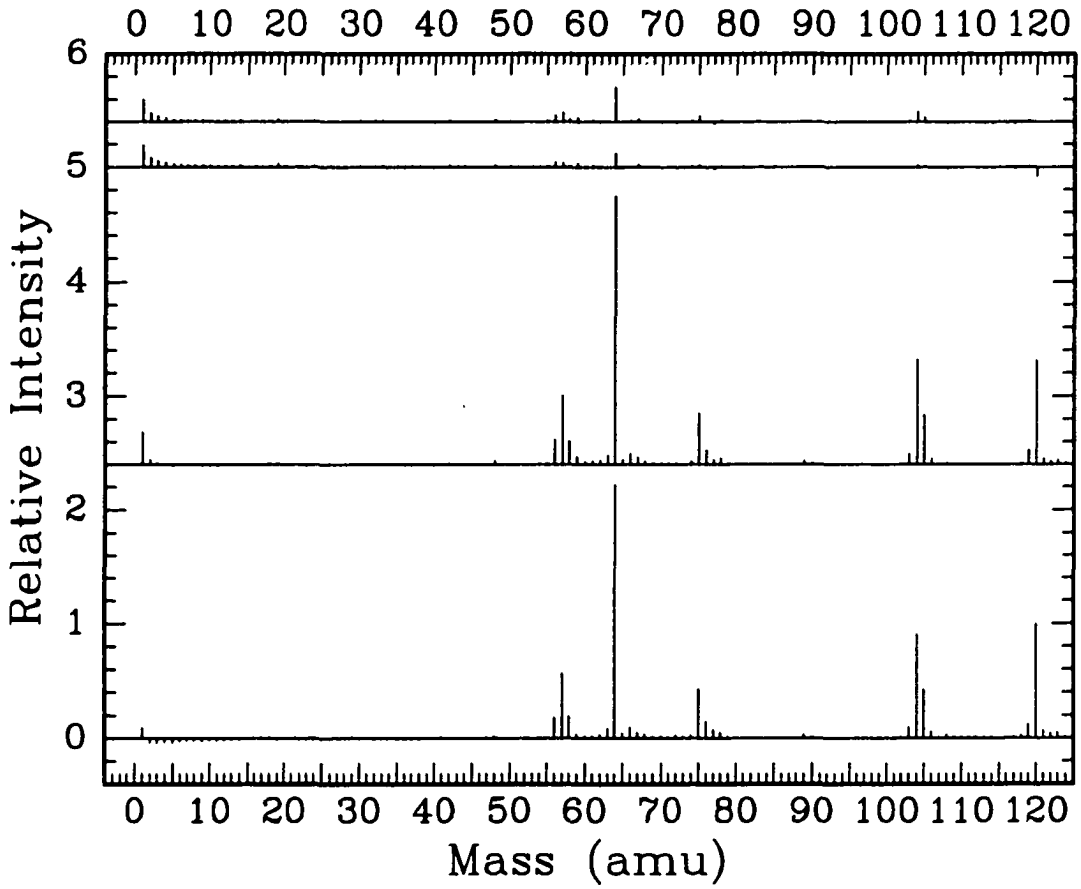

Figure 3.45: Mass spectra (9P34 CO_2 laser line) for *sec*-butyl methyl sulfoxide. The bottom spectrum is the corresponding stick mass spectrum to the photoionization mass spectrum in the previous figure (page 153). The second spectrum from the bottom correlates to the photofragmentation / photoionization mass spectrum in the previous figure. The second spectrum from the top represents the difference mass spectrum in the previous figure. The top spectrum indicates the photofragmentation species production due to the CO_2 laser. The intensities in all of the spectra were normalized to the value of the parent molecular ion at 120 amu in the photoionization mass spectrum.

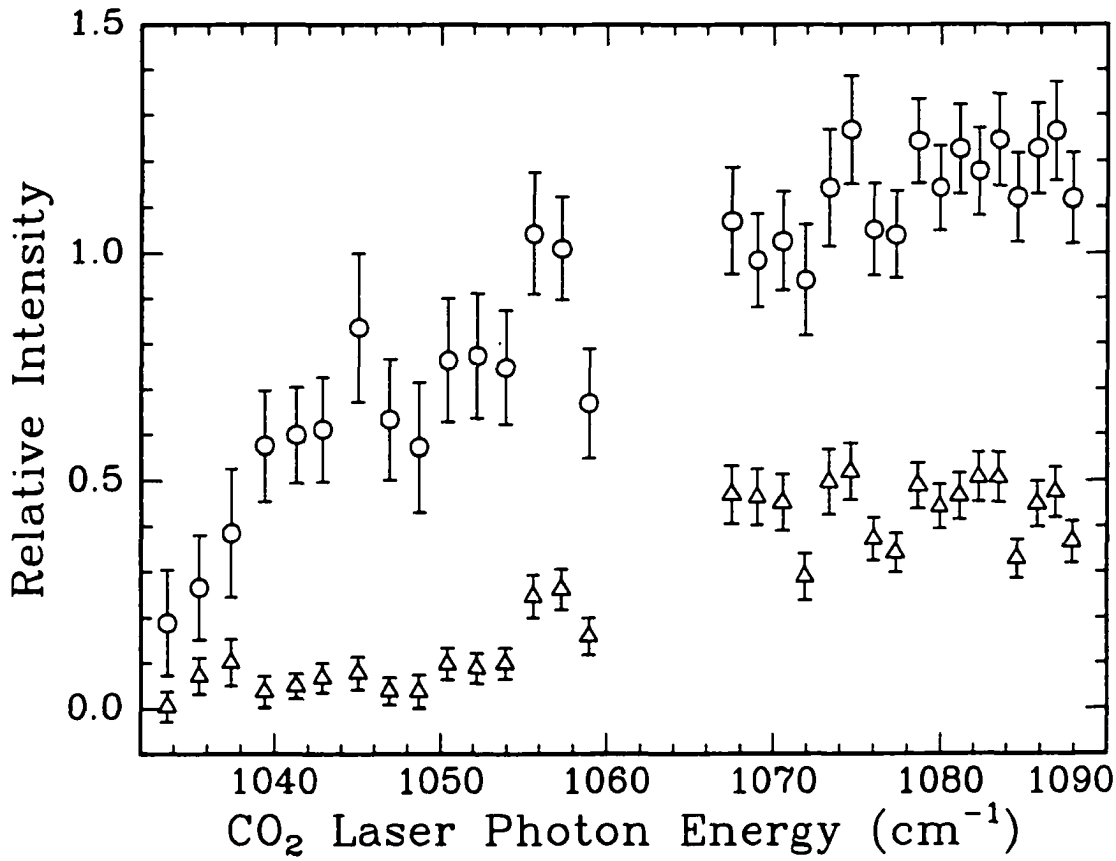

Figure 3.46: Photolysis wavelength dependence for masses 57 and 63 amu from *sec*-butyl methyl sulfoxide. The open circle data correspond to $[C_4H_9]^+$ (57 amu) and have been shifted up by 0.1. The open triangle data represent $[OSCH_3]^+$ (63 amu). The intensities were obtained from the CO_2 laser production mass spectra and have been normalized to the abundance of the parent molecular ion at 120 amu in the corresponding photoionization mass spectra.

dependence for this pair of simple cleavage products did not show a sharp increase in intensity at any of the wavelengths in this region. However, both $[C_4H_9]^+$ and $[OSCH_3]^+$ exhibited an increase in abundance as the wavenumber was increased from 1033.6 to 1087.9 cm^{-1}.

Another product species which displayed a similar behaviour was $[SCH_3]^+$ (mass of 47 amu) and is presented in figure 3.47 on page 157. For the 9P CO_2 laser band (1033.6 to 1058.9 cm^{-1}), small quantities of $[SCH_3]^+$ were produced. However, when the wavelength was changed to the 9R CO_2 laser band (1067.5 to 1087.9 cm^{-1}), the abundance increased by a factor of about six. This sharp increase was caused by the parent molecule absorbing more energy from the CO_2 laser for the 9R band and yielding more photofragmentation products.

An interesting development seems to have occurred with the wavelength dependent measurements for several other species and $[C_4H_8]^{+\bullet}$ will be the first to be considered. In general, the wavelength dependence was similar to that for $[C_4H_9]^+$ where a gradual increase in abundance was observed for the 9P CO_2 laser band and an intensity maximum occurred in the 9R band (figure 3.48 on page 158). Although the abundance for $[C_4H_9]^+$ continued to increase across the 9R band, $[C_4H_8]^{+\bullet}$ seemed to have a maximum around 1075 cm^{-1} followed by a slight decrease in abundance at higher wavenumbers. This can be attributed to the parent molecule absorbing more energy at the higher wavenumbers which would lead to an increase in the formation of cleavage products from a mechanism that is faster to develop than the one involved in the

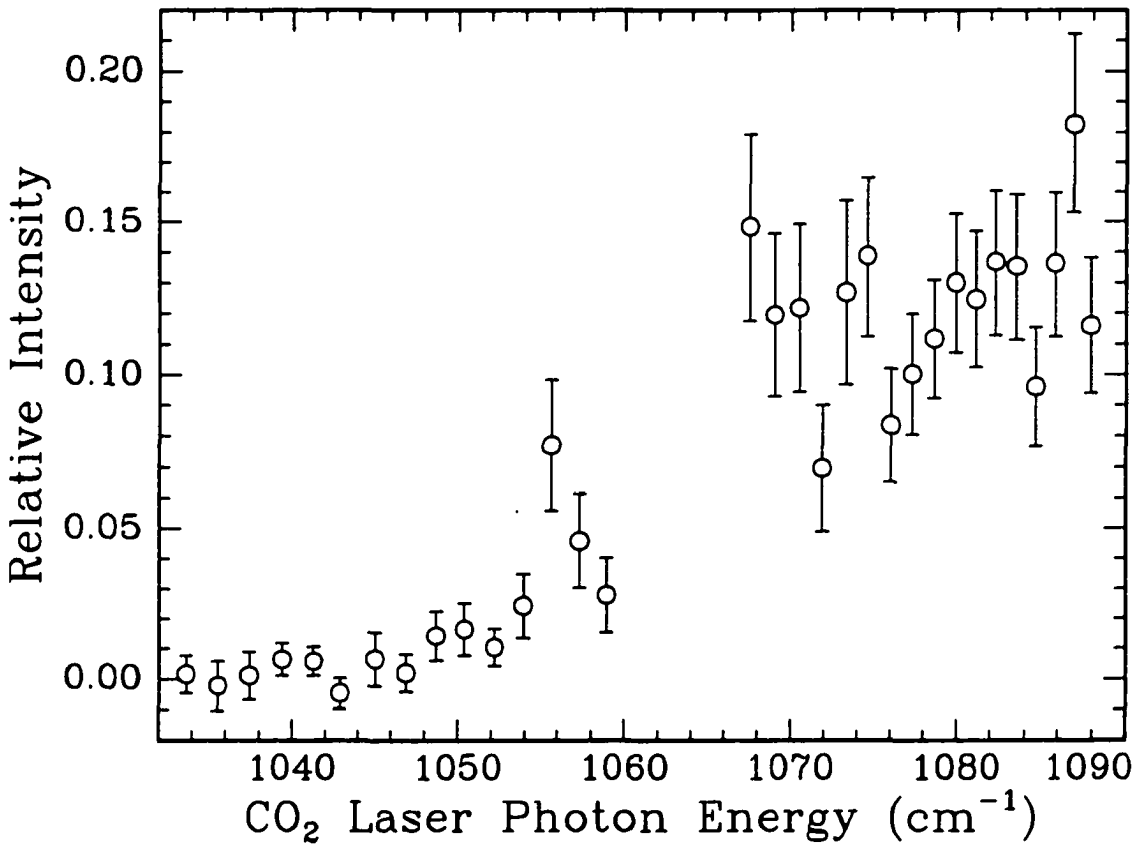

Figure 3.47: Photolysis wavelength dependence for mass 47 amu ($[SCH_3]^+$) from *sec*-butyl methyl sulfoxide. The intensities were obtained from the CO_2 laser production mass spectra and have been normalized to the abundance of the parent molecular ion at 120 amu in the corresponding photoionization mass spectra.

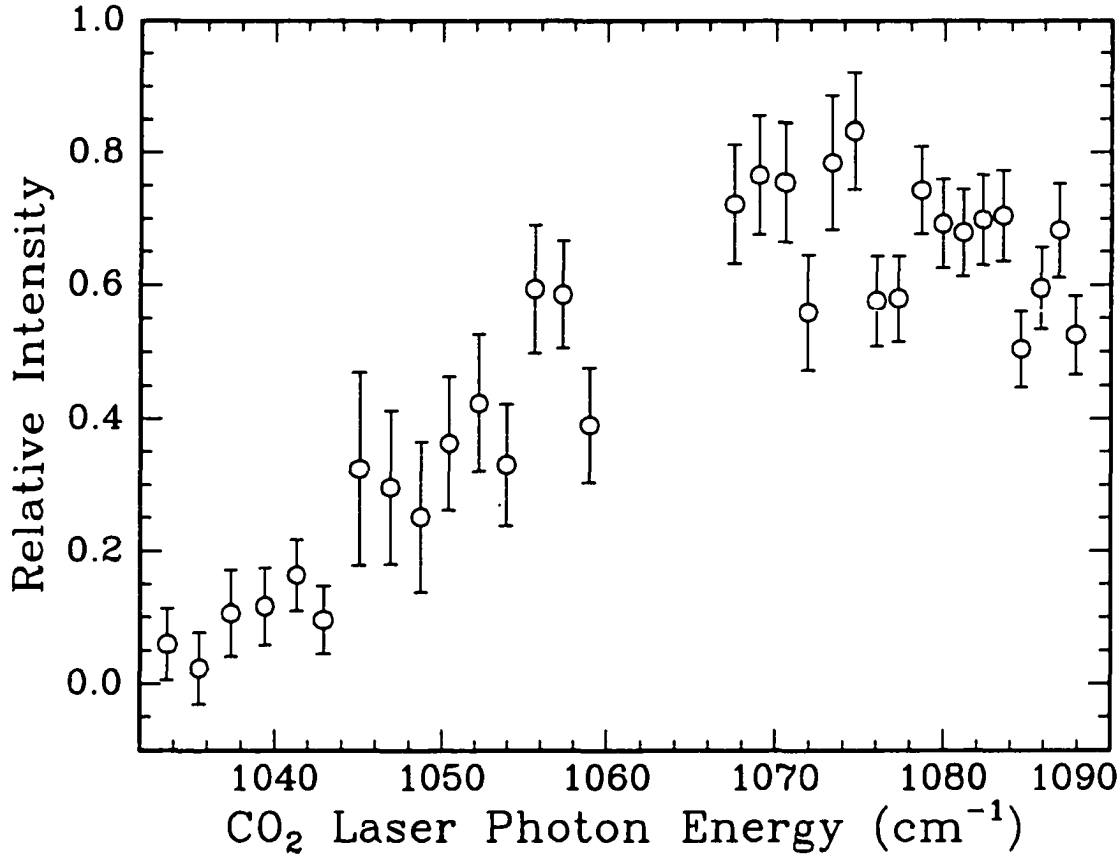

Figure 3.48: Photolysis wavelength dependence for mass 56 amu ($[C_4H_8]^{+\bullet}$) from *sec*-butyl methyl sulfoxide. The intensities were obtained from the CO_2 laser production mass spectra and have been normalized to the abundance of the parent molecular ion at 120 amu in the corresponding photoionization mass spectra.

generation of $[C_4H_8]^{+\bullet}$. This seems reasonable because in order to form $[C_4H_8]^{+\bullet}$, a hydrogen atom was lost from the butyl group as well as the cleavage of the bond to the sulfur atom.

A similar wavelength dependence was observed for $[C_3H_6]^{+\bullet}$, $[C_3H_5]^+$, $[C_2H_5]^+$ and $[CH_3]^+$ and is presented in figures 3.49 (page 160) and 3.50 (page 161). In all four cases, a small abundance was observed for the 9P CO_2 laser band but a sharp increase was observed for the 9R band. In addition, all four species showed an intensity maximum near 1070 cm^{-1}. Because $[C_3H_6]^{+\bullet}$, $[C_3H_5]^+$ and $[C_2H_5]^+$ all must originate from the butyl group in the parent molecule, they must have formed by mechanisms which were slower to develop than for $[C_4H_9]^+$. The one exception for this group of fragmentation species was $[CH_3]^+$ which could have originated from the butyl group or as a simple cleavage product where the bond between the sulfur atom and the methyl group was broken in the parent molecule. However, because of the similar wavelength for the intensity maximum, it is possible that the $[CH_3]^+$ also originated from the butyl group like the three other species previously stated. Another explanation for the different wavelength for the maximum abundance for these product species is that the primary photoproduct (a butyl group) absorbs additional photons to generate the secondary photofragment species.

$[C_4H_{10}]^{+\bullet}$ was one product species which exhibited a different wavelength dependence and is presented in figure 3.51 on page 162. Unlike all of the other fragmentation product species previously presented, $[C_4H_{10}]^{+\bullet}$ seems to have an intensity maximum

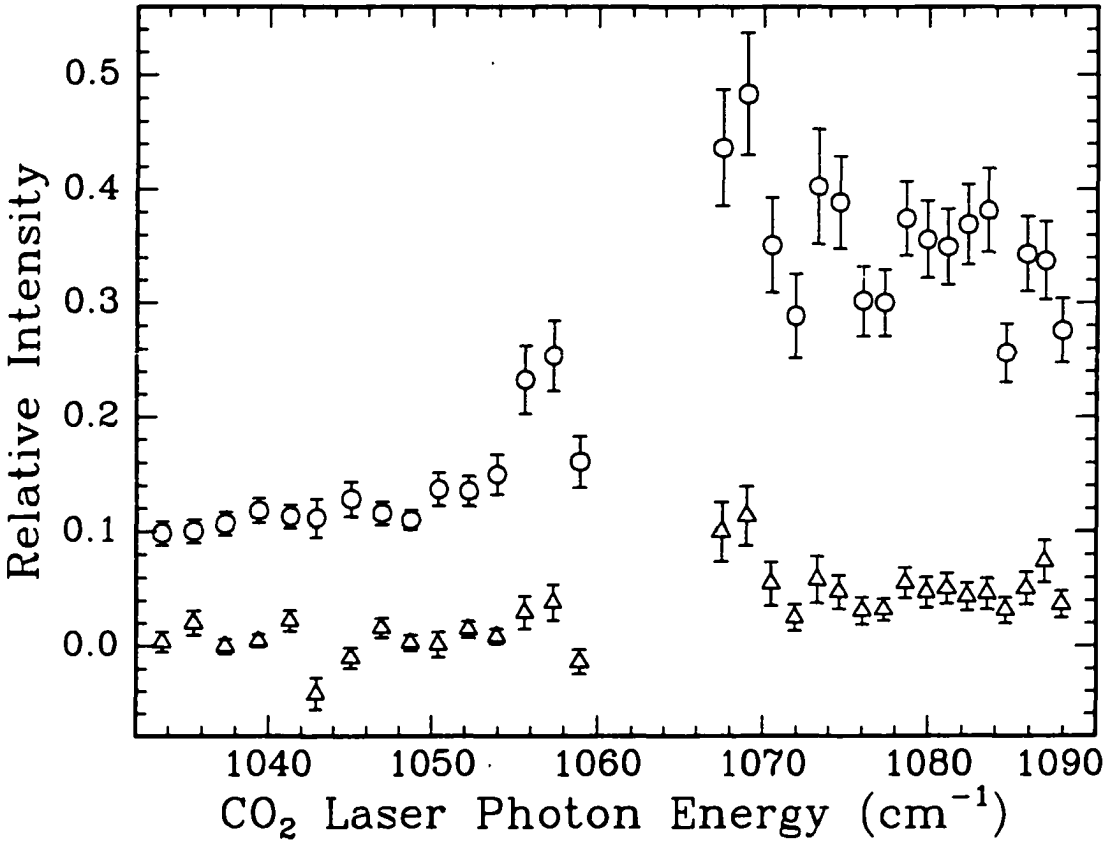

Figure 3.49: Photolysis wavelength dependence for masses 15 and 29 amu from *sec*-butyl methyl sulfoxide. The open triangle data are for $[CH_3]^+$ (15 amu). The open circle data correspond to $[C_2H_5]^+$ (29 amu) and have been shifted up by 0.1. The intensities were obtained from the CO_2 laser production mass spectra and have been normalized to the abundance of the parent molecular ion at 120 amu in the corresponding photoionization mass spectra.

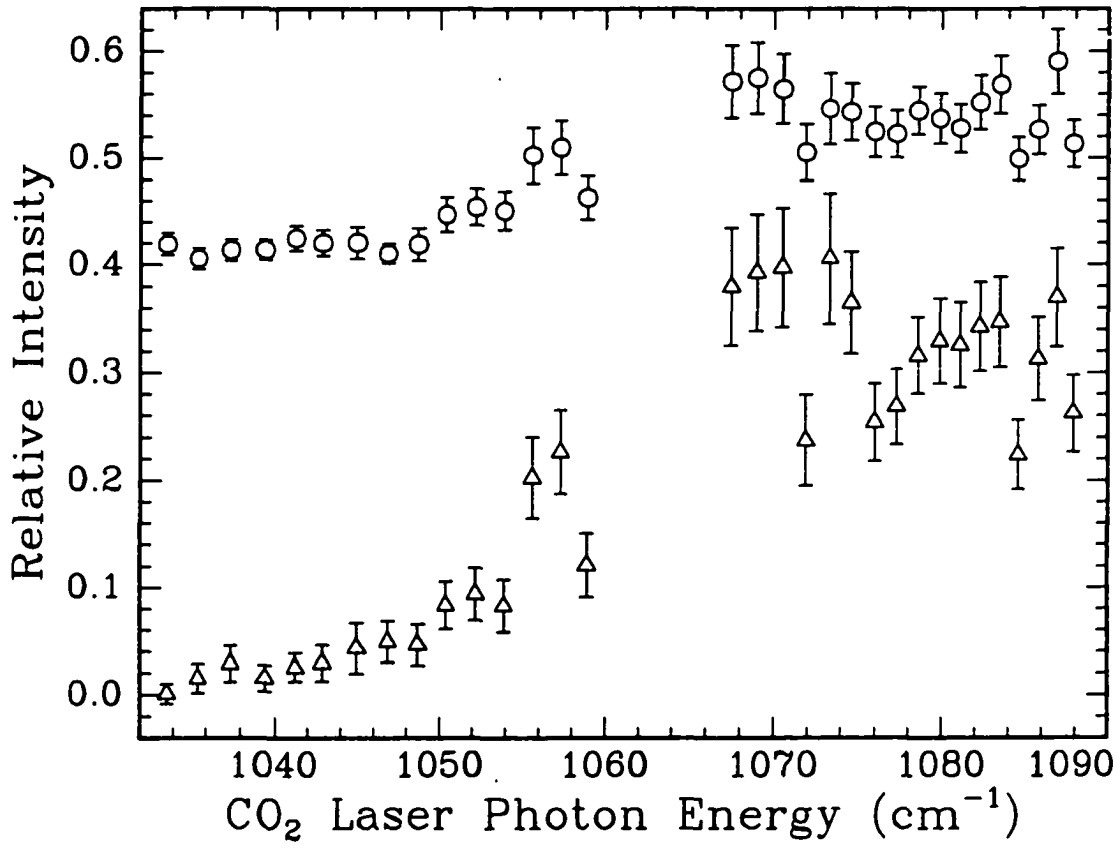

Figure 3.50: Photolysis wavelength dependence for masses 41 and 42 amu from *sec*-butyl methyl sulfoxide. The open triangle data are for $[C_3H_5]^+$ (41 amu). The open circle data correspond to $[C_3H_6]^{+\bullet}$ (42 amu) and have been shifted up by 0.4. The intensities were obtained from the CO_2 laser production mass spectra and have been normalized to the abundance of the parent molecular ion at 120 amu in the corresponding photoionization mass spectra.

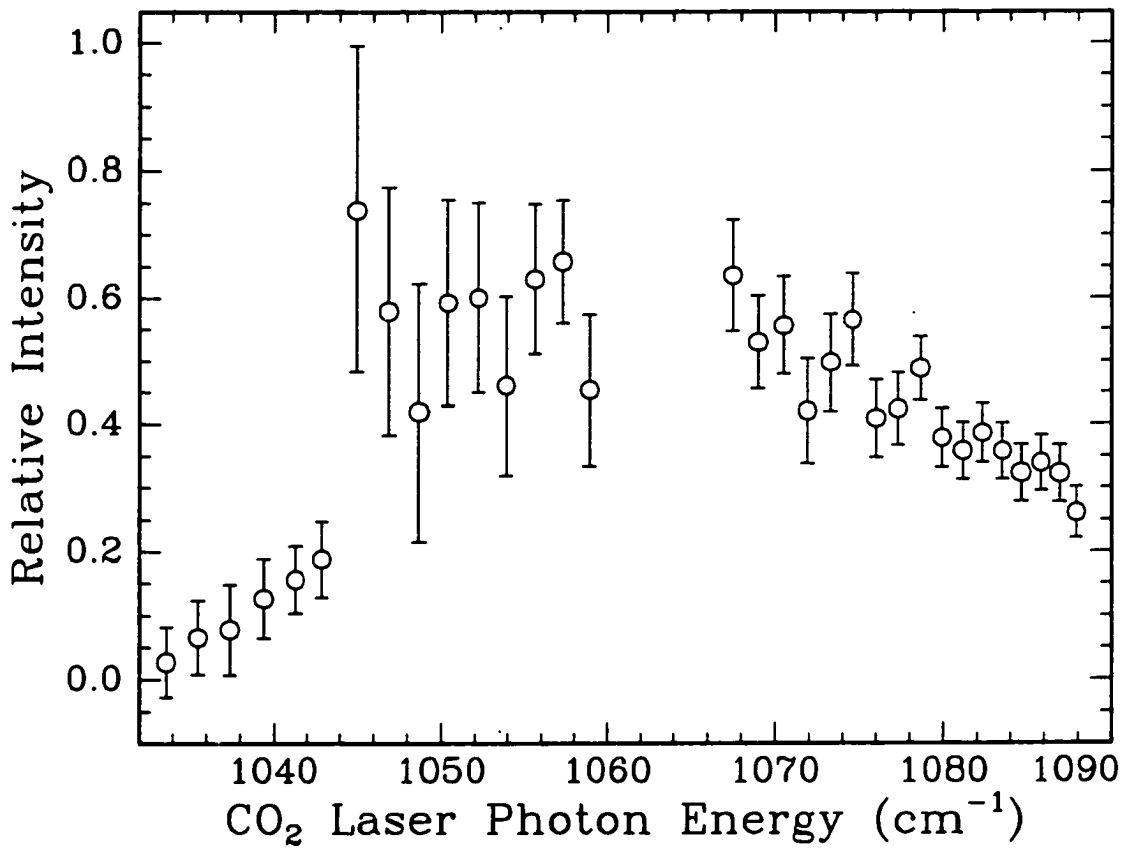

Figure 3.51: Photolysis wavelength dependence for mass 58 amu ($[C_4H_{10}]^{+\bullet}$) from *sec*-butyl methyl sulfoxide. The intensities were obtained from the CO_2 laser production mass spectra and have been normalized to the abundance of the parent molecular ion at 120 amu in the corresponding photoionization mass spectra.

in the 9P CO_2 laser band region. The steady decline in abundance across the 9R band and the increase in abundance for the other fragmentation species is an indication that the other mechanisms involved with the butyl group in this wavenumber region were dominating over the one which migrated a hydrogen atom from the methyl group to the butyl group (possibly by hydrogen migration to the oxygen atom and then migration from the oxygen atom to the butyl group) and formed a butane molecule.

3.4.2 Power Dependence

Increasing the output power of the CO_2 laser at the 9R32 line (1085.8 cm^{-1}) for *sec*-butyl methyl sulfoxide, once again, increased the number of photofragmentation species and the abundance for the product ions. Figures 3.52 (page 164) and 3.53 (page 165) present the time of flight mass spectra and regular mass spectra, respectively, at a *sec*-butyl methyl sulfoxide sample pressure of 2.1×10^{-6} Torr and at 1.6 W for the 9R32 CO_2 laser line. The major product species were determined to be $[C_4H_8]^{+\bullet}$ (56 amu), $[C_4H_9]^+$ (57 amu), $[C_4H_{10}]^{+\bullet}$ (58 amu), $[OSCH_3]^+$ (63 amu) and $[HOSCH_3]^{+\bullet}$ (64 amu). Minor fragmentation species were $[CH_3]^+$ (15 amu), $[C_2H_5]^+$ (29 amu), $[C_3H_5]^+$ (41 amu), $[C_3H_6]^{+\bullet}$ (42 amu) and $[SCH_3]^+$ (47 amu). Additional minor product species which arose due to the photoionization process appeared at 75 (possibly $[C_2H_3SO]^+$), 104 ($[C_4H_8SO]^{+\bullet}$) and 105 amu ($[C_4H_9SO]^+$).

The low CO_2 laser output power behaviour of *sec*-butyl methyl sulfoxide was significantly different than what was observed for dimethyl sulfoxide and methyl phenyl

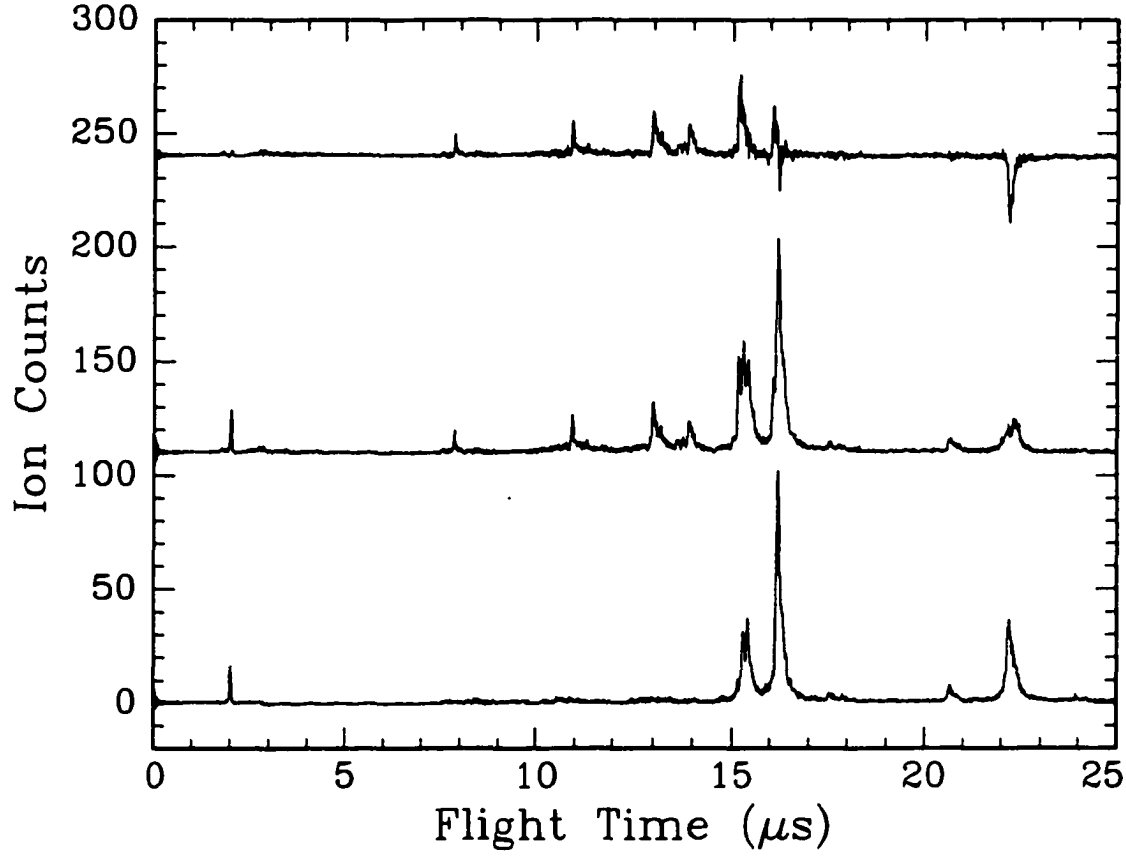

Figure 3.52: Time of flight mass spectra (9R32 CO_2 laser line, 1.6 W) for *sec*-butyl methyl sulfoxide. The bottom spectrum was obtained with only the photoionization laser interacting with the molecule. The middle spectrum was obtained with first the CO_2 laser interacting with the sample followed by the photoionization laser. The top spectrum represents the difference between the two lower spectra. The sample pressure was 2.1×10^{-6} Torr.

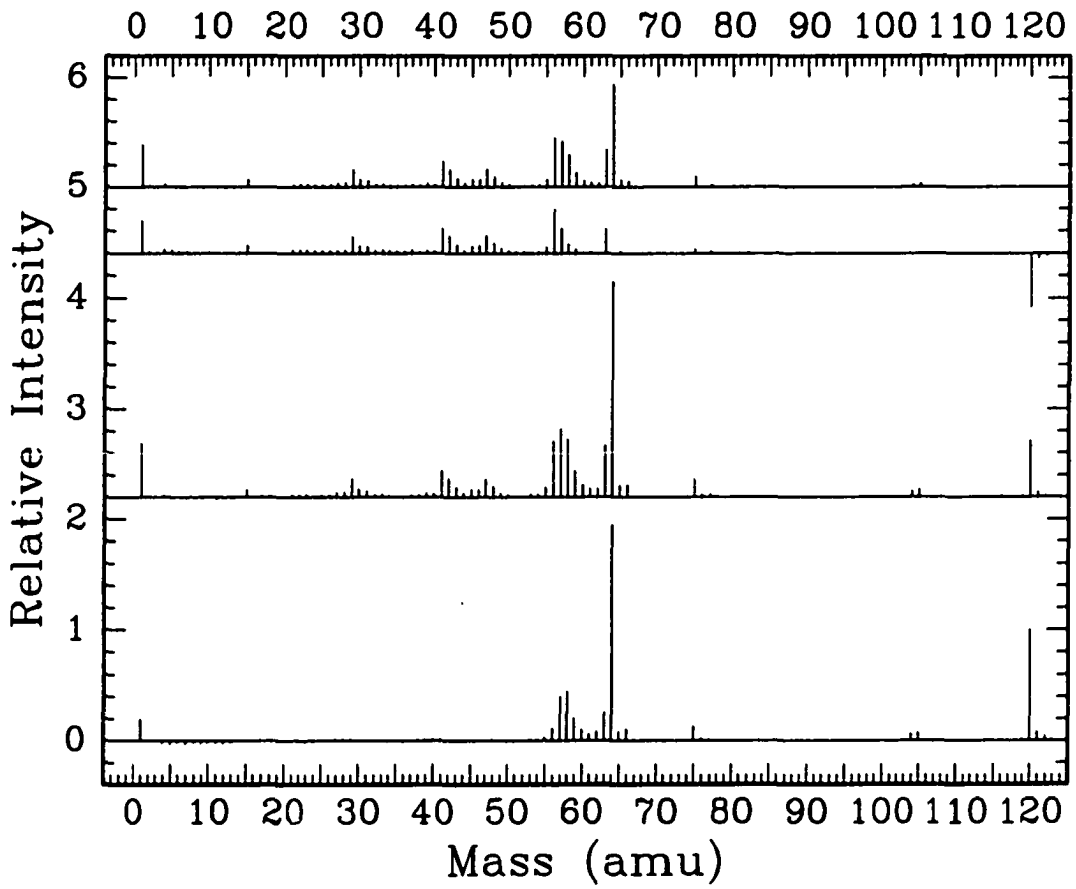

Figure 3.53: Mass spectra (9R32 CO_2 laser line, 1.6 W) for *sec*-butyl methyl sulfoxide. The bottom spectrum is the corresponding stick mass spectrum to the photoionization mass spectrum in the previous figure (page 164). The second spectrum from the bottom correlates to the photofragmentation / photoionization mass spectrum in the previous figure. The second spectrum from the top represents the difference mass spectrum in the previous figure. The top spectrum indicates the photofragmentation species production due to the CO_2 laser. The intensities in all of the spectra were normalized to the value of the parent molecular ion at 120 amu in the photoionization mass spectrum.

sulfoxide. In figure 3.19 (page 110) for dimethyl sulfoxide and figure 3.36 (page 139) for methyl phenyl sulfoxide, whatever photofragmentation species were present had negligible abundance at the low CO_2 laser output power. With *sec*-butyl methyl sulfoxide, however, a different result was observed in figures 3.54 (page 167) and 3.55 (page 168). It was rather surprising that even at the low output power of 0.1 W from the CO_2 laser, a significant amount of $[C_4H_9]^+$ (57 amu) and $[HOSCH_3]^{+\bullet}$ (64 amu) were produced.

A different, and somewhat unusual, CO_2 laser output power dependent behaviour was observed for the butane fragmentation species. Figure 3.56 on page 170 presents the power dependence for the butane ion (58 amu, open circles, solid line), butyl ion (57 amu, open triangles, dashed line), butene ion (56 amu, filled in circles, dot-dashed line) and the intensity sum of these three ions (filled in triangles, dot-dot-dashed line). For clarity purposes, the butyl ion intensities have been shifted up by 0.2, the butene ion intensities by 1.0 and the sum by 1.2. Below 0.2 W, the butane and butyl ions displayed a slope with a sharp increase in abundance while virtually no butene ions were present at these low output power values. Above this power, the slope for the butane and butyl ions decreased while the slope for the butene ion increased. At about 0.7 W the slope for the butyl ion decreased while for the butane ion, the decrease in the slope occurred around 1.1 W. Although the slope for the butene ion also decreased at around 1.0 W, there was also a jump in abundance associated with the change in the slope. This behaviour was highly unusual because a gradual change in abundance

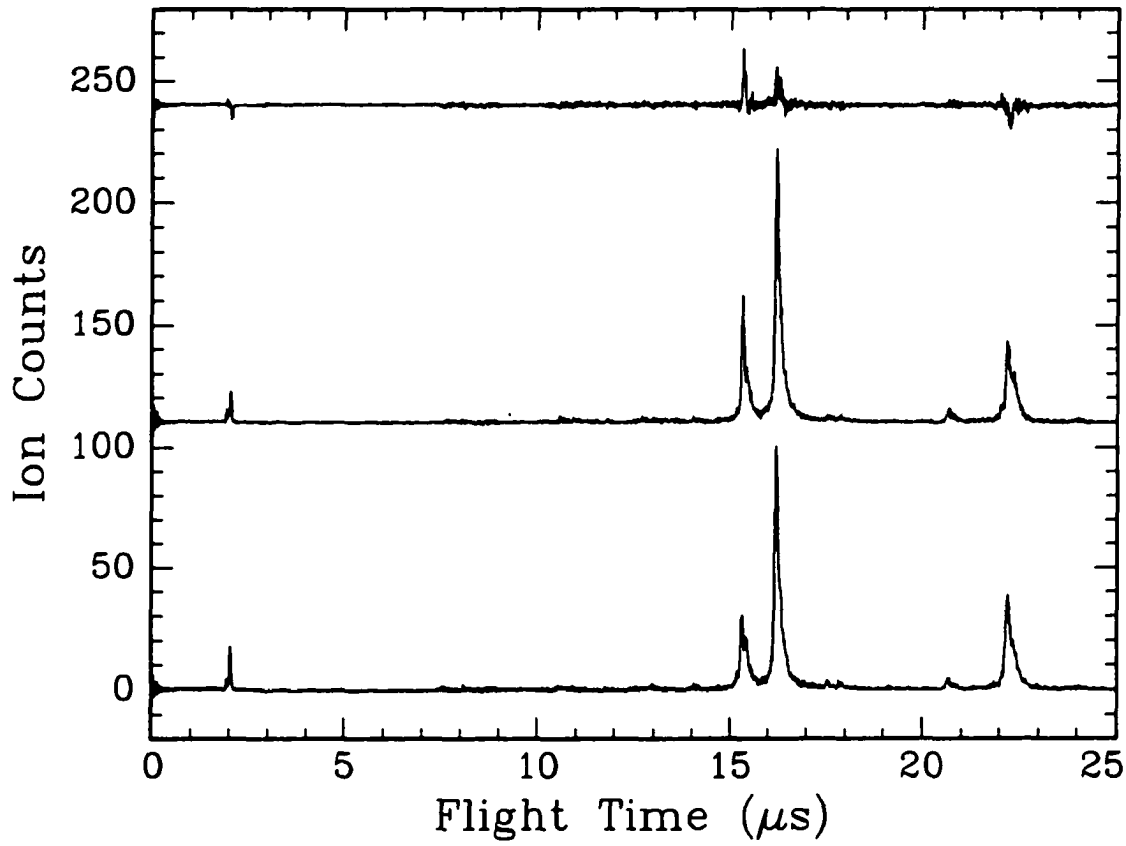

Figure 3.54: Time of flight mass spectra (9R32 CO_2 laser line, 0.1 W) for *sec*-butyl methyl sulfoxide. The bottom spectrum was obtained with only the photoionization laser interacting with the molecule. The middle spectrum was obtained with first the CO_2 laser interacting with the sample followed by the photoionization laser. The top spectrum represents the difference between the two lower spectra. The sample pressure was 2.1×10^{-6} Torr.

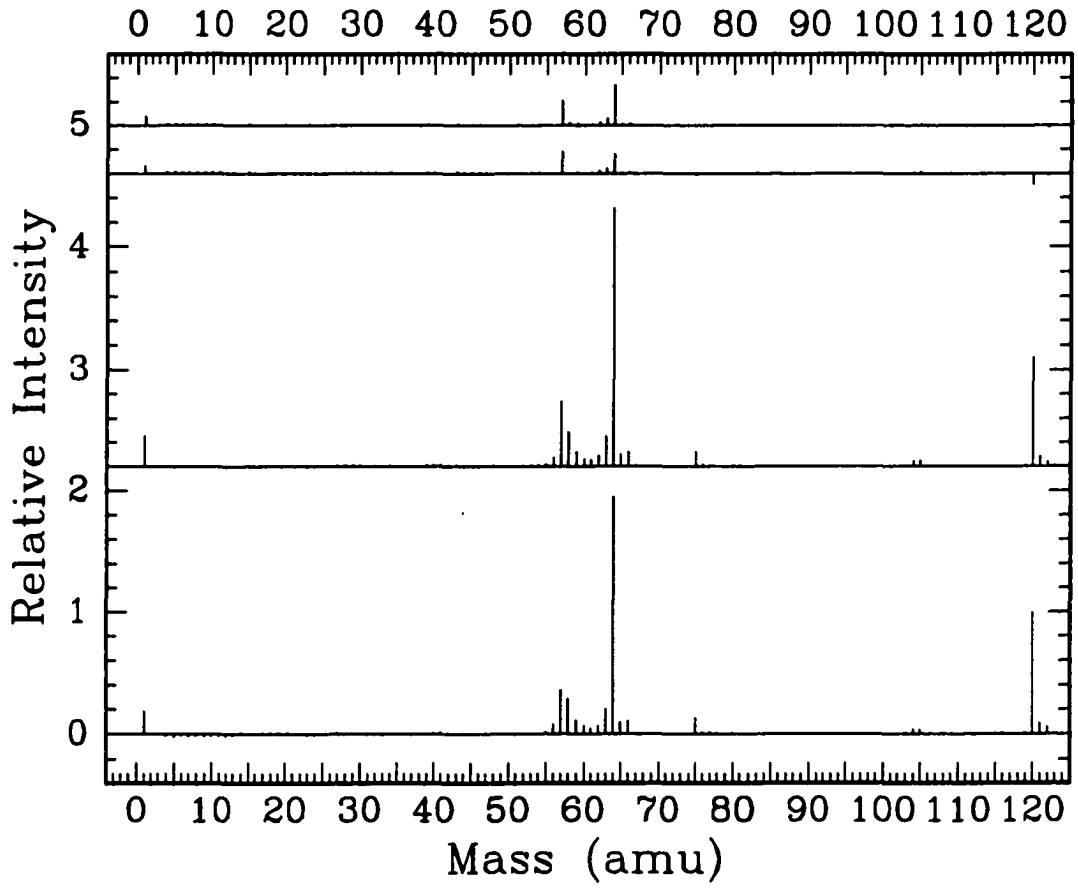

Figure 3.55: Mass spectra (9R32 CO_2 laser line, 0.1 W) for *sec*-butyl methyl sulfoxide. The bottom spectrum is the corresponding stick mass spectrum to the photoionization mass spectrum in the previous figure (page 168). The second spectrum from the bottom correlates to the photofragmentation / photoionization mass spectrum in the previous figure. The second spectrum from the top represents the difference mass spectrum in the previous figure. The top spectrum indicates the photofragmentation species production due to the CO_2 laser. The intensities in all of the spectra were normalized to the value of the parent molecular ion at 120 amu in the photoionization mass spectrum.

had been observed with most of the other fragmentation species presented in this chapter.

This odd behaviour might be an artifact of the analysis procedure caused by an overlap of the butyl and butane ions in the time of flight mass spectra. Since these three ions are not clearly resolved in the time of flight mass spectra, it would be better to consider the sum of the intensities and deal with the group as a whole instead of individually analyzing each ion species. The behaviour of the sum resembles the power dependence for the butane ion for the power at which the change in slope occurred. However, the value of the slopes seem to be closer to the slopes of the most intense species, the butyl ion. At low output powers, there was a sharp increase in abundance, followed by a more gradual increase at intermediate powers (0.2 to 1.1 W) which, in turn, was followed by a gradual decrease in abundance. This behaviour can be explained by the butyl ion group being the only fragmentation species associated with the butyl moiety in the parent molecule at low output powers, but as the CO_2 laser output power was increased, other mechanisms compete to decrease the slope of the intensity. At higher output powers, additional mechanisms also compete with the mechanism(s) that produced the butyl ion group such that the abundance for this group now decreased.

Figure 3.57 on page 171 illustrates the power dependence for $[SCH_3]^+$ and it exhibited the usual behaviour. Below 0.8 W, very little $[SCH_3]^+$ was observed while above this threshold value a sharp increase in abundance was observed.

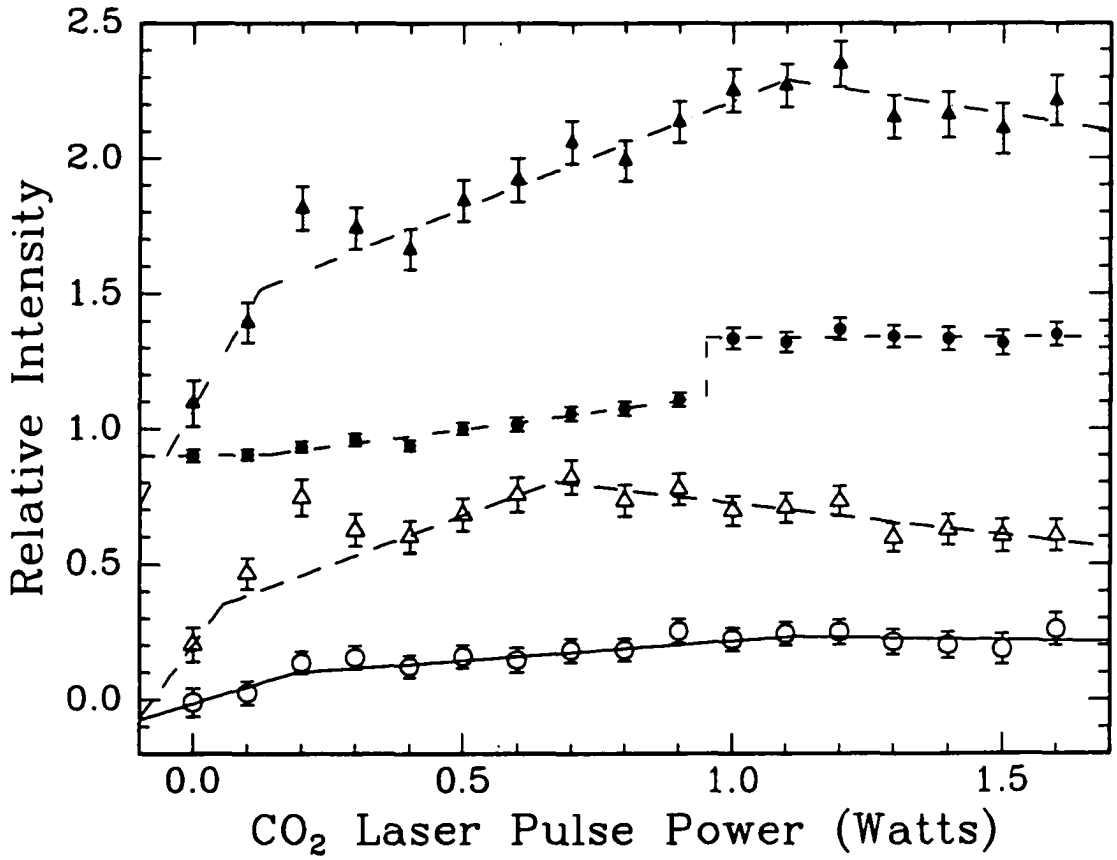

Figure 3.56: Photolysis power dependence for masses 56, 57 and 58 amu from *sec*-butyl methyl sulfoxide. The filled in circle data fitted by the dot-dashed line are for $[C_4H_8]^{+\bullet}$ (56 amu) and have been shifted up by 0.9. The open triangle data fitted by the dashed line correlate to $[C_4H_9]^+$ (57 amu) and have been shifted up by 0.2. The open circle data fitted by the solid line represent $[C_4H_{10}]^{+\bullet}$ (58 amu). The filled in triangle data fitted by the dot-dot-dashed line correspond to the intensity sum of all three species and have been shifted up by 1.1. The intensities were obtained from the CO_2 laser production mass spectra and have been normalized to the abundance of the parent molecular ion at 120 amu in the corresponding photoionization mass spectra.

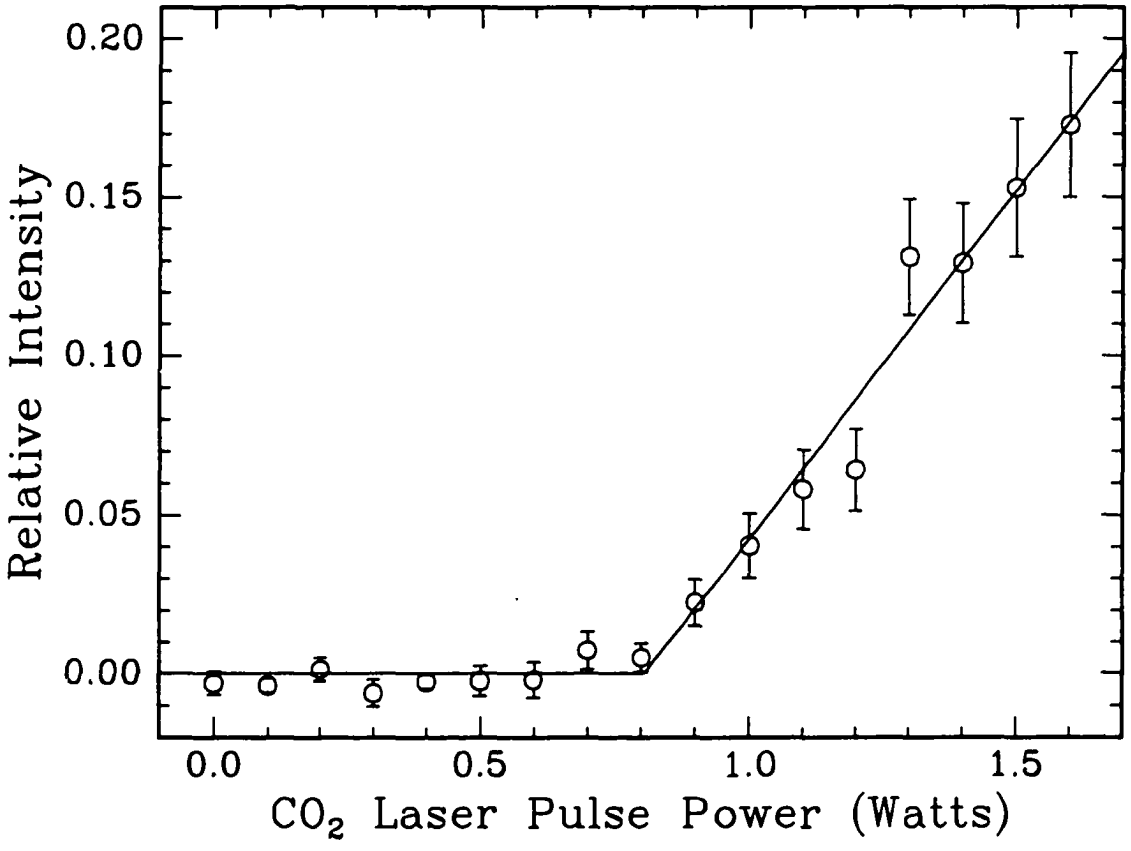

Figure 3.57: Photolysis power dependence for mass 47 amu ($[SCH_3]^+$) from *sec*-butyl methyl sulfoxide. The intensities were obtained from the CO_2 laser production mass spectra and have been normalized to the abundance of the parent molecular ion at 120 amu in the corresponding photoionization mass spectra.

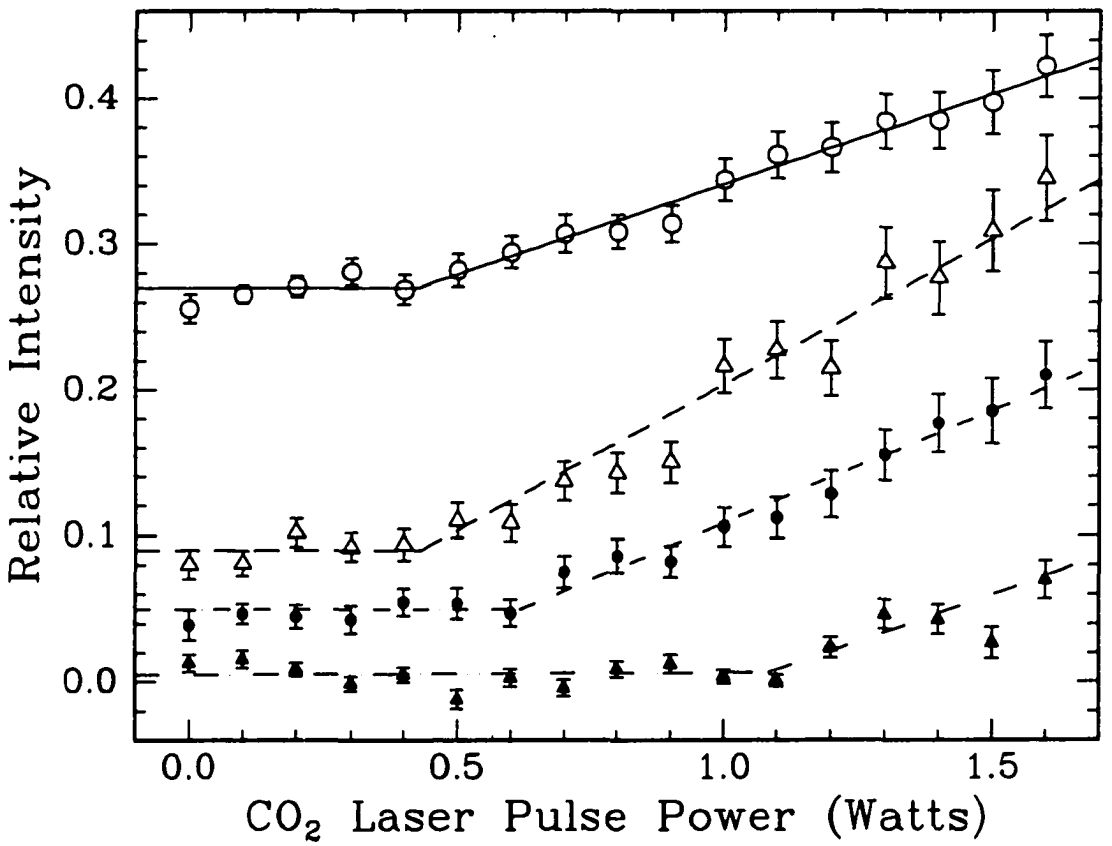

Figure 3.58: Photolysis power dependence for masses 15, 29, 41 and 42 amu from *sec*-butyl methyl sulfoxide. The filled in triangle data fitted by the dot-dot-dashed line represent $[CH_3]^+$ (15 amu). The filled in circle data fitted by the dot-dashed line are for $[C_2H_5]^+$ (29 amu) and have been shifted up by 0.05. The open triangle data fitted by the dashed line correlate to $[C_3H_5]^+$ (41 amu) and have been shifted up by 0.09. The open circle data fitted by the solid line correspond to $[C_3H_6]^{+\bullet}$ (42 amu) and have been shifted up by 0.27. The intensities were obtained from the CO_2 laser production mass spectra and have been normalized to the abundance of the parent molecular ion at 120 amu in the corresponding photoionization mass spectra.

The CO_2 laser output power dependence for $[C_3H_6]^{+\bullet}$ (42 amu), $[C_3H_5]^+$ (41 amu) and $[C_2H_5]^+$ (29 amu) are presented in figure 3.58 on page 172. The power dependence data for $[C_3H_6]^{+\bullet}$ (open circles, solid line) has a threshold at 0.4 W. The threshold for generating $[C_3H_5]^+$ (open triangles, dashed line) also occurred at 0.4 W while for $[C_2H_5]^+$ (filled in circles, dot-dashed line) the threshold was at 0.6 W. For all of these fragmentation species, the abundance increased as the CO_2 laser output power was increased further above the threshold value.

The power dependence for the methyl ion (filled in triangles, dot-dot-dashed line) was also presented in figure 3.58. Below 1.1 W, essentially no $[CH_3]^+$ was produced. The fluctuations in the data about the best fit line was due to the variations in the baseline of the time of flight mass spectra. However, above 1.1 W a sharp increase in abundance was observed.

Since the methyl ion was also observed in the photolysis of both dimethyl sulfoxide and methyl phenyl sulfoxide, a comparison might provide some further insight into the mechanism involved in generating this species. With dimethyl sulfoxide, the power threshold occurred at 0.5 W (figure 3.20, page 112) while with methyl phenyl sulfoxide the threshold was at 0.6 W (figure 3.39, page 144). It seems that as the parent molecule becomes more complicated (in the sense of having more atoms), the power threshold increased. However, it was quite surprising that there was such a large difference in the threshold between methyl phenyl sulfoxide (0.6 W) and *sec*-butyl methyl sulfoxide (1.1 W) when there is only a difference of two atoms between these

molecules. An explanation for this large difference is that the mechanism responsible for generating the methyl ion in *sec*-butyl methyl sulfoxide is different than for methyl phenyl sulfoxide and dimethyl sulfoxide. The similar threshold values for $[CH_3]^+$ formation from methyl phenyl sulfoxide and dimethyl sulfoxide suggests the same mechanism for these two molecules. Since there is only one source of a methyl group for these two molecules, $[CH_3]^+$ originated from a cleavage reaction. With *sec*-butyl methyl sulfoxide, however, the methyl group could either be from the methyl moiety or be part of the butyl group. From the work of Smakman and de Boer, a sulfoxide molecule was more likely to lose the larger group [52]. Applying this to *sec*-butyl methyl sulfoxide suggests that the butyl group is more likely to be lost than the methyl group. The much higher threshold value for $[CH_3]^+$ formation from *sec*-butyl methyl sulfoxide than from methyl phenyl sulfoxide or dimethyl sulfoxide could be an indication that the methyl group originated from the butyl moiety.

Chapter 4

Concluding Remarks

In the previous chapter, the experimental results presented the mass spectra and laser photolysis of some small organic sulfoxide molecules. A similar arrangement will be used in this chapter. The first section will provide some concluding remarks for the various electron impact and photoionization mass spectra of the small organic sulfoxide molecules. The next three sections will deal with the infrared multiple-photon dissociation laser photolysis work performed on dimethyl sulfoxide, methyl phenyl sulfoxide and *sec*-butyl methyl sulfoxide. The last section will include some final thoughts for this work.

4.1 Mass Spectra

The mass spectra for dimethyl sulfoxide in figure 3.1 on page 71 contained fewer fragmentation species than was observed by Bowie *et al.* [45] and Smakman and de Boer [52]. The species at 63, 61 and 45 amu have all been observed and identified by both of these two previous works as $[H_3CSO]^+$, $[H_3CSCH_2]^+$ and $[HCS]^+$. The only new feature in figure 3.1 was the unidentified peak at 40 amu. The only interesting result presented in figure 3.1 was that the photoionization mass spectrum had very little fragmentation of the parent molecular ion when compared with the electron impact mass spectrum.

It was rather surprising that Bowie *et al.* did not report results for diethyl sulfoxide because they did consider larger dialkyl molecules like dipropyl sulfoxide and dibutyl sulfoxide as well as the smallest dialkyl sulfoxide, dimethyl sulfoxide [45]. The presence of the strong peak at 63 amu in the electron impact mass spectrum in figure 3.2 on page 74 for diethyl sulfoxide follows the general observation made by Bowie *et al.* that the dialkyl sulfoxides all formed this common product species. Another generalization made by Bowie *et al.* was that one of the alkyl groups migrated a hydrogen atom to the sulfoxide group followed by loss of the alkene group. With diethyl sulfoxide, this would correspond to the loss of H_2CCH_2 from the parent molecular ion which resulted in a species of mass 78 amu. Clearly, the results presented in this work for diethyl sulfoxide follow the same trends as observed by Bowie *et al.* for other, larger, dialkyl sulfoxide molecules.

The mass spectra for methyl phenyl sulfoxide in figure 3.3 on page 76 also had fewer fragmentation species than was observed by Bowie *et al.* [45] but the photoionization mass spectrum did contain some new features. The major peaks in the electron impact mass spectrum in figure 3.3 (140 amu for the parent molecular ion, 125 amu for $[C_6H_5SO]^+$, 97 amu for $[C_5H_5S]^+$, 77 amu for $[C_6H_5]^+$ and 51 amu for $[C_4H_3]^+$) were also seen and identified by Bowie *et al.* Although the major fragmentation species in the photoionization mass spectrum at 78 and 124 amu were also observed in the electron impact mass spectrum, the relative intensities were vastly different. It was rather surprising that the product channel for the formation of $[C_6H_6]^{+\bullet}$ was favoured over the one which would have generated $[C_6H_5]^+$. The 77 amu species would have been generated by a cleavage of the bond between the sulfur atom and the phenyl group whereas the 78 amu species involved hydrogen migration to the phenyl group prior to the bond breaking. This is another example of the bond rupturing reaction requiring hydrogen migration as was observed by Smakman and de Boer for aliphatic sulfoxides [52].

The strong peak at 78 amu in the electron impact mass spectrum of ethyl phenyl sulfoxide in figure 3.4 on page 78 could either be $[C_6H_6]^{+\bullet}$ or $[C_2H_6SO]^{+\bullet}$. The odd electron species $[C_6H_6]^{+\bullet}$ could be formed from ethyl phenyl sulfoxide by a similar mechanism which resulted in $[C_6H_6]^{+\bullet}$ from methyl phenyl sulfoxide, namely, hydrogen migration from the alkyl group to the phenyl moiety followed by cleavage of the bond to the sulfur atom. $[C_2H_6SO]^{+\bullet}$, however, could be formed by hydrogen

migration from the phenyl group to the sulfoxide group followed by loss of C_6H_4.

There were other similarities between ethyl phenyl sulfoxide and methyl phenyl sulfoxide. The species at 126 amu corresponds to the loss of CO from the parent molecular ion of ethyl phenyl sulfoxide. A similar peak was observed by Bowie *et al.* [45] for methyl phenyl sulfoxide but at a much weaker intensity than was observed in the present work for ethyl phenyl sulfoxide. The increased intensity could indicate that the phenyl group is more likely to migrate to the oxygen atom with ethyl phenyl sulfoxide than for methyl phenyl sulfoxide.

An interesting similarity with the electron impact mass spectra of the butyl sulfoxide molecules involved the fragmentation species $[H_3CSOH]^{+\bullet}$ from *tert*-butyl methyl sulfoxide and *sec*-butyl methyl sulfoxide and $[(H_3C)(CH_2)SOH]^{+\bullet}$ from *sec*-butyl ethyl sulfoxide. The common part to the parent molecules is the butyl group connected to the sulfoxide group. A hydrogen atom migrated from the butyl group to the sulfoxide group and the bond connecting the remaining alkyl group to the sulfur atom was broken. This result can be generalized by the following chemical equation:

$$[C_4H_9-SO-R]^{+\bullet} \rightarrow C_4H_8 + [HOS-R]^{+\bullet} \tag{4.1}$$

where R is either a methyl or ethyl group.

As a final point on the discussion of the electron impact mass spectra of the small organic sulfoxide molecules, it seems that the statement made by Bowie *et al.* that the

mass spectra are "relatively simple" may have been a bit misleading [45]. Although the fragmentation species are readily characterized, the mechanisms involved are not simple, single step reactions. The results presented in this thesis, by Bowie *et al.* [45] and by Smakman and de Boer [52] all indicate that a migration of some species usually occurred before a fragment was lost from the parent molecule.

4.2 Dimethyl Sulfoxide Photolysis

The CO_2 laser wavelength which generated the maximum intensity for the various photofragment species was found to be 1085.8 cm^{-1} (as seen in table 3.1 on page 91) which is in agreement with the work by Gross *et al.* [41]. The results presented in section 3.2 (starting on page 89) indicate that the dimethyl sulfoxide molecules were not vibrationally excited to the same extent as Gross *et al.* as determined by the low $[SO]^{+\bullet}$ abundance in the present work. However, the higher excitation obtained by Gross *et al.* can be attributed to the much higher sample pressure (0.24 Torr as opposed to 3.1×10^{-6} Torr for the present work) resulting in collision induced fragmentation.

One skeletal rearrangement fragmentation species obtained from the infrared photolysis of dimethyl sulfoxide is $[H_3CO]^{\bullet}$ and its complementary species $[SCH_3]^{\bullet}$. The fact that the amount of $[H_3CO]^{+}$ produced was larger than that for $[SCH_3]^{+}$ was a rather unexpected result. This disagrees with the results reported by Amos *et al.* [47] previously presented on page 95. Another problem associated with the results depicted

in figure 3.15 (page 103) was that the fragment with the lower ionization potential was expected to be the more abundant ion [75]. Since this rule to predict the relative abundance applies to the case of a parent ion fragmenting to produce an ion and a radical, it may not apply here although the sharp increase in only one species ($[H_3CO]^+$) in the wavelength dependent CO_2 laser photolysis of dimethyl sulfoxide seems to suggest that this was precisely what was happening. The CO_2 laser output power dependent photolysis of dimethyl sulfoxide also generated more $[H_3CO]^+$ than $[SCH_3]^+$ but the relative abundances were more similar to each other than for the wavelength dependent results.

The previous vacuum ultraviolet photolysis work on dimethyl sulfoxide at 193 nm that generated SO was believed to occur by a stepwise process which first produced H_3CSO [64, 65]. The large abundance of $[H_3CSO]^+$ generated in the present work does lend some support to this proposed mechanism. More conclusive evidence for the two-step mechanism would have been given by an increased $[SO]^{+\bullet}$ production with a decreased $[H_3CSO]^+$ intensity as the CO_2 laser output power was increased. As was shown in figure 3.21 (page 113), there was no significant increase in the $[SO]^{+\bullet}$ abundance as the CO_2 laser power was increased. In addition, the power dependence for $[H_3CSO]^+$ in figure 3.20 (page 112) did not exhibit a drop in intensity at the higher photolysis laser output powers. Unfortunately, the present work cannot differentiate between a concerted single step reaction or a sequential two-step mechanism for the generation of $[SO]^{+\bullet}$ from dimethyl sulfoxide.

4.3 Methyl Phenyl Sulfoxide Photolysis

The infrared photolysis of methyl phenyl sulfoxide was summarized in table 3.2 on page 117 and provided some interesting results. Unlike dimethyl sulfoxide, the wavelength dependent investigation indicated the fragment species had a maximum abundance at significantly different wavelengths. In particular, $[C_6H_8S]^{+\bullet}$ had a maximum at 1050.4 cm^{-1} while $[OSCH_3]^+$ had a maximum at 1087.9 cm^{-1}. The power dependent study also had some results not seen with dimethyl sulfoxide where some of the larger mass fragment species plateaued in abundance at higher CO_2 laser output powers.

The infrared photolysis wavelength dependence for methyl phenyl sulfoxide in section 3.3.1 (starting on page 118) clearly showed that as the wavenumber was increased, the fragment abundance also increased. Fragmentation species, like $[C_5H_5S]^+$, which required extensive rearrangement of the parent molecule, had a slow increase over the whole wavenumber region. This gradual behaviour was not observed for all of the photofragmentation species. In particular, $[OSCH_3]^+$ and $[CH_3]^+$ exhibited a sharp increase in abundance as the CO_2 laser wavenumber approached 1090 cm^{-1}. Like the other fragmentation species, these two ions showed a slow increase below 1080 cm^{-1}. The increase corresponds to the molecule gradually absorbing more photons from the laser beam as the wavenumber was increased. The sharp increase indicates that an additional mechanism became energetically accessible as the molecule absorbed a greater number of photons and the energy threshold was surpassed.

The power dependence for the complementary fragmentation species from the two simple dissociation reactions of methyl phenyl sulfoxide exhibited an interesting behaviour for the pairs $[C_6H_5SO]^+$ / $[CH_3]^+$ and $[C_6H_5]^+$ / $[OSCH_3]^+$. The similarity in the results was that the two fragments representing one complementary pair have a different power dependence. This means that a different mechanism was responsible for forming the complementary fragment species. The sharp increase in abundance for $[C_6H_5]^+$ while the slope for the complementary species $[OSCH_3]^+$ remained unchanged, suggests a new mechanism became energetically accessible because the abundance changed for only one species of the pair. As the CO_2 laser output power was increased, the parent molecule absorbed more energy from the laser beam and more energetically excited parent molecules (which did not fragment) were formed. When the energetically excited molecule was photoionized, the parent molecular ion subsequently fragmented to produce one ion ($[C_6H_5]^+$) and one radical ($[OSCH_3]^\bullet$). The complementary pair $[CH_3]^+$ and $[C_6H_5SO]^+$ also showed a similar behaviour where $[CH_3]^+$ suddenly increased in abundance at 0.6 W. However, this pair showed a different behaviour for $[C_6H_5SO]^+$ because the intensity appeared to level off just when the $[CH_3]^+$ abundance started to increase. This plateauing of the intensity can be explained by the energy threshold for the competing dissociative reactions which form fragmentation species that require skeletal rearrangements being surpassed at a CO_2 laser output power of 0.6 W.

4.4 *sec*-Butyl Methyl Sulfoxide Photolysis

The infrared photolysis of *sec*-butyl methyl sulfoxide was summarized in table 3.3 on page 149 and provided interesting results, similar to what was observed with methyl phenyl sulfoxide. The wavelength for maximum yield ranged from 1057.3 cm^{-1} for $[C_4H_8]^{+\bullet}$ to 1086.9 cm^{-1} for $[SCH_3]^+$. Unlike dimethyl sulfoxide and methyl phenyl sulfoxide, most of the fragment species from *sec*-butyl methyl sulfoxide had a maximum yield near 1070 cm^{-1} instead of just below 1090 cm^{-1}. The power dependent results for *sec*-butyl methyl sulfoxide were similar to the results for methyl phenyl sulfoxide, namely that some smaller mass species had a threshold which was surmounted before the abundance became significant while the abundance for some larger mass species plateaued at a certain power.

In section 3.4.1 (starting on page 148), it was shown that the various product species from the infrared multiple-photon dissociation of *sec*-butyl methyl sulfoxide exhibited a wavelength dependence. As the CO_2 laser wavelength was varied, the molecule absorbed a different amount of radiation from the laser beam. In general, as the molecule absorbed more infrared photons, more dissociation of the parent molecule would occur. This was indicated by the increased abundance as the wavelength changed. Eventually, as the molecule absorbed even greater numbers of photons, additional fragmentation species were generated by way of the various competing product channels. This could result in a decreased abundance of a product species which was formed at a lower excitation level. This would explain why the wavelength

for maximum formation of $[C_4H_{10}]^{+\bullet}$ (1057.3 cm^{-1}) was so different from all of the other fragmentation species (which were mostly around 1070 cm^{-1}).

The photolysis laser power dependence of *sec*-butyl methyl sulfoxide presented in section 3.4.2 (starting on page 163) also showed that the fragmentation species abundance changed as the molecule absorbed more photons. The smaller fragmentation species like $[SCH_3]^+$ and $[C_2H_5]^+$, were essentially not produced at lower laser output powers but increased in abundance once some threshold level was surpassed. Larger species, like the butyl group, increased in abundance at lower powers as the laser output power was increased but then decreased in abundance at even higher CO_2 laser output powers. This decrease in the photofragment species intensity can be explained by this large species further fragmenting to generate smaller mass products.

One product species of particular interest is $[CH_3]^+$ which could have been generated by simple cleavage of the methyl moiety in *sec*-butyl methyl sulfoxide or it could have originated from the butyl moiety. Isotope labelling of specific atoms, allowed Siegel to determine which carbon atom in the phenyl group of methyl phenyl sulfoxide migrated to the oxygen atom [46]. A similar approach could be used with *sec*-butyl methyl sulfoxide to determine the origin of the methyl ion fragment. Differentiating the methyl moiety by using a ^{13}C atom would solve this problem. An increase in intensity for a species with a mass of 16 amu would indicate that the methyl ion originated from the methyl moiety whereas a 15 amu product species would mean that the methyl ion came from the butyl moiety.

4.5 Final Comments

Although a fair amount of electron impact mass spectroscopy work has been done on organic sulfoxides, only two of the seven molecules investigated in this work have been previously presented in the literature. The unusual results for this class of molecules which involve extensive skeletal rearrangements could be misinterpreted as impurities in the samples. However, the repeated occurrence of the skeletal rearrangement mechanisms which explained the origins of various fragment species in the present work and also as reported by other researchers [45, 52], suggests that the unusual results are not caused by sample impurities.

The bulk of the work presented in this thesis represents a different approach to studying the photolysis of small organic sulfoxide molecules. When this work was first started, it was believed that the CO_2 laser would fragment the target molecules and then the Nd:YAG laser would ionize the fragments. Unfortunately, this assumption is incorrect as shown by the numerous examples from the present work that indicate fragmentation also occurred after photoionization. The infrared multiple-photon dissociation of dimethyl sulfoxide in the present work resulted in a gentler fragmentation of the parent molecule than what was observed by Gross *et al.* [41]. As previously mentioned, this is a result of the much lower sample pressure used in the present work (3.1×10^{-6} Torr) than was used by Gross *et al.* (0.24 Torr). This gentler technique allowed the vibrationally excited parent molecule to undergo skeletal rearrangement reactions which were not observed by Gross *et al.*

Even though the infrared multiple-photon dissociation of methyl phenyl sulfoxide and *sec*-butyl methyl sulfoxide resulted in readily explainable fragmentation species, the mechanisms were not anticipated prior to this work being started. It was, somewhat naively, believed that the only reactions that would occur would involve simple cleavage mechanisms. It was rather surprising that photofragmentation of these molecules also involved skeletal rearrangement reactions.

Bibliography

[1] J.B. Farmer, in: *Mass Spectrometry*, C.A. McDowell, Editor (McGraw-Hill Book Company Inc., New York, New York, U.S.A., 1963) 7.

[2] F.W. Aston, *Philosophical Magazine and Journal of Science*, **38** (1919) 707.

[3] F.W. Aston, *Philosophical Magazine and Journal of Science*, **39** (1920) 611.

[4] J. Mattauch, *Physical Review*, **50** (1936) 617.

[5] F.W. McLafferty, *Interpretation of Mass Spectra* (University Science Books, Mill Valley, California, U.S.A., 1980) p. 12.

[6] W.C. Wiley and I.H. McLaren, *The Review of Scientific Instruments*, **26** (1955) 1150.

[7] B.A. Mamyrin, V.I. Karataev, D.V. Shmikk and V.A. Zagulin, *Soviet Physics JETP*, **37** (1973) 45.

[8] J. Perrin, *Transactions of the Faraday Society*, **17** (1922) 546.

[9] F. Daniels and E.H. Johnston, *Journal of the American Chemical Society*, **43** (1921) 53.

[10] F. Daniels and E.H. Johnston, *Journal of the American Chemical Society*, **43** (1921) 72.

[11] R.A. Ogg, Jr., *Journal of Chemical Physics*, **15** (1947) 337.

[12] R.A. Ogg, Jr., *Journal of Chemical Physics*, **18** (1950) 572.

[13] R.A. Ogg, Jr., W.S. Richardson and M.K. Wilson, *Journal of Chemical Physics*, **18** (1950) 573.

[14] R.L. Mills and H.S. Johnston, *Journal of the American Chemical Society*, **73** (1951) 938.

[15] K.J. Laidler, *Chemical Kinetics* (HarperCollins*Publishers* Inc., New York, New York, U.S.A., 1987) p. 303.

[16] I. Langmuir, *Transactions of the Faraday Society*, **17** (1922) 600.

[17] F.A. Lindemann, *Transactions of the Faraday Society*, **17** (1922) 598.

[18] F.A. Lindemann, *Transactions of the Faraday Society*, **17** (1922) 606.

[19] J. Perrin, *Transactions of the Faraday Society*, **17** (1922) 605.

[20] W.C.M. Lewis, *Transactions of the Faraday Society*, **17** (1922) 573.

[21] H.C. Ramsperger, *Journal of the American Chemical Society*, **49** (1927) 1495.

[22] C.N. Hinshelwood, *Proceedings of the Royal Society of London*, Series A **113** (1927) 230.

[23] O.K. Rice and H.C. Ramsperger, *Journal of the American Chemical Society*, **49** (1927) 1617.

[24] O.K. Rice and H.C. Ramsperger, *Journal of the American Chemical Society*, **50** (1928) 617.

[25] L.S. Kassel, *Journal of Physical Chemistry*, **32** (1928) 225.

[26] L.S. Kassel, *Journal of Physical Chemistry*, **32** (1928) 1065.

[27] R.A. Marcus and O.K. Rice, *Journal of Physical and Colloid Chemistry*, **55** (1951) 894.

[28] R.A. Marcus, *Journal of Chemical Physics*, **20** (1952) 359.

[29] G.M. Wieder and R.A. Marcus, *Journal of Chemical Physics*, **37** (1962) 1835.

[30] P.J. Robinson and K.A. Holbrook, *Unimolecular Reactions* (John Wiley and Sons Ltd., New York, New York, U.S.A., 1972) p. 64.

[31] J.I. Steinfeld, J.S. Francisco and W.L. Hase, *Chemical Kinetics and Dynamics* (Prentice Hall, Englewood Cliffs, New Jersey, U.S.A., 1989) p. 362.

[32] R.G. Gilbert and S.C. Smith, *Theory of Unimolecular and Recombination Reactions* (Blackwell Scientific Publications, Oxford, Great Britain, 1990) p. 64.

[33] B.A. Lengyel, *Introduction to Laser Physics* (John Wiley and Sons Inc., New York, New York, U.S.A., 1966) p. 278.

[34] K.J. Laidler, *Chemical Kinetics* (HarperCollins*Publishers* Inc., New York, New York, U.S.A., 1987) p. 362.

[35] M.F. Goodman, J. Stone and E. Thiele, in: *Multiple Photon Excitation and Dissociation of Polyatomic Molecules*, C.D. Cantrell, Editor (Springer-Verlag, New York, New York, U.S.A., 1986) 159.

[36] J.L. Lyman, R.J. Jensen, J. Rink, C.P. Robinson and S.D. Rockwood, *Applied Physics Letters*, **27** (1975) 87.

[37] V.S. Letokhov, in: *Laser Spectroscopy of Highly Vibrationally Excited Molecules*, V.S. Letokhov, Editor (Adam Hilger, New York, New York, U.S.A., 1989) 1.

[38] J.D. Rynbrandt and B.S. Rabinovitch, *Journal of Chemical Physics*, **54** (1971) 2275.

[39] P.W. Atkins, *Physical Chemistry* (W.H. Freeman and Company, Fourth Edition, New York, New York, U.S.A., 1990) p. 822.

[40] G.W. Castellan, *Physical Chemistry* (Addison-Wesley Publishing Company, Third Edition, Reading, Massachusetts, U.S.A., 1983) p. 893.

[41] H. Gross, Y. He, M. Quack, A. Schmid and G. Seyfang, *Chemical Physics Letters*, **213** (1993) 122.

[42] D.R. Rayner, E.G. Miller, P. Bickart, A.J. Gordon and K. Mislow, *Journal of the American Chemical Society*, **88** (1966) 3138.

[43] D.R. Rayner, A.J. Gordon and K. Mislow, *Journal of the American Chemical Society*, **90** (1968) 4854.

[44] J.Ø. Madsen, C. Nolde, S.-O. Lawesson, G. Schroll, J.H. Bowie and D.H. Williams, *Tetrahedron Letters*, (1965) 4377.

[45] J.H. Bowie, D.H. Williams, S.-O. Lawesson, J.Ø. Madsen, C. Nolde and G. Schroll, *Tetrahedron*, **22** (1966) 3515.

[46] A. Siegel, *Journal of the Chemical Society, Chemical Communications*, (1976) 327.

[47] D. Amos, R.G. Gillis, J.L. Occolowitz and J.F. Pisani, *Organic Mass Spectrometry*, **2** (1969) 209.

[48] R.G. Gillis, J.L. Occolowitz and J.F. Pisani, *Organic Mass Spectrometry*, **2** (1969) 425.

[49] T.H. Kinstle and W.R. Oliver, *Organic Mass Spectrometry*, **6** (1972) 699.

[50] R.A. Khmel'nitskii and Y.A. Efremov, *Russian Chemical Reviews*, **46** (1977) 83.

[51] K. Pihlaja, in: *The Chemistry of Sulphones and Sulphoxides*, S. Patai, Z. Rappoport and C. Stirling, Editors (John Wiley & Sons, Chichester, Great Britain,

1988) 125.

[52] R. Smakman and T.J. de Boer, *Organic Mass Spectrometry*, **3** (1970) 1561.

[53] R.G.W. Norrish, *Transactions of the Faraday Society*, **30** (1934) 103.

[54] R.G.W. Norrish and M.E.S. Appleyard, *Journal of the Chemical Society*, (1934) 874.

[55] R.G.W. Norrish and C.H. Bamford, *Nature (London)*, **138** (1936) 1016.

[56] R.G.W. Norrish and C.H. Bamford, *Nature (London)*, **140** (1937) 195.

[57] C.H. Bamford and R.G.W. Norrish, *Journal of the Chemical Society*, (1938) 1521.

[58] K. Gollnick and H.U. Stracke, *Tetrahedron Letters*, **3** (1971) 203.

[59] K. Gollnick and H.U. Stracke, *Tetrahedron Letters*, **3** (1971) 207.

[60] K. Gollnick and H.U. Stracke, *Pure and Applied Chemistry*, **33** (1973) 217.

[61] W.O. Ranky and D.C. Nelson, in: *Organic Sulfur Compounds*, N. Kharasch, Editor (Pergamon Press, New York, New York, U.S.A., 1961) 170.

[62] X. Chen, F. Asmar. H. Wang and B.R. Weiner, *Journal of Physical Chemistry*, **95** (1991) 6415.

[63] X. Chen, H. Wang, B.R. Weiner, M. Hawley and H.H. Nelson, *Journal of Physical Chemistry*, **97** (1993) 12269.

[64] H.-Q. Zhao, Y.-S. Cheung, D.P. Heck, C.Y. Ng, T. Tetzlaff and W.S. Jenks, *Journal of Chemical Physics*, **106** (1997) 86.

[65] D.A. Blank, S.W. North, D. Stranges, A.G. Suits and Y.T. Lee, *Journal of Chemical Physics*, **106** (1997) 539.

[66] R.N. Rudolph, S.W. North, G.E. Hall and T.J. Sears, *Journal of Chemical Physics*, **106** (1997) 1346.

[67] F.C. Gozzo and M.N. Eberlin, *Journal of Mass Spectrometry*, **30** (1995) 1553.

[68] H. Schwarz, *Organic Mass Spectrometry*, **15** (1980) 491.

[69] A.H. Kung, J.F. Young and S.E. Harris, *Applied Physics Letters*, **22** (1973) 301.

[70] W.W. Duley, *CO_2 Lasers–Effects and Applications* (Academic Press, New York, New York, U.S.A., 1976) p. 57.

[71] O. Svelto, *Principles of Lasers* (Plenum Press, Third Edition, New York, New York, U.S.A., 1989) p. 310.

[72] *Quanta-Ray GCR-3 and GCR-4 Pulsed Nd:YAG Laser Instruction Manual* (Spectra-Physics Lasers, Mountain View, California, U.S.A., 1991) p. **3**-10.

[73] *Lumonics Series TEA-820 CO_2 Laser Instruction Manual* (Lumonics Inc., Kanata, Ontario, Canada, 1985) p. **5**-5.

[74] D.R. Lide, Editor, *CRC Handbook of Chemistry and Physics* (CRC Press Inc., 73rd. Edition, Boca Raton, Florida, U.S.A., 1992) p. **10**-71.

[75] F.W. McLafferty, *Interpretation of Mass Spectra* (University Science Books, Mill Valley, California, U.S.A., 1980) p. 46.

[76] G.A. McGibbon, P.C. Burgers and J.K. Terlouw, *Chemical Physics Letters*, **218** (1994) 499.